
EXPRESSION AND CHARACTERIZATION OF VEGF RECEPTORS: THEIR USE IN DRUG DISCOVERY

Rossella Di Stasi

Dottorato in Scienze Biotecnologiche –XXI ciclo
Indirizzo Biotecnologie Molecolari
Università di Napoli Federico II



Dottorato in Scienze Biotecnologiche –XXI ciclo
Indirizzo Biotecnologie Molecolari
Università di Napoli Federico II



**EXPRESSION AND
CHARACTERIZATION OF VEGF
RECEPTORS: THEIR USE IN DRUG
DISCOVERY**

Rossella Di Stasi

Dottoranda: Rossella Di Stasi

Relatore: Prof. Ettore Benedetti

Correlatore: Dr. Luca D. D'Andrea

Coordinatore: Prof. Giovanni Sannia

Index

ABBREVIATIONS	pag.	1
SUMMARY	pag.	4
RIASSUNTO	pag.	6
INTRODUCTION	pag.	11
How does a blood vessel form? Vasculogenesis and angiogenesis	pag.	12
Promoters and inhibitors of angiogenesis	pag.	14
Promoters of angiogenesis	pag.	15
Inhibitors of angiogenesis	pag.	19
The vascular endothelial growth factor (VEGF) family	pag.	20
VEGFs	pag.	21
Regulation of VEGF-A expression	pag.	23
VEGF receptors	pag.	24
VEGFR-1	pag.	24
VEGFR-2	pag.	25
VEGFR-3	pag.	26
Neuropilins	pag.	26
Structure and functional analysis of VEGF receptors Flt-1 and KDR	pag.	27
Structures of VEGF-A and PlGF	pag.	28
Structure of VEGF-A in the free form and bound to D2 of VEGFR-1	pag.	28
Structure of PlGF in the free form and bound to D2 of VEGFR-1	pag.	29
VEGF and the induction of pathological angiogenesis: therapeutic implications and perspectives	pag.	30
<i>De novo</i> engineered VEGF mimicking peptides	pag.	31
The aim of the work	pag.	32
MATERIALS AND METHODS	pag.	34
Strains, enzymes and reagents	pag.	34
Antibiotics	pag.	34
<i>E. coli</i> cells transformation techniques	pag.	34
Preparation of <i>E. coli</i> TOPF'10 cells and transformation by electroporation	pag.	34
Preparation of <i>E. coli</i> BL21 (DE3) competent cells and transformation by heat shock	pag.	35
Proteins analyses	pag.	35
Determination of the protein concentration	pag.	35
Electrophoretic analysis of proteins (SDS-PAGE)	pag.	35

Bioinformatic tools	pag.	36
Domains cloning of human KDR and Flt-1 receptors	pag.	36
Cloning of 1-3, 2-3, 1-2 and 2 KDR receptor domains	pag.	36
<i>kdr</i>_{D2} gene mutagenesis	pag.	38
Cloning of 1-4, 2-4, 2-3 and 2 Flt-1 receptor domains	pag.	40
Expression and purification of recombinant KDR and Flt-1 extracellular domains	pag.	41
Expression	pag.	41
Batch purification of 6xHis-tagged proteins under denaturing conditions	pag.	41
Expression and refolding of ¹⁵N-labeled recombinant Flt-1_{D2} for NMR studies	pag.	42
Western blot analysis	pag.	42
TEV digestion of 6xHis-tagged proteins	pag.	43
Flt-1_{D2} alkylation by iodoacetamide and trypsin digestion	pag.	43
Flt-1_{D2} CD analysis	pag.	44
Flt-1_{D2}-VEGF binding competition assay on ECs by Fluorescence activated cell sorting (FACS)	pag.	44
NMR Spectroscopy	pag.	45
Preparation of NMR samples	pag.	45
Peptide-protein interactions	pag.	45
Chemical Shift Mapping	pag.	45
Saturation Transfer Difference	pag.	45
RESULTS	pag.	46
Domains cloning of human KDR and Flt-1 receptors	pag.	46
Cloning of 1-3, 2-3, 1-2 and 2 KDR receptor domains	pag.	46
Cloning of 1-4, 2-4, 2-3 and 2 Flt-1 receptor domains	pag.	48
Expression and purification of recombinant human KDR and Flt-1 extracellular domains	pag.	50
Expression of 1-3, 2-3, 1-2 and 2 KDR receptor domains	pag.	50
<i>kdr</i>_{D2} gene mutagenesis	pag.	54
Expression of 1-4, 2-4 and 2-3 Flt-1 receptor domains	pag.	55
Expression, refolding and purification of 2 Ig-like Flt-1 receptor domain cloned into the pETM11 expression vector	pag.	57
TEV digestion and native-PAGE analysis of Flt-1_{D2}	pag.	58
LC-MS analyses of Flt-1_{D2} after TEV cleavage, alkylation and trypsin digestion	pag.	60
Flt-1_{D2} VEGF-binding competition assay by Fluorescence Activated Cell Sorting (FACS)	pag.	64

Expression, refolding and purification of ^{15}N-Flt-1_{D2}	pag.	65
CD spectroscopic analysis	pag.	65
Proteins secondary structure content	pag.	66
NMR Characterization of Flt-1_{D2}	pag.	69
NMR analysis of peptide-protein interaction	pag.	71
Identification of the binding site on Flt-1_{D2} <i>via</i> Chemical Shift Mapping	pag.	71
Epitope mapping of QK and MA peptides bound to Flt-1_{D2} <i>via</i> Saturation Transfer Difference	pag.	74
DISCUSSION	pag.	76
REFERENCES	pag.	80
PUBLICATIONS and COMUNICATIONS	pag.	90

Abbreviations

AMBIC	ammonium bicarbonate
Ang	angiopoietins
APS	ammonium persulfate
BM	basement membrane
bp	base pair
BSA	albumin from bovine serum
CD	circular dichroism
<i>dam</i>	DNA adenine methylase
D2, D1-2, D2-3, D1-3, D1-4, D2-4	domain 2, domain 1-2, domain 2-3, domain 1-3, domain 1-4, domain 2-4 of VEGFRs
DNA	deoxyribonucleic acid
dNTP	deoxy nucleotide tri-phosphate
DTT	dithiothreitol
EBM	endothelial basal medium
<i>E. coli</i>	<i>Escherichia coli</i>
EC	endothelial cell
ECL	enhanced chemi-luminescence
ECM	extracellular matrix
EDTA	ethylene-diamino-tetraacetic acid
EGF	epithelial growth factor
EGM	endothelial growth medium
ESI	electron spray ionization source
FACS	fluorescence activated cell sorting
FCS	fetal calf serum
FDA	Food and Drug Administration
FGF	fibroblast growth factor
FGFR	fibroblast growth factor receptor
FID	free induction delay
FITC	fluorescein isothiocyanate
Flt-1	fms-like tyrosine kinase-1
F.T.	flow-through
<i>gor</i>	glutathione reductase gene

GTE	Glucose-Tris-EDTA
h	hour
HF	hypotensive factor
HIF-1	hypoxia-inducible factor-1
HPLC	high performance liquid chromatography
HSC	haematopoietic stem cells
HSPG	heparan sulfate proteoglycan
HSQC	heteronuclear single quantum coherence
HUVEC	Human umbilical vein endothelial cell
Ig	immunoglobulin
Kd	dissociation constant
IPTG	isopropyl-beta-D-thiogalactopyranoside
KDa	Kilo Dalton
KDR	kinase domain region
LB	Luria-Bertani Broth (10 g/L bacto-triptone, 5 g/L yeast extract, 10 g/L NaCl)
LC-MS	liquid chromatography mass spectrometry
MCS	multi cloning site
MAPK	mitogen-activated protein kinase
min	minute
MMP	metalloproteinase
ms	millisecond
MWCO	molecular weight cut off
NIH-3T3	Mouse embryonic fibroblast cell line
nm	nanometer
NMR	Nuclear Magnetic Resonance
NOESY	Nuclear Overhauser Effect Spectroscopy
NRP	neuropilin
NRTK	non receptor tyrosine kinase
Ni-NTA	nickel-nitrilotriacetic acid
O.D.	optical density
<i>orf</i>	open reading frame
PAI-1	plasminogen activator inhibitor 1
PBS	phosphate buffer saline

PC	pericyte
PCR	polymerase chain reaction
PDGF	platelet derived growth factor
PDGFR	platelet derived growth factor receptor
pI	isoelectric point
PIGF	placenta growth factor
PVDF	polyvinylidene fluoride
RT	room temperature
RTK	receptor tyrosine kinase
SDS-PAGE	sodium dodecyl sulfate polyacrylamide gel electrophoresis
sec	second
SMC	smooth muscle cells
STD	saturation transfer difference
svVEGF	snake venom vascular endothelial growth factor
TAE	Tris acetate EDTA
TE	10 mM Tris/HCl pH 8, 1 mM EDTA pH 8
TEMED	N,N,N',N'-tetramethyl ethylene diamine
TEV	tobacco etch virus
TFA	trifluoroacetic acid
TIC	total ion current
TK	tyrosine kinase
TM	trans-membrane domain
TnI	troponin I
Tris	Tris (hidroxy methyl) amino methane
<i>trx</i>B	thioredoxin reductase gene
TrxA	thioredoxin A
TSP-1	thrombospondin-1
U	units
uPA	urokinase-type plasminogen activator
UV	ultra violet
VEGF	vascular endothelial growth factor
VEGFR	VEGF receptor
VPF	vascular permeability factor

The one letter code is used for amino acids.

Summary

Angiogenesis is the process of remodeling of the vascular tissue characterized by the branching out of a new blood vessel from a pre-existing one. The angiogenesis is particularly active during embryogenesis, while during adult life it is quiescent and limited to particular physiological phenomena. In the last years, the study of molecular mechanisms of angiogenesis has stirred renewed interest due to the recognition of the role played by angiogenesis in several pathologies of large social impact, such as tumors and cardiovascular diseases, but also to the pharmacological interest rising from the possibility of modulating this phenomenon (Carmeliet, P. *Nat. Med.* 9, 653-660, 2003). Antibodies, peptides and small molecules targeting active endothelial cells (ECs) represent an innovative tool in therapeutic and diagnostic fields (D'Andrea, L. D. *et al.*, 2008, submitted). In the process of angiogenesis, vascular endothelial growth factor (VEGF) is essential for growth, mitogenesis, and tube formation of ECs. VEGF binds to two tyrosine kinase receptors, fms-like tyrosine receptor (Flt-1) and kinase insert domain containing receptor (KDR), on the surface of ECs, thereby activating signal transduction and regulating physiological and pathological angiogenesis. The extracellular portion of these receptors is comprised of 7 immunoglobulin domains; domains deletion studies on Flt-1 have shown that the ligand binding function resides within the first three domains (Barleon, B. *et al.*, *J. Biol. Chem.* 272, 10382-10388, 1997). Deletion experiments on KDR show that only domains 2 and 3 are critical for ligand binding (Fhu, G. *et al.*, *J. Biol. Chem.* 273, 11197-11204, 1998). Actually, of these receptors, are not well known structural data, done exception for the domain 2 of Flt-1 of which, in the literature, is reported the crystal structure complexed with VEGF (Wiesmann, C *et al.*, *Cell* 91, 695-704, 1997) and PIGF (Christinger, H. W. *et al.*, *J. Biol. Chem.* 279, 10382-10388, 2004) and the three-dimensional, uncomplexed form determined by NMR spectroscopy (Starovasnik, M. A. *et al.*, *J. Mol. Biol.* 293, 531-544, 1999). Both VEGF and its receptors are overexpressed in pathological angiogenesis, so the heightened interest in the study of this process is due to the realization that aberrant angiogenesis contributes to pathology. The aim of this PhD thesis is the characterization of proteins involved in the angiogenesis for a better understanding of this crucial process. Because the angiogenic response strictly depends on VEGF and on functions and signaling properties of its receptors, we centred our efforts on the expression of some of the extracellular Ig-like domains of VEGF receptors, focusing the attention on their structural characterization *via* NMR and on their employment in the identification and improvement of new organic or peptide-based molecules targeting the protein system VEGF/VEGFRs. First of all, once expressed and purified Flt-1_{D2}, it was identified by LC-MS, before and after TEV protease cleavage; then we used the second domain of VEGFR-1 for CD analysis. Recorded spectra showed that the protein assumes a β -sheet conformation prevalently, as expected for the structural organization of an Ig-like domain. In addition, with Flt-1_{D2} was performed an *in vitro* assay on HUVEC cells. This assay verified the binding ability of Flt-1_{D2} to VEGF-biotin, delivering the growth factor from membrane receptors and acting as an antibody.

After these preliminary investigations, Flt-1_{D2} was employed in interaction studies with QK and MA peptides (D'Andrea *et al.*, *PNAS* 102, 14215-14220, 2005 and Del Gatto, A. PhD thesis, 2005), in order to better understand their biological behavior as agonist or antagonist in angiogenesis process. This is necessary for the optimization and stabilization of that features which these molecules need to be used as good

modulators in angiogenesis. The interaction between peptides and Flt-1_{D2} has been studied through NMR techniques founded on the observation of ligand (Saturation Transfer Difference) and protein (Chemical Shift Mapping). These experiments showed that QK is able to bind on Flt-1 receptor the same region tied by VEGF. Therefore, the recombinant Flt-1_{D2} was employed for a NMR screening of a library of small molecules, in order to find other VEGF agonist/antagonist and design new molecules more specific and selective in their targeting VEGFRs system. These are preliminary data.

Riassunto

Scopo di questo progetto di dottorato è stata l'espressione in forma ricombinante e la caratterizzazione di proteine coinvolte nel processo di angiogenesi, al fine di impiegarle nello *screening* di molecole in grado di fungere da modulatori della crescita di nuovi vasi sanguigni. L'angiogenesi, infatti, è un processo di rimodellamento del tessuto vascolare caratterizzato dalla formazione di nuovi vasi sanguigni a partire da strutture preesistenti. La formazione di un nuovo vaso sanguigno, così come quella di ogni tessuto, è garantita dall'interazione dinamica tra le cellule che lo costituiscono ed il loro microambiente che risulta essere sostanzialmente costituito dalla matrice extracellulare e da altri citotipi con i quali la popolazione cellulare interagisce. La matrice extracellulare è composta da proteine fibrose e da proteoglicani, ma in essa sono presenti anche citochine e fattori di crescita, generalmente associati a componenti della matrice stessa. L'angiogenesi è regolata prevalentemente da uno di questi fattori di crescita, il VEGF (Vascular Endothelial Growth Factor), potente fattore angiogenico e mitogeno specifico per le cellule endoteliali che, insieme alla matrice extracellulare dell'endotelio vascolare, alla membrana basale, alle cellule muscolari lisce e a quelle di supporto, concorrono alla formazione dei canali che dirigono e contengono il flusso sanguigno. La funzione biologica del VEGF si esplica attraverso il suo legame a due recettori di membrana con attività tirosin-chinasica: il Kinase Domain Receptor (KDR) e l'Fms-like tyrosin kinase (Flt-1), entrambi presenti sulla superficie di diversi tipi di cellule endoteliali, ma in grado di attivare vie di trasduzione distinte, nonostante condividano un elevato grado di omologia (Figura R1) (Ferrara, N *et al.*, *Endocr. Rev.* 18, 4-25, 1997 and Ferrara, N. *Curr. Opin. Biotechnol.* 11, 617-624, 2000).

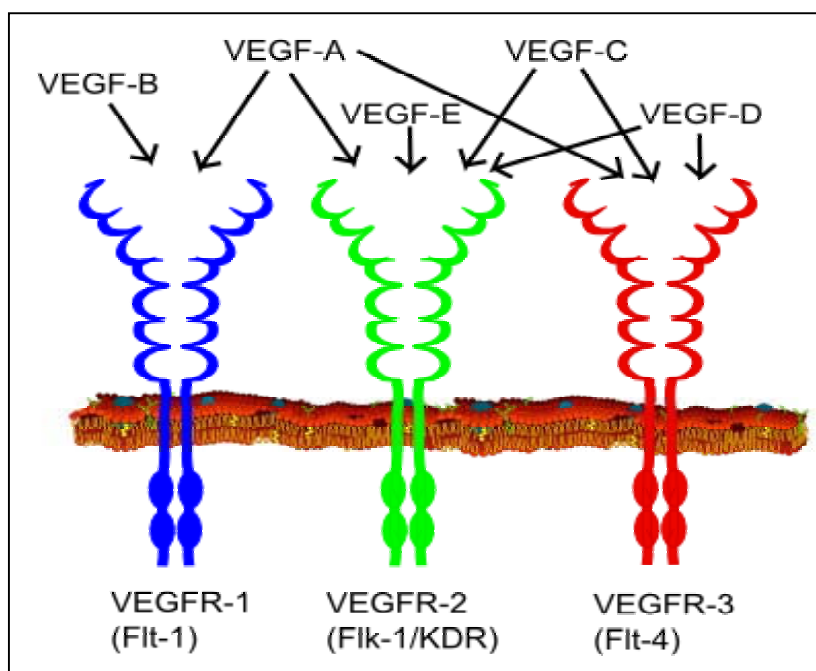


Figura R1_ Rappresentazione delle interazioni del VEGF e dei suoi analoghi con alcuni recettori espressi sulla superficie delle cellule endoteliali.

Per quanto riguarda la porzione extracellulare di queste proteine, attualmente, non sono noti dati strutturali, fatta eccezione per il dominio 2 di Flt-1 di cui, in letteratura, è riportata la struttura cristallografica complessata al VEGF (Figura R2) e al PlGF (Wiesmann, C. *et al.*, *Cell* 91, 695-704, 1997 and Christinger, H. W. *et al.*, *J. Biol. Chem.* 279, 10382-10388, 2004) e quella libera in soluzione (Starovasnik, M. A. *et al.*, *J. Mol. Biol.* 293, 531-544, 1999).

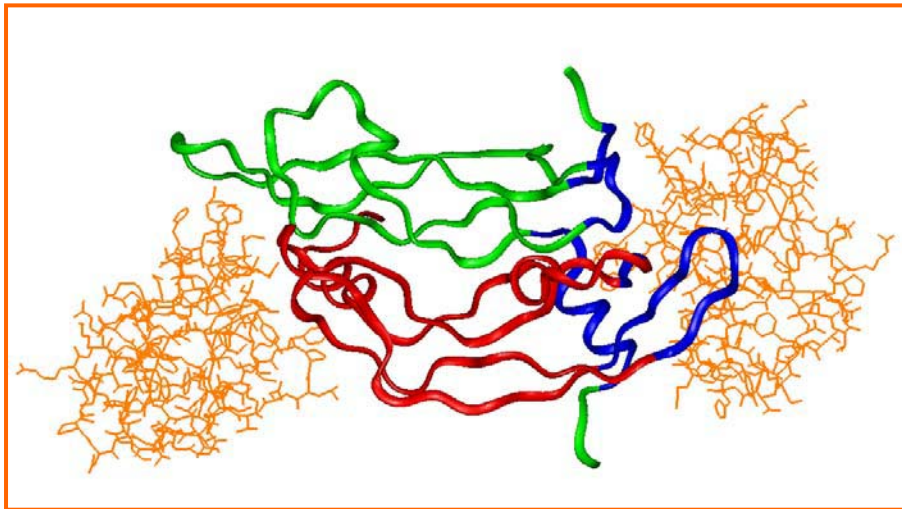


Figura R2_ Dominio 2 del recettore Flt-1 (in arancione) complessato al VEGF₈₋₁₀₉ (in rosso e verde). In blu sono rappresentati i residui del VEGF a contatto con il recettore.

Studi di delezione hanno dimostrato che i maggiori responsabili del riconoscimento specifico per il VEGF sono i primi 3 domini extracellulari per il recettore Flt-1 (Barleon, B. *et al.*, *J. Biol. Chem.* 272, 10382-10388, 1997) e i domini 2 e 3 per KDR (Fhu, G. *et al.*, *J. Biol. Chem.* 273, 11197-11204, 1998). Affinché l'angiogenesi possa svolgersi correttamente, le interazioni che hanno luogo tra le cellule endoteliali e la matrice extracellulare debbono svolgersi secondo una sequenza precisa ed ordinata. In più, l'angiogenesi, come la maggior parte dei processi biologici, è il risultato di un equilibrio tra fattori "pro-angiogenici" ed "anti-angiogenici". Lo spostamento da questa situazione di equilibrio (noto come switch angiogenico) è alla base di manifestazioni patologiche di varia natura quali tumori ed ischemie (Carmeliet, P. *Nat. Med.* 9, 653-660, 2003). Alla luce di queste conoscenze, lo studio del sistema costituito dal VEGF e dai suoi recettori risulta, pertanto, di notevole interesse. La possibilità di disporre di nuovi composti capaci di modulare la risposta angiogenica del VEGF avrebbe così numerose applicazioni in campo terapeutico e diagnostico. Difatti, negli ultimi anni lo studio dei meccanismi dell'angiogenesi è stato uno tra i campi maggiormente investigati e finanziati nell'ambito della ricerca medica. Al momento, tra gli inibitori del processo approvati come agenti terapeutici si annoverano l'Avastin, un anticorpo monoclonale contro il VEGF, usato per il trattamento del tumore del colon-retto, ed un suo derivato, il Lucentis, in uso per patologie oculari. Sono invece pochi i farmaci disponibili che stimolano l'angiogenesi VEGF-dipendente. Attualmente un solo composto pro-angiogenico è stato approvato, il Regranex (PDGF umano

ricombinante), per il trattamento delle ulcere del piede diabetico. L'utilizzo farmacologico di fattori di crescita come il VEGF è stato finora precluso a causa di numerosi effetti collaterali (Carmeliet, P. *Nat. Med.* 6, 1102-1103, 2000b; Lee, C. G. *et al.*, *Nat. Med.* 10, 1095-1103, 2004; Weis, S. M. *et al.*, *Nature* 437, 497-504, 2005). Recentemente è stata riportata in letteratura la caratterizzazione strutturale e le proprietà biologiche di un peptide sintetico che mima il VEGF. Il peptide, QK, modellato sulla regione 17-25 dell'elica del VEGF, lega i recettori del VEGF, attivando poi il processo di proliferazione cellulare VEGF-dipendente. Tale peptide potenzia la risposta biologica del VEGF, e promuove la formazione di capillari *in vitro* ed *in vivo* (D'Andrea, L. D. *et al.*, *PNAS* 102, 14215-14220, 2005). Dunque, si rende necessario lo sviluppo di inibitori di basso peso molecolare e di nuovi agonisti in modo da modulare la crescita di nuovi vasi sanguigni e, in tal modo, la progressione di patologie derivanti da un alterato funzionamento del processo angiogenico. Nel caso dello sviluppo di un tumore, occorre considerare che l'angiogenesi e la formazione di una metastasi costituiscono due esempi paradigmatici del ruolo cruciale svolto dal microambiente all'interno del quale questi due processi si svolgono, nella dinamica spazio-temporale del loro accadere. Il microambiente diventa allora anche un potenziale bersaglio terapeutico per mantenere l'angiogenesi in un ambito fisiologico o per deregolare il potenziale metastatico di una popolazione cellulare. In tal senso sono tuttora allo studio molecole in grado di bloccare l'interazione tra i recettori e i fattori di crescita angiogenici, impedendo così a questi ultimi di interagire con le cellule endoteliali che esprimono sulla loro superficie i recettori. Tale progetto di dottorato si inserisce dunque in questo ampio discorso ed ha come obiettivo la caratterizzazione di proteine coinvolte nell'angiogenesi, in particolare, dei domini extracellulari dei recettori KDR e Flt-1. La loro espressione in forma ricombinante ed il loro impiego in studi condotti mediante analisi NMR, offrirebbe, infatti, la possibilità di uno *screening* di piccoli peptidi o di collezioni di molecole organiche al fine di trovare nuovi ligandi per i recettori e quindi probabili modulatori dell'angiogenesi, in qualità di antagonisti e/o agonisti del processo. La mia attività scientifica nell'ambito di questo progetto si è focalizzata, pertanto, sul clonaggio e l'espressione di alcuni dei domini extracellulari dei recettori del VEGF Flt-1 e KDR. A tal fine sono stati utilizzati diversi vettori per il clonaggio delle sequenze geniche di interesse e diversi ceppi batterici per l'ottimizzazione dei livelli di espressione delle corrispondenti proteine ricombinanti. I sistemi di espressione scelti, sfruttando la presenza di un promotore forte ed inducibile qual è quello regolato dalla RNA polimerasi T7, sono stati in grado di fornire alti livelli di espressione delle proteine di interesse; essi recano marcatori di selezione costituiti da geni che conferiscono resistenza ad un antibiotico (Canamicina o Ampicillina), presentano un'origine di replicazione riconosciuta dall'ospite batterico ed un sito di policlonaggio. La maggior parte dei suddetti sistemi consente, inoltre, di esprimere le proteine di interesse con una coda di poli-istidine all'N-terminale della catena polipeptidica, permettendone una più efficace ed immediata purificazione dai contaminanti di *E. coli* mediante cromatografia di affinità. Le sequenze geniche corrispondenti ai domini extracellulari di Flt-1 e KDR (*flt-1*_{D1-4}, *flt-1*_{D2-4}, *flt-1*_{D2-3} e *flt-1*_{D2}; *kdr*_{D1-3}, *kdr*_{D2-3}, *kdr*_{D1-2} e *kdr*_{D2}) sono state amplificate tramite PCR, utilizzando come stampo il cDNA degli interi recettori e come iniziatori della reazione di amplificazione a catena della polimerasi coppie di oligonucleotidi disegnate sulla base delle sequenze geniche in esame. Il DNA dei costrutti ricombinanti è stato opportunamente purificato e verificato tramite sequenziamento. I clonaggi di tutte le sequenze geniche amplificate sono riusciti con successo ed i costrutti ottenuti nei diversi sistemi di espressione

sono stati utilizzati per l'espressione nei ceppi di *E. coli* scelti per tale scopo. Tutti i costrutti espressi nei diversi ceppi batterici hanno prodotto proteine insolubili, il cui processo di rinaturazione, dopo estrazione in presenza di agenti denaturanti quali urea 8M o Gu-HCl 6M, non sempre è stato portato a termine con successo o ha permesso di ottenere quantità di proteina non sufficienti per essere impiegate in studi di caratterizzazione. Il nostro interesse si è pertanto focalizzato maggiormente sul costrutto pETM11-*flt-1*_{D2}, che siamo riusciti ad esprimere a buoni livelli nel ceppo BL21 *Codon Plus* (DE3) RIL di *E. coli* (60 mg/L) e a rinaturare con rese soddisfacenti. In seguito a trasformazione chimica nel suddetto ceppo batterico, i cloni selezionati su piastra sono stati propagati in terreno liquido. La proteina di interesse è stata espressa in forma insolubile, sia a 22°C che a 37°C, pertanto è stata purificata in condizioni denaturanti mediante cromatografia di affinità su resina funzionalizzata con ioni Nickel (Ni²⁺-NTA *resin*) e sottoposta, successivamente, ad un protocollo di *refolding* su colonna, in modo tale da sottrarle gradualmente l'agente denaturante (urea) utilizzato per la sua estrazione dai corpi di inclusione. Terminato il *refolding*, la proteina Flt-1_{D2} è stata eluita con alte concentrazioni di imidazolo, dializzata e, mediante taglio con la proteasi TEV, è stata allontanata dalla sua estremità N-terminale la coda di poli-istidine con cui è stata espressa. La proteina è stata purificata all'omogeneità, mediante un ulteriore step su resina Ni²⁺-NTA per allontanare da essa sia la TEV che l'HIS-TAG e sottoposta ad un'ampia caratterizzazione. Flt-1_{D2} è stata infatti identificata mediante spettrometria di massa (LC-MS) prima e dopo il taglio con la proteasi; è stata trattata con iodoacetammide (prima e dopo riduzione con DTT) per stabilire l'eventuale alchilazione a carico delle due cisteine presenti nella sequenza amminoacidica del dominio proteico; è stata infine sottoposta ad una proteolisi limitata con tripsina. I dati ottenuti attraverso queste prove ci hanno fornito informazioni utili, seppure indirette, riguardo lo stato assunto dalla proteina in seguito al *refolding* su colonna. Infatti, il trattamento con iodoacetammide ha lasciato invariata la massa di Flt-1_{D2} non ridotta, mentre ha alchilato la proteina precedentemente trattata con DTT. Ciò ci ha dato conferma del fatto che le due cisteine presenti nella sequenza di Flt-1_{D2} sono impegnate in un ponte disolfurico, così come confermato da dati strutturali (Wiesmann, C. *et al.*, *Cell* 91, 695-704, 1997). In più, la reazione di proteolisi limitata, esaminata alla massa a tempi diversi (dopo 45 e dopo 90 minuti) ha mostrato una struttura abbastanza compatta, non intaccata drasticamente dalla tripsina, così come atteso per un dominio immunoglobulinico quale è il dominio 2 del recettore Flt-1. Di Flt-1_{D2} sono state effettuate analisi mediante dicroismo circolare e gli spettri acquisiti hanno mostrato che la proteina assume una conformazione prevalentemente di tipo β -sheet, così come atteso per l'organizzazione strutturale di un dominio di tipo immunoglobulinico. La temperatura di denaturazione di Flt-1_{D2} è stata stimata intorno ai 60°C ed il processo è risultato reversibile. Parallelamente, il dominio proteico è stato utilizzato in un saggio funzionale di fluorescenza condotto *in vitro* su cellule HUVEC (Human umbelical vein endothelial cells). Tale saggio ha dimostrato la capacità di legame del VEGF-biotina ai recettori di membrana presenti sulla superficie delle HUVEC e allo stesso tempo la capacità di Flt-1_{D2} di spiazzare il VEGF da tale interazione. In presenza di un anticorpo anti-VEGF, l'intensità della fluorescenza registrata inviando sulle HUVEC il solo VEGF-biotina è diminuita significativamente. Un decremento analogo si è osservato anche quando le cellule sono state incubate con VEGF-biotina pretrattato con Flt-1_{D2}, indicando che il recettore è in grado di legare il VEGF e di competere per tale legame con i recettori di membrana, comportandosi alla stregua di un anticorpo. In seguito all'ottenimento

di questi dati preliminari, si è passati alla caratterizzazione vera e propria della proteina che, per tale scopo, è stata marcata con ^{15}N , mediante espressione in terreno minimo contenente, come unica fonte di azoto, il cloruro di ammonio marcato ($^{15}\text{NH}_4\text{Cl}$). Flt-1_{D2} è stata espressa e purificata secondo lo stesso protocollo utilizzato per la proteina non marcata, quindi è stata concentrata (0.3 mM) e sottoposta a studi di caratterizzazione mediante NMR. L'acquisizione degli spettri protonici mono- e bidimensionali di Flt-1_{D2} ha messo in evidenza la presenza di numerosi picchi relativi ai protoni ammidici, con una buona dispersione dei *chemical shifts*, così come atteso per la proteina nativa (Starovasnik, M. A. *et al.*, *J. Mol. Biol.* 293, 531-544, 1999). È stato pertanto possibile asserire che il dominio proteico ottenuto in forma ricombinante e purificato all'omogeneità dopo *refolding* ha una conformazione correttamente ripiegata. Successivamente, la proteina è stata impiegata in studi di interazione con due piccoli peptidi di quindici amminoacidi sintetizzati e caratterizzati nel laboratorio in cui è stato svolto questo lavoro di tesi; i peptidi in esame sono QK (Ac-KLTWQELYQLKYKGI-NH₂) ed MA (Ac-KLTWMELYQLAYKGI-NH₂) (D'Andrea, L. D. *et al.*, *PNAS* 102, 14215-14220, 2005 and Del Gatto, A. PhD thesis 2005). Entrambi rappresentano un esempio di quello che viene definito approccio di sintesi mediante *rational-design* e riproducono l'elica 17-25 del VEGF; infatti, l'analisi accurata dei dati strutturali, così come gli studi di mutagenesi, hanno permesso di identificare i residui amminoacidici coinvolti nel legame del VEGF ai suoi recettori. Essi sono distribuiti su una superficie discontinua costituita appunto dall'elica 17-25 presente all'estremità N-terminale di ciascun monomero del VEGF (Keyt, B. A. *et al.*, *J. Biol. Chem.* 271, 5638-5646, 1996; Muller, Y. A. *et al.*, *Proc. Natl. Acad. Sci. USA* 94, 7192-7197, 1997; Wiesmann, C. *et al.*, *Cell* 91, 695-704, 1997). Attualmente, la stragrande maggioranza delle molecole peptidiche in grado di modulare l'interazione tra il VEGF ed i suoi recettori deriva da *screening* di collezioni fagiche, mentre sono pochi gli esempi derivanti da un approccio di tipo razionale. L'interazione dei due peptidi con il secondo dominio del recettore Flt-1 è stata studiata attraverso tecniche NMR basate sull'osservazione del ligando (*Saturation Transfer Difference*) e della proteina (*Chemical Shift Mapping*). Tale interazione ha permesso di identificare, sia per QK che per MA, le regioni impegnate nel *binding* con la proteina, dimostrando che il peptide QK lega sul recettore la stessa regione di legame del VEGF. Flt1_{D2} è stata infine impiegata in uno studio di *drug discovery*, attraverso lo screening di una collezione di piccole molecole organiche con l'intento di selezionare nuovi ligandi a basso peso molecolare capaci di bloccare l'interazione tra il VEGF ed i suoi recettori. I dati ottenuti sono del tutto preliminari.

Introduction

Angiogenesis is a phenomenon intimately associated with endothelial cells (ECs) migration and proliferation. During embryonic development, ECs rapidly proliferate, thereby forming new blood vessels. In adult life, however, ECs turnover is very low, except for physiological wound healing and female reproductive functions. Angiogenesis is also implicated in pathological conditions associated with tumors, intraocular neovascular disorders, chronic ischemia and other diseases (Carmeliet, P. 2003). The mediators of this process have been identified in a series of vascular growth factors such as the Vascular Endothelial Growth Factor (VEGF). VEGF represents a key regulator of angiogenesis; its biological effects are prevalently mediated by two receptor tyrosine kinases (RTK): VEGFR-1 and VEGFR-2 which are localized on the cell surface of various endothelial cell types. VEGF and its receptors are over-expressed in pathological angiogenesis, making this protein system a target for therapeutic and diagnostic applications (Ferrara, N *et al.*, 1997 and Ferrara, N. 2000). Therapeutic angiogenesis is sought as the ultimate intervention to solve chronic ischemia in those conditions that cannot be treated alternatively; its converse, the anti-angiogenic treatment, with the blockage of the VEGF/VEGFRs pathway, is a promising therapy in oncology. To date, a number of different strategies to inhibit VEGF signal transduction are available and they include the use of humanized neutralizing anti-VEGF monoclonal antibodies, receptor antagonists, soluble receptors and inhibitors of VEGF receptors function (Moreira, I. S. *et al.*, 2007). Moreover, new molecular entities as peptides have been reported to bind to the extracellular region of the VEGF receptors. A large number of them show an antagonist activity and only few behave as agonists (D'Andrea, L. D. *et al.*, 2008, submitted).

The introduction is not meant to cover the VEGF/VEGFR field completely, but rather to emphasize selected aspects of these molecules which are important for the aims described in this PhD thesis.

How does a blood vessel form? Vasculogenesis and Angiogenesis

Blood vessel formation occurs through the processes of vasculogenesis and angiogenesis (Folkman, J. *et al.*, 1996; Risau, W. 1997; Beck, L. *et al.*, 1997). Vasculogenesis is the differentiation *de novo* of vascular endothelial cells from precursor cells, known as angioblasts, during embryonic development. This process is distinct from angiogenesis, which is a remodeling process characterized by the sprouting of new blood vessels from pre-existing ones (Figure 1). Vasculogenesis was thought to occur only in early embryogenesis. The existence of endothelial progenitor stem cells has been established, however, and these bone marrow-derived cells have been found in the adult, including injured corneas and tumor vasculature, suggesting that vasculogenesis can occur in the adult (Asahara, T. *et al.*, 1997; Shi, Q. *et al.*, 1998; Takahashi, T. *et al.*, 1999a). Although developmentally significant, angiogenesis is rare in the adult. One exception is the female reproductive system where it has been demonstrated that angiogenesis is correlated with vascularization of ovarian follicles, development of the corpus luteum, repair of endometrial vessels and implantation of embryo *in utero* (Shweiki, D. *et al.*, 1993). Angiogenesis is involved in physiological wound healing and tissue repair. It is stimulated by factors such as VEGF and fibroblast growth factor (FGF), which will be described at greater length below. An early response to angiogenesis-stimulating factors is the degradation of endothelial cell basement membrane (BM) by proteases such as the members of the matrix metalloproteinase (MMP) family. MMPs degrade collagen and other extracellular matrix components, disrupting the BM barrier, enabling ECs to migrate from pre-existing vessels towards angiogenic stimuli and to proliferate (Moses, M.A. 1997). Vascular cell-adhesion molecules contribute to ECs migration by mediating cell-extracellular-matrix interactions. An important mediator is the integrin $\alpha_V\beta_3$, a receptor for proteins such as fibronectin, which is expressed at low levels in quiescent blood vessels (Eliceiri, B.P. *et al.*, 1998). Antagonists of $\alpha_V\beta_3$ inhibit the growth of new blood vessels but not pre-existing ones, suggesting that cell adhesion is a critical step in angiogenesis (Brooks, P.C. *et al.*, 1994). Following migration and proliferation, ECs assemble into tubes with a lumen (Figure 2). Lumen formation may be dependent on E-selectin, a trans-membrane cell-adhesion glycoprotein that mediates endothelial cell-cell contacts (Nguyen, M. *et al.*, 1992). An important step in producing a mature blood vessel is the recruitment of mesenchymal cells and their subsequent differentiation into smooth muscle cells-like pericytes (PC) that stabilize the newly forming vasculature. Platelet-derived growth factor (PDGF) plays a role in pericytes recruitment, acting as a potent chemoattractant and mitogen for pericytes and smooth muscle cells (SMC) (Lindahl, P. *et al.*, 1997).

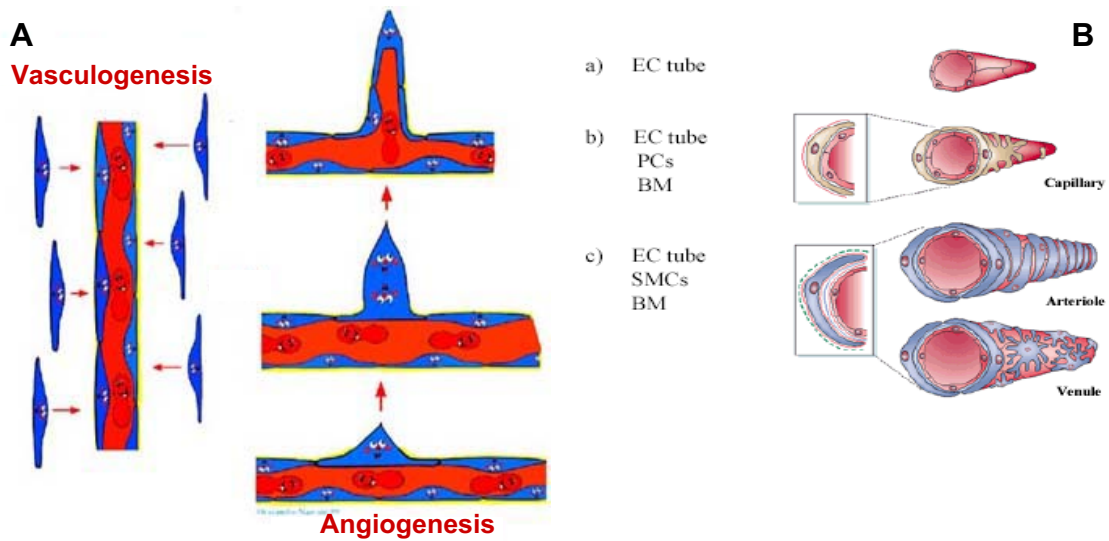


Figure 1_ A) Vasculogenesis versus angiogenesis; B) Wall composition of nascent and mature vessels: schematic representation of cells involved in vasculogenesis and angiogenesis (Yancopoulos, G. D. *et al.*, 2000).

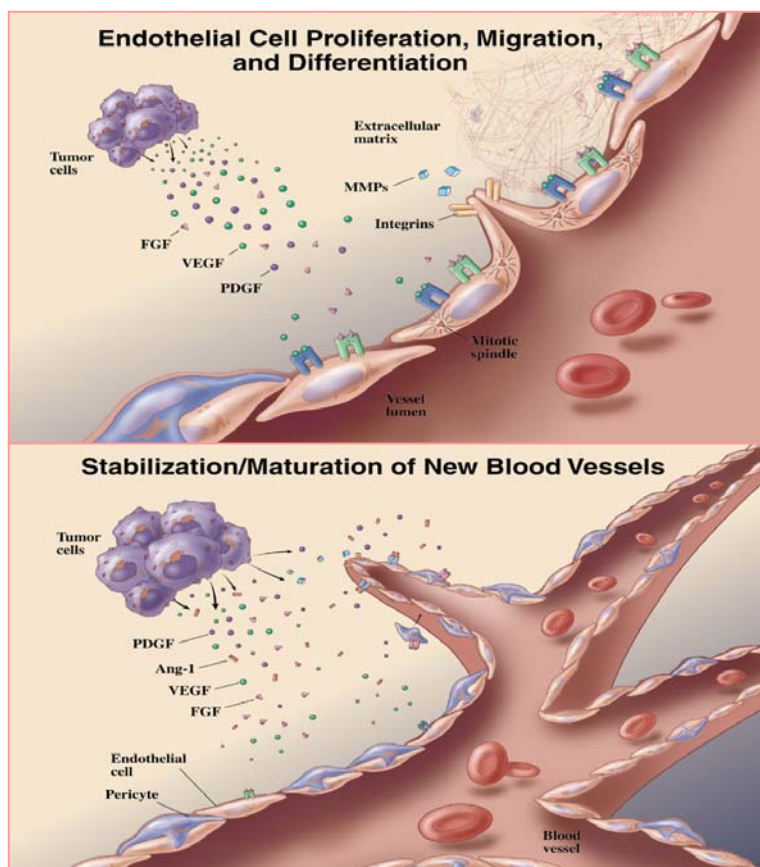


Figure 2_ Processes in pathological angiogenesis: the various steps in blood vessel formation.

Promoters and inhibitors of angiogenesis

Formation of the normal blood vasculature is thought to depend from the balanced secretion, in appropriate amounts and temporal sequence, of a large number of chemically diverse molecules (Beck, L. *et al.*, 1997; Yancopoulos, G.D. *et al.*, 2000; Carmeliet, P. 2000a). These include VEGF and other members of the VEGF/VEGFR family, in addition to other growth factors (e.g. PDGF, FGF, angiopoietins) and various endogenous inhibitors (**Table 1**).

Table 1: Endogenous angiogenic regulators

Pro-angiogenic	Anti-angiogenic
Acidic fibroblast growth factor	2-Methoxyoestradiol
Angiogenin	Angioarrestin
Angiopoietin-1	Angiostatin
B61/LERK-1	Angiotensin
Basic fibroblast growth factor	Antiangiogenic antithrombin III
Del-1	Endostatin
Erythropoietin	Fibronectin peptide
Follistatin	Gro- β
Gangliosides	Human chorionic gonadotropin (hCG)
Granulocyte colony-stimulating factor	Hyaluronan
Granulocyte macrophage colony-stimulating factor	Interferon γ -inducible protein 10
Hepatocyte growth factor	Interferons
Hyaluronan oligosaccharides	Interleukin 12
Insulin-like growth factor	Kringle 5
Interleukin 8	Laminin peptide
Leptin	Plasminogen activator inhibitors
Midkine	Platelet factor 4

Monocyte chemoattractant protein 1	Prolactin 16kD fragment
Oestrogens	Proliferin-related protein
Placenta growth factor	Thrombospondin-1
Platelet-derived growth factor	Tissue inhibitors of metalloproteinase
Pleiotrophin	Transforming growth factor-beta (TGF-b)
Progranulin	Tumour necrosis factor α (high dose)
Proliferin	Tumstatin
Prostaglandin E ₁ , E ₂	Vasculostatin
Transforming growth factor α and β	Vasostatin (calreticulin fragment)
Tumour necrosis factor α (low dose)	
Vascular endothelial growth factor	

Promoters of angiogenesis

Angiopoietins and Tie receptors

Tie receptors and their ligands, the angiopoietins, play a critical role in embryonic angiogenesis (Partanen, J. *et al.*, 1999 and Davis, S. *et al.*, 1999). Tie receptors, Tie1 and Tie2, are tyrosine kinases expressed by ECs. Mice deficient in Tie2 are embryonic lethal with defects in the proper development of the endothelial lining of the heart. Tie1 is required for the structural integrity of ECs and mice deficient in Tie1 die by birth (Dumont, D.J. *et al.*, 1994 and Sato, T.N. *et al.*, 1995). Angiopoietin-1 (Ang1) is a ligand for Tie2 (Davis, S. *et al.*, 1996). Ang1 induces phosphorylation of Tie2 in ECs, but does not induce cell proliferation. Over-expression of Ang1 results in more numerous and more highly branched vessels. Targeted disruption of Ang1 is embryonic lethal and the defects in these mice resemble those in the Tie2 deficient mice. In addition to heart defects, there are a reduced number of vessels and remodeling of the initial primary capillary network does not occur. Importantly, there is a lack of recruitment of periendothelial supporting cells to the ECs in Ang1-deficient mice, which leads to lack of blood vessels stabilization and maturation (Suri, C. *et al.*, 1998). Ang1 is expressed embryonically, most prominently in heart myocardium. In adult tissue Ang1 is constitutively and widely expressed especially in platelets, megakaryocytes as well as in highly vascularized tissues, but not in tissues with low vascularization (Thurston, G. *et al.*, 2000). It has been suggested that mesenchymal cells produce Ang1, which activates Tie2 which in turn leads to the production and release of factors (e.g. PDGF-BB) that recruit pericytes and smooth muscle cells

(Folkman, J. *et al.*, 1996). Angiopoietin 2 (Ang2) is 60% identical to Ang1, but does not stimulate Tie2 tyrosine phosphorylation. Ang2 might be a natural antagonist of Ang1 that blocks Ang1 activation of Tie2 receptor (Maisonpierre, P.C. *et al.*, 1997). Neither Ang1 nor Ang2 alone could trigger an angiogenic response, but could enhance VEGF-induced angiogenesis, leading to the notion of an angiogenic balance: Ang1 signaling *via* Tie2 leads to vessel maturation, whereas Ang2 blocks the Ang1/Tie2 signal and leads to angiogenesis or vessel regression and apoptosis, depending on the presence of VEGF (Hanahan, D. 1997 and Asahara, T. *et al.*, 1998).

Platelet derived growth factor (PDGF)

PDGF has been shown to be one of the most potent angiogenesis inducers and is licensed for the treatment of neuropathic diabetic foot ulcers (Bennett, S.P. *et al.*, 2003). The Platelet-derived Growth Factor belongs to a family of structurally and functionally related growth factors containing cysteine knots, which includes also the VEGF (Fredriksson, L. *et al.*, 2004a). The currently known PDGFs include the PDGF-A, PDGF-B, PDGF-C, PDGF-D chains. All members harbour a growth factor core domain, containing a conserved set of cysteine residues, which is necessary and sufficient for receptor binding activation. PDGF-A and PDGF-B contain N-terminal pro-domains, which are removed intracellularly by furin or other convertases; cleavage of these domains result in protein activation and receptor binding (Heldin, C. H. *et al.*, 1999 and Fredriksson, L. *et al.*, 2004a). PDGF-C and PDGF-D instead are processed in the extracellular space (Fredriksson, L. *et al.*, 2004b). PDGFs act through two tyrosine kinase receptors, PDGFR α and PDGFR β . The receptors are transmembrane proteins, composed of an extracellular ligand-binding domain, a transmembrane domain and a cytoplasmic tyrosine kinase domain (Fantl, W. J. *et al.*, 1993). The extracellular region contains five immunoglobulin-like domains, while the intracellular domain carries a tyrosine kinase domain and a unique sequence with no homology to kinases (Matsui, T. *et al.*, 1989). Upon ligand binding, the PDGF receptors dimerize and phosphorylate each other in trans on specific tyrosine residues (Kelly, J. D. *et al.*, 1991). Although in theory there are several possible combinations of ligand and receptors, the functional *in vivo* interaction has been proved only for PDGF-AA and PDGF-CC with PDGFR α and for PDGF-BB with PDGFR β (Andrae, J. *et al.*, 2008) (Figure 3). PDGFR interacts with several other proteins involved in multiple cellular and developmental responses including integrins (Hynes, R.O. 2002) and transcription factors. PDGFs play key roles in embryonal development, being involved in the formation of blood vessels, kidney, lungs, connective tissues and central nervous system. Furthermore, together with other growth factors, PDGF regulate the wound healing process; it has been shown that wounds treated with PDGF exhibit an increase in the re-epithelization and neovascularization rates (Heldin, C. H. *et al.*, 1999 and Sundberg, C. *et al.*, 1997). Overexpression of the PDGFs has been associated with several diseases associated with increased cell proliferation. Experimental evidences show that PDGF is involved in pulmonary fibrosis (Yi, E. S. *et al.*, 1996) and in the formation of cholesterol induced atherosclerosis (Rutherford, C. *et al.*, 1997). PDGF overexpression was also observed in human solid tumors, as gastrointestinal stromal and central nervous system tumors (Heldin, C. H. *et al.*, 1999 and Alvarez, R. H. *et al.*, 2006).

Fibroblast growth factor (FGF)

In the 1980s purification of pro-angiogenic proteins led to the identification, and sequencing of the two prototypic *heparin-binding angiogenic growth factors* FGF1 (acidic FGF) and FGF2 (basic FGF) (Abraham, J. A. *et al.*, 1986a-b). Since then the FGF family has increased in number and complexity as many more members of the family (23 in total) with a variety of biological activities, have been discovered (Powers, C. J. *et al.*, 2000). Acidic and basic fibroblast growth factors (FGF-1 and FGF-2, respectively) are very potent inducers of EC migration, proliferation and tube formation *in vitro* and are highly angiogenic *in vivo* (Klagsbrun, M. *et al.*, 1991a). All FGFs share 30–70% homology in their amino acid sequences and consist of two highly conserved core-domains that fold in 12 antiparallel β -strands, leading to the formation of a cylindrical barrel (Ago, H. *et al.*, 1991; Eriksson, A. E. *et al.*, 1991; Zhu, X. *et al.*, 1991; Zhang, J. D. *et al.*, 1991). These domains are separated by a central spacer region of variable length as well as variable are the C- and N-terminal regions of the different FGFs (Reuss, B. *et al.*, 2003). Many studies have shown that FGFs can act on different cell types inducing cell proliferation, differentiation, migration and survival (Ornitz, D. M. *et al.*, 2001). All these actions are made possible through the dual interaction of FGFs with high-affinity tyrosine kinase receptors (FGFRs) and with a large number of low affinity sites on the cell surface and within the surrounding extracellular matrix (ECM) (Klagsbrun, T. *et al.*, 1991b). These sites were identified as heparan sulfate proteoglycans (HSPGs) obligatory partners of the FGF interaction with FGFR (Ornitz, D. M. *et al.*, 1992 and Mansukhani, A. *et al.*, 1992). To date four FGF transmembrane receptors (FGFRs1-4) and one soluble receptor (FGFR5) are known (Chaffer, C. L. *et al.*, 2007). Isolation and structural characterization in 1989 of a protein with high affinity for FGF1 (Lee, P. L. *et al.*, 1989) led to the identification of the prototypic of all FGF receptors, which are transmembrane proteins with three extracellular immunoglobulin-like domains (Igl, IgII, and IgIII), an acidic box and heparin-binding domain between Igl and IgII, a hydrophobic transmembrane domain, and an intracellular region containing a split tyrosine kinase domain (Figure 4). In the structure of the FGF receptor gene four possible splice sites exist, generating an FGFR α subtype that expresses only two Ig-like domains, and an FGFR β subtype that expresses all the three Ig-like domains. Those splice events alter FGF/FGFR specificity by exposing or obscuring the acidic box that lies between the Igl and IgII domains.

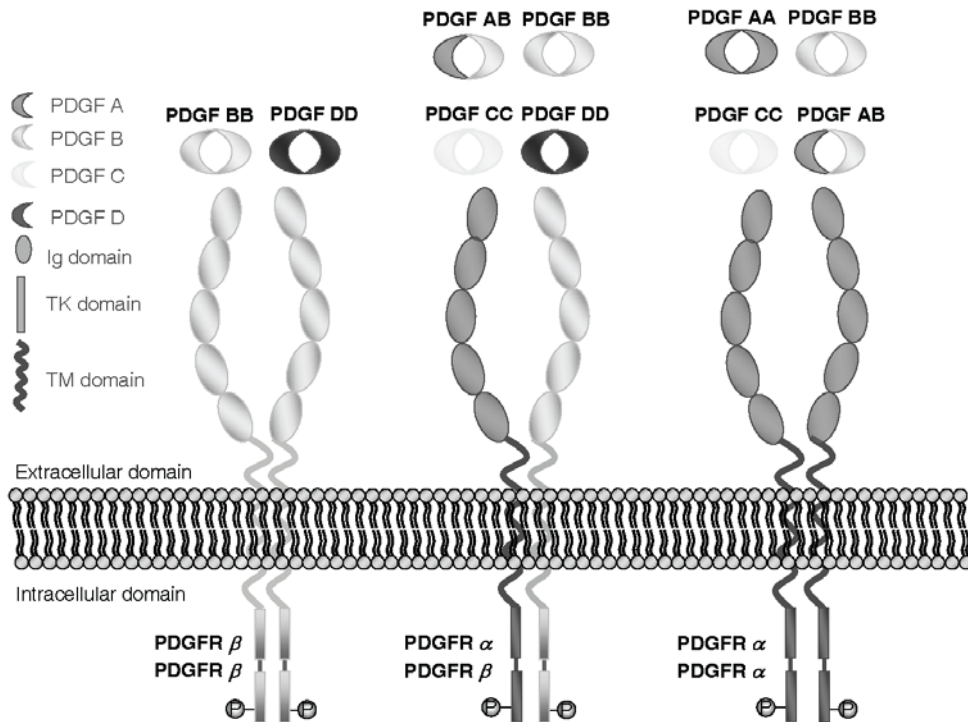


Figure 3_ Schematic representation of the PDGFs/PDGFRs interaction. Three different PDGFR isoforms are showed: the homodimers aa and bb and the heterodimer ab. The extracellular domains of all PDGFRs contain five immunoglobulin-like (Ig) domains which interact with the four different homodimeric PDGF isoforms AA, BB, CC, DD, and the heterodimeric isoform AB. PDGFRs also have a transmembrane (TM) region and an intracellular region containing a tyrosine kinase (TK) domain.

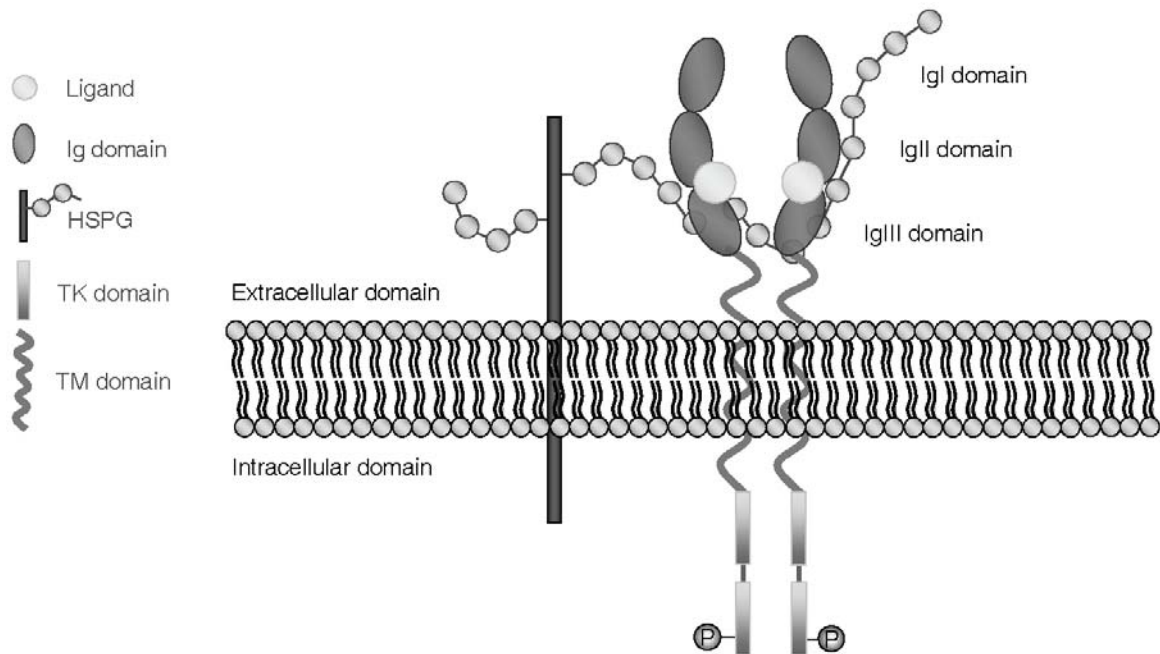


Figure 4_ Schematic representation of the FGFs/FGFRs interaction. The extracellular domain of FGFRs contains three immunoglobulin-like (Igl–III) domains. FGFs interact with the second and third of these domains, and heparan sulfate proteoglycans (HSPG) are integral to the FGF–FGFR signaling complex. FGFRs also have a transmembrane (TM) region and an intracellular region containing a split tyrosine kinase (TK) domain.

Inhibitors of angiogenesis

A large number of angiogenesis inhibitors have been described. For example, there are natural molecules that apparently act directly on ECs to block their migration, proliferation and/or their ability to form capillary-like tubes. These include proteins such as angiostatin, endostatin, thrombospondin-1, troponin-1 and others (Hanahan, D. *et al.*, 1996).

Angiostatin

Angiostatin is a 38 KDa internal fragment of plasminogen (O' Reilly, M.S. *et al.*, 1994). Angiostatin enables micrometastasis to remain dormant by increasing the tumor cell apoptotic rate. Tumor cells do not synthesize angiostatin directly, but may instead produce and secrete an as yet an unidentified enzyme that enters the circulation and interacts with plasminogen to release the angiostatin portion (Holmgren, L. *et al.*, 1995).

Thrombospondin-1

A 140 KDa fragment of Thrombospondin-1 (TSP-1) was one of the first natural angiogenesis inhibitors to be described. TSP-1 is an inhibitor of tumor growth and metastasis in a number of animal models. Its expression is inversely correlated with angiogenic activity (Rastinejad, F. *et al.*, 1989). In studies of fibroblasts cultured from patients with Li-Fraumeni disease, it was shown that TSP-1 is regulated by the *p53* tumor suppressor gene. Loss of *p53* results in suppression of TSP-1 and in a concomitant increase in angiogenic activity (Dameron, K.M. *et al.*, 1994).

Endostatin

Endostatin is a 20 KDa carboxy-terminal fragment of collagen XVIII. The identity of the enzyme that releases endostatin from collagen XVIII is unknown. Endostatin specifically inhibits capillary ECs proliferation *in vitro* and is a potent inhibitor of the growth of primary and metastatic tumors (O' Reilly, M.S. *et al.*, 1997; Dnanabal, M. *et al.*, 1999; Bergers, G. *et al.*, 1999). Endostatin has several properties that suggest it might be of potential clinical use as an anti-angiogenic agent. One is that endostatin does not induce drug resistance as do conventional chemotherapy and radiation. In addition, in mouse tumor models, repeated cycles of administering systemic endostatin results in prolonged tumor dormancy without further treatment, suggesting that endostatin could completely suppress a tumor rather than just inhibit it transiently (Boehm, T. *et al.*, 1997).

Troponin

Troponin I (TnI) is a 22 KDa angiogenesis inhibitor isolated from cartilage (Moses, M.A. *et al.*, 1999); it is an endothelial cell-specific inhibitor of FGF- and VEGF-driven capillary ECs proliferation *in vitro* and of neovascularization in cornea models. Interestingly, TnI is used clinically as a sensitive serum marker to assess the degree of myocardial damage during infarction. It is speculated that the anti-angiogenic properties of TnI might be responsible for the difficulty in revascularizing ischemic myocardium following injury.

The vascular endothelial growth factor (VEGF) family

The VEGF family and its receptors play a central, specific role in angiogenesis, mediating vascular permeability, endothelial cells proliferation, migration and survival (Ferrara, N. 2002). New vessel growth and maturation are highly complex and coordinated processes, requiring the sequential activation of a series of receptors by numerous ligands (Ferrara, N. 1999; Yancopoulos, G.D. *et al.*, 2000; Carmeliet, P. 2000a). VEGF (also referred to as VEGF-A) belongs to a gene family that includes placental growth factor (PlGF), VEGF-B, VEGF-C and VEGF-D. Homologous of VEGF have also been identified in the genome of the sheep parapoxvirus and shows to have VEGF-like activities (Ferrara, N. *et al.*, 1997 and Neufeld, G. *et al.*, 1999) (Figure 5).

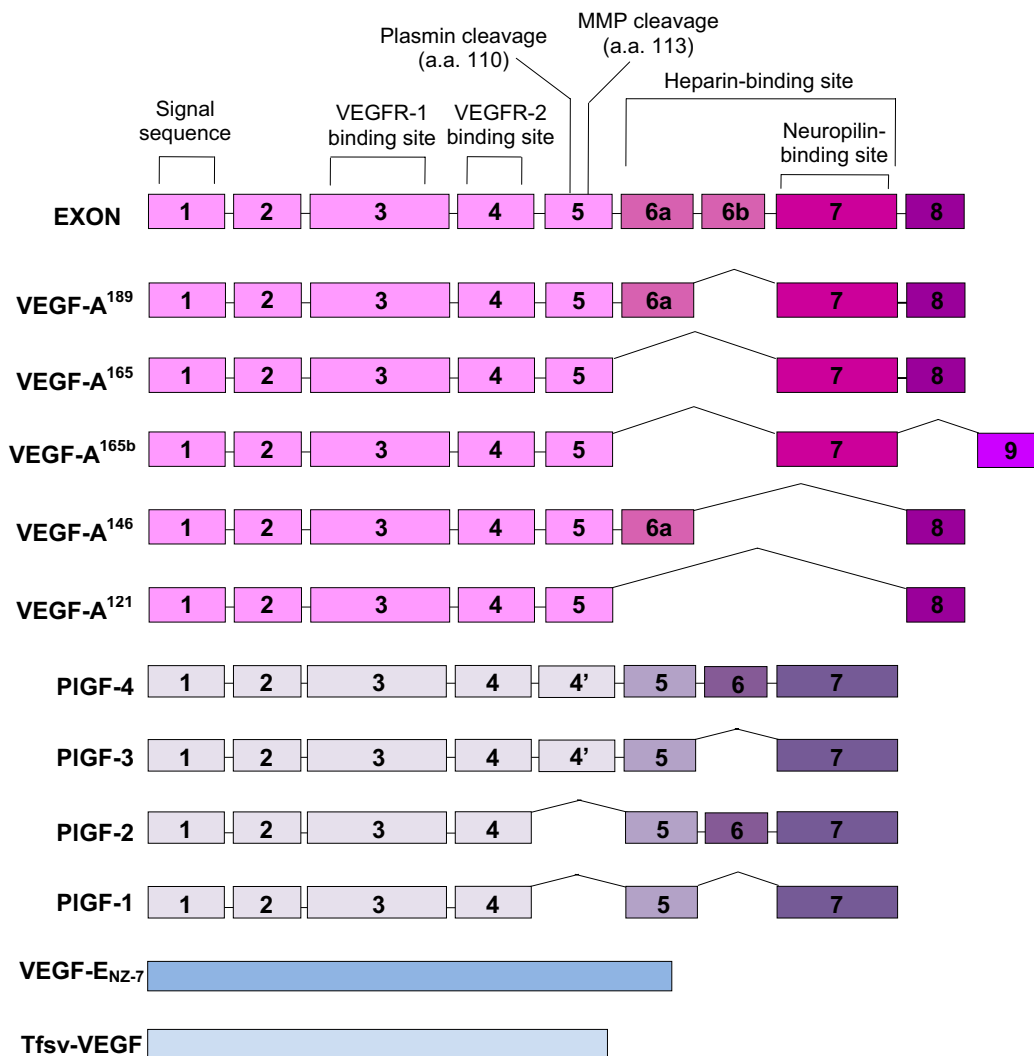


Figure 5_ Structure of some VEGF family members. Alternative splicing results in the generation of several VEGF-A and PlGF isoforms. VEGF-A gene possesses eight exons, the first of which encodes a hydrophobic leader sequence typical of secreted proteins. VEGF-A¹⁸⁹ lacks a portion of exon 6, whereas VEGF-A¹⁶⁵, generally the most commonly expressed isoform, lacks all of exon 6. VEGF-A¹⁴⁵ lacks both exons 6b and 7, and VEGF-A¹²¹ lacks all of exons 6 and 7. VEGF-A^{165b} is an inhibitory form of VEGF-A that lacks exons 6 and 8 and terminates with a portion of the supposed 3' untranslated region, here designated as exon 9 (Nagy *et al.* 2007). VEGF receptor and heparin-binding sites, as well as protease cleavage sites, are shown. Viral VEGF-E and snake venom VEGFs are encoded by one transcript.

VEGFs

A well documented *in vitro* activity of VEGF is the ability to promote growth of vascular ECs derived from arteries and veins. VEGF induces a potent angiogenic response in a variety of *in vivo* models (Leung, D.W. *et al.*, and Plouet, J. *et al.*, 1989) and its delivery also induces lymphangiogenesis in mice (Nagy, J.A. *et al.*, 2002). VEGF is a survival factor for ECs, both *in vitro* and *in vivo*. *In vitro*, it prevents apoptosis induced by serum starvation, *in vivo* induces expression of the anti-apoptotic proteins Bcl-2 and A1 in ECs (Gerber, H.P. *et al.*, 1998 a and b). VEGF is known also as vascular permeability factor (VPF), based on its ability to induce vascular leakage (Senger, D.R. *et al.*, 1983 and Dvorak, H.F. *et al.*, 1995). It is now well established that such permeability-enhancing activity underlies significant roles of this molecule in inflammation and other pathological circumstances (Bates, D.O. *et al.*, 1997).

VEGF-A

VEGF-A is the most comprehensively studied member of the VEGF family and has singular importance in vascular development (Brown, L.F. *et al.*, 1997; Dvorak, H.F. 2003; Ferrara, N. *et al.*, 2003; Dvorak, H.F. 2006). Encoded by a single gene of eight exons separated by seven introns (Figure 5), VEGF-A is a highly conserved, disulfide-bonded dimeric glycoprotein. It shares low, but significant, sequence homology with PDGF, and, like PDGF, has cysteines that form inter- and intra-chain bonds. Crystal structure reveals that the two chains, that comprise VEGF-A, are arranged antiparallel with receptor binding sites at either end (Muller, Y.A. *et al.*, 1997). Upon reduction, VEGF-A separates into its individual chains and loses all biological activity (Dvorak, H.F. 2003). The importance of VEGF-A as a central regulator of angiogenesis and vasculogenesis was demonstrated in mice targeted gene disruption studies. Even animals that lack one of the two VEGF alleles die before birth because of defects in the development of the cardiovascular system (Ferrara, N. *et al.*, 1996 and Carmeliet, P. *et al.*, 1996). These observations indicate that the development of the cardiovascular system depends on the generation of precise VEGF concentration gradients and that a decrease in the amounts of the VEGF produced during the development of the embryo may lead to decreased angiogenesis with fatal consequences. The human VEGF-A gene is located on the short arm of chromosome 6 and is differentially spliced to yield predominant isoforms that encode polypeptides of 206, 189, 165, 145 and 121 amino acids in human cells; corresponding murine proteins are one amino acid shorter. An additional splice variant, 165b, has been found in normal kidneys; it is an endogenous inhibitor of VEGF-A¹⁶⁵ and is downregulated in renal tumors and therefore may be antiangiogenic (Woolard, J. *et al.*, 2004). All VEGF-A isoforms differ significantly in their binding to cells and matrices (Park, J.E. *et al.*, 1993; Grunstein, J. *et al.*, 2000; Maes, C. *et al.*, 2002; Yu, J.L. *et al.*, 2002; Ruhrberg, C. 2003). VEGF-A¹⁶⁵, the most prominently expressed isoform in most normal tissues and in pathological angiogenesis, is a positively charged molecule, with an iso-electric point (pI) of 8.5, that binds to proteoglycans and to other negatively charged matrices (Ferrara, N. *et al.*, 1992); in fact, VEGF-A was originally purified on heparin affinity columns (Senger, D.R. *et al.*, 1983). VEGF-A¹⁸⁹ contains the peptides encoded by exon 6 and binds to heparin more strongly than VEGF-A¹⁶⁵, whereas VEGF-A¹²¹ lacks amino acids encoded by exons 6 and 7 of the VEGF gene and is acidic, so does not bind to heparin and diffuses freely in tissues. These different properties have consequences

for VEGF-A function *in vivo*. Developing blood vessels require both long- and short-range guidance cues for directional migration (Ruhrberg, C. 2003 and Eichmann, A. *et al.*, 2005). VEGF-A¹⁶⁵, which is both soluble and matrix bound, can supply both types of cues, but when only VEGF-A¹²¹ is present, ECs lack guidance over short distances. However, when only proteoglycan-bound VEGF-A¹⁸⁹ is present, there is a deficit in long-range guidance, and migrating ECs fail to branch appropriately. It is not surprising, therefore, that mice engineered to express only VEGF-A¹⁶⁴ isoform develop normally, whereas those engineered to express only VEGF-A¹²⁰ or VEGF-A¹⁸⁸ develop severe anomalies (Carmeliet, P. 1997 and Yu, J.L. *et al.*, 2002). Matrix VEGF-A may be inactive or ineffectual and in such circumstances proteases such as plasmin or metalloproteinases, which cleave the C-terminal portion of VEGF-A, are required to generate a biologically active peptide (Park, J.E. *et al.*, 1993).

PlGF (placental growth factor)

PlGF is another member of the VEGF family mainly expressed in the placenta and tumors. It forms disulphide-linked homodimers, but can also form heterodimers with VEGF. PlGF exists in four splice variants that all bind to VEGFR-1, but only PlGF-2 can also bind to heparin and to the co-receptors neuropilin-1 and 2, due to the insertion of a highly basic 21 amino acid sequence encoded by exon 6 of PlGF gene (Persico, M. G. *et al.*, 1999). PlGF knock out studies in mice indicate that PlGF is not crucial in embryonic vasculogenesis but affects angiogenesis and plasma extravasation under pathological conditions (Carmeliet, P. *et al.*, 2001). The bioavailability of VEGF and FGF-2 and therefore their capacity to induce angiogenesis might be controlled by PlGF-2. PlGF can induce angiogenesis *in vivo* to an extent comparable to VEGF (Bacillari *et al.*, 1998 and Lutun, A. *et al.*, 2002).

VEGF-B, C and D

VEGF-B is approximately 44% identical to VEGF-A; it exists in the two isoforms VEGF-B167 and VEGF-B186 and can form heterodimers with VEGF. VEGF-B binds only to VEGFR-1, inducing expression and increased activity of urokinase-type plasminogen activator (uPA) and plasminogen activator inhibitor 1 (PAI-1), suggesting a role in extracellular matrix (ECM) degradation and ECs migration. VEGF-C and VEGF-D form a subgroup within the VEGF family as they consist of a central VEGF homology domain with N- and C-terminal extensions that are cleaved during protein maturation and are not seen in the other VEGFs or PlGF. Both, VEGF-C and VEGF-D consist of non-covalent dimers and bind to VEGFR-2 and VEGFR-3. VEGF-C is mainly expressed during embryogenesis, whereas VEGF-D is also expressed in adult heart and skeletal muscle (Jussila, L. *et al.*, 2002).

VEGF-E

VEGF-E is a novel VEGF variant that was found in different strains of Orf viruses (Lyttle, D. J. *et al.*, 1994). Orf viruses belong to the parapox virus family and produce a dermatitis in sheep and humans. The lesion produced after infection show extensive proliferation of vascular ECs and dilatation of blood vessels. All this could be attributed to the presence of a gene encoding for a VEGF family member which was designated VEGF-E (Savory, L. J. *et al.*, 2000). The VEGF-E genes of more than 20 independent parapox virus variants show an extraordinary degree of sequence variation (Mercer, A. A. *et al.*, 2002). It was shown that VEGF-E variants exclusively bind to VEGFR-2 stimulating proliferation of human ECs *in vitro* and

vascularization of sheep skin *in vivo*, with potencies equivalent to VEGF-A¹⁶⁵ (Wise, L. M. *et al.*, 2003). VEGF-E family members show only ~25-35% amino acid identity with VEGF-A; interestingly, VEGF-E variants are most closely related to VEGF-A¹²¹, in fact there is no heparin-binding site comparable to exon 7 of VEGF-A¹⁶⁵.

Snake venom VEGFs (vammin and VR-1)

Vammin and VR-1 are two anti-HF antiserum reactive proteins isolated from the venoms of *Vipera ammodytes ammodytes* and *Daboia russelli russelli*, respectively. Each chain of vammin contains a total of 110 amino acid residues, while the number of residues in each chain of VR-1 is 109 (Yamazaki, Y. *et al.*, 2003). The primary structure of vammin and VR-1 shares identity with members of VEGF family, and the cysteine knot motif, a characteristic of the VEGF family proteins is completely conserved. Snake venom VEGFs (svVEGFs) specifically bind only to VEGFR-2 with essentially an equal affinity to VEGF-A¹⁶⁵. In fact, most of the important residues for KDR binding are highly conserved in vammin and VR-1, but some critical residues involved in Flt-1 binding are altered to other amino acid residues (Muller, Y.A. *et al.*, 1997 and Pan, B. *et al.*, 2002).

Regulation of VEGF-A expression

A number of factors regulate low-level expression of VEGF-A in normal tissues and induce its over-expression in pathological angiogenesis. One of these, hypoxia, acts stimulating both VEGF-A transcription and mRNA stabilization (Claffey, K.P. *et al.*, 1996 and Levy, A.P. *et al.*, 1997). VEGF-A transcription is under the control of hypoxia-inducible factor-1 (HIF-1), a heterodimeric protein transcription factor. One HIF-1 subunit, HIF-1 β , is constitutively expressed, while the other, HIF-1 α , is rapidly degraded under normoxic conditions through the ubiquitin pathway. In fact, in the presence of oxygen, proline 564 in the HIF-1 α subunit is hydroxylated by a prolyl hydroxylase (Ivan, M. *et al.*, 2001). Then, the product of von Hippel-Lindau tumor-suppressor gene, pVHL, which is the main regulator of HIF-1, attaches to hydroxylated proline within HIF-1. Once bound, pVHL mediates the ubiquitination of HIF-1 α , which is designated for destruction by the proteasome. Instead, in the absence of oxygen, stabilized by hypoxia, HIF-1 α translocates into the nucleus, dimerizes with HIF-1 β and the complex binds to and activates a hypoxia-responsive element in the VEGF-A promoter (Fukumura, D. *et al.*, 2001). HIF-1 also activates the transcription of other hypoxia-inducible genes such as PDGF, TGF- β and erythropoietin (George, D. J. *et al.*, 2003). Hypoxic regulation of VEGF-A expression has been demonstrated in many tumors; however, many other tumors express VEGF-A constitutively at high levels even under normoxic conditions. In these instances, regulation must be achieved by other means. One important mechanism is that mediated by oncogenes (i.e. *ras*) and tumor suppressor genes (i.e. *p53*). It is now clear that these genes, once thought to exert their effects solely on the growth properties of tumor cells, have an additional function, inducing VEGF-A expression and thereby angiogenesis (Rak, J. *et al.*, 2004 and Mukhopadhyay, D. *et al.*, 2004).

VEGF receptors

The biological activity of the VEGF family proteins is mediated through the binding to three types of receptor tyrosine kinases (RTKs), VEGFR-1, -2, -3. Activation of these receptors by VEGFs triggers the phosphorylation of a multitude of proteins that are active in signal transduction cascades (Matsumoto, T. *et al.*, 2001). Different members of the VEGF family show disparate receptor binding specificities and trigger several signaling pathways. Both VEGFR-1 and VEGFR-2 have seven immunoglobulin-like (Ig-like) domains in the extracellular portion, a single trans-membrane region and a consensus tyrosine kinase sequence that is interrupted by a kinase insert domain (Shibuya, M. *et al.*, 1990 and Terman, B.I. *et al.*, 1991). VEGFR-3 is a member of the same family of RTKs but is not a receptor for VEGF-A, binding instead to VEGF-C and VEGF-D (Karkkainen, M.J. *et al.*, 2002) In addition to these RTKs, VEGF interacts with a family of co-receptors, the neuropilins (Figure 6).

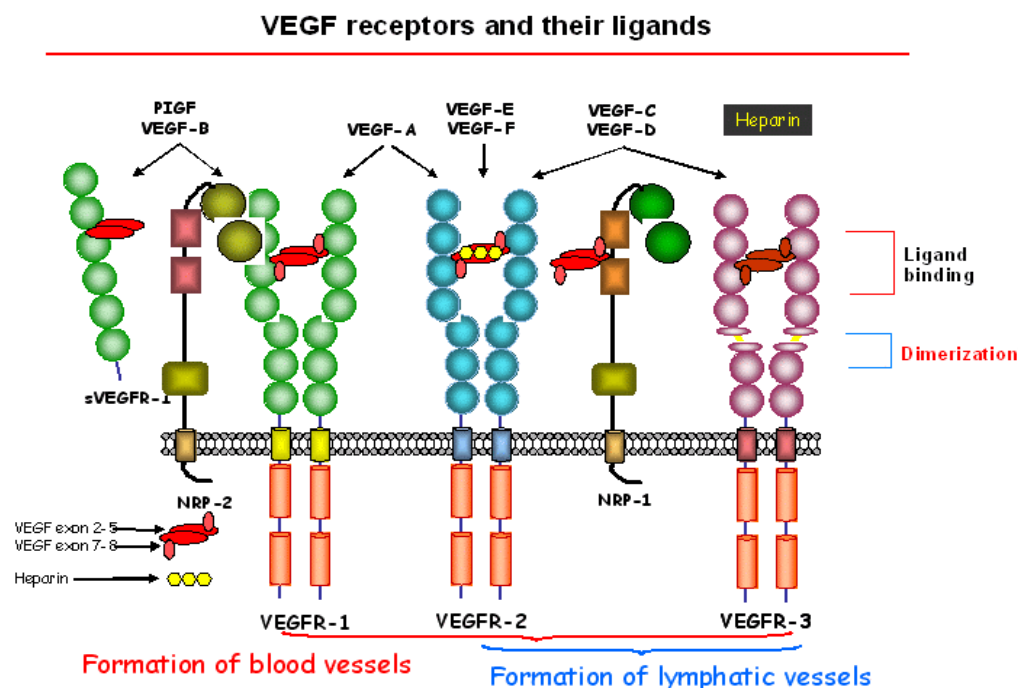


Figure 6_ Schematic diagram illustrating the receptor binding specificity of VEGF family members and VEGFR/NRP receptors. The VEGF family of ligands and their receptor-binding patterns are shown at the top. The activation of downstream signal transduction molecules leads to formation of blood and lymphatic vessels through several EC functions such as migration, vascular permeability, survival and proliferation.

VEGFR-1

VEGFR-1 [also known as Flt-1 (fms-like tyrosine kinase-1) receptor] is a 180 KDa high affinity receptor for VEGF-A, VEGF-B and PIGF with a Kd for VEGF-A of approximately 10-30 pM (Park, J.E. *et al.*, 1994 and Olofsson, B. *et al.*, 1998) (Figure 6). It is expressed in vascular ECs and a range of non-endothelial cells including haematopoietic stem cells (HSC), macrophages and monocytes. Although Flt-1 was

the first RTK to be identified as a VEGF receptor more than a decade ago (de Vries, C. *et al.*, 1992), the precise function of this molecule is still under debate. Recent evidences indicate that the functions and signaling properties of Flt-1 can be different depending on the developmental stage of the animal and the cell type. The mechanisms responsible for VEGFR-1 over-expression are not yet fully understood, but hypoxia, which stimulates the expression of VEGF may also upregulate Flt-1 by the HIF-1 dependent mechanism (Gerber, H.P. *et al.*, 1997). A natural soluble Flt-1 receptor (sFlt-1), produced by endothelial and tumor cells has been identified as an alternative splice product that contains the first six of the seven amino-terminal immunoglobulin-like domains of Flt-1 (Kendall, R. L. *et al.*, 1996). Soluble Flt-1 binds to VEGF with high affinity and forms a heterodimeric complex with VEGFR-2. sFlt-1 protein inhibits VEGF-induced endothelial cell proliferation, in fact, transfection of tumor cells with sFlt-1 resulted in reduced tumor growth and metastasis (Goldman, C.K. *et al.*, 1998). These results suggest that sFlt-1 acts as an angiogenesis inhibitor by sequestering VEGF and/or by acting as a dominant negative effector by forming heterodimers with trans-membrane VEGFR tyrosine kinases. Therefore, sFlt-1 and Flt-1 receptors have been demonstrated to suppress retinal neovascularization in a murine model of ischemic retinopathy (Aiello, L.P. *et al.*, 1995). Besides, gene targeting studies have demonstrated that Flt-1^{-/-} mice die *in utero* between days 8.5 and 9.5 due to obstruction of vessels by an overgrowth of ECs. In fact, ECs develop, but do not organize into vascular channels, indicating that, at least during early development, Flt-1 is a negative regulator of VEGF action (Fong, G.H. *et al.*, 1995 and Fong, G.H. *et al.*, 1999). It was determined that the VEGF (and PlGF) binding site is located primarily to the first three immunoglobulin-like domains of Flt-1 and that two Flt-1 receptors can be linked by a VEGF bridge. It was also determined that the fourth immunoglobulin-like loop contains a receptor dimerization domain (Wiesmann, C. *et al.*, 1997). Although Flt-1 receptor binds to VEGF with high affinity, it is a kinase-impaired receptor; Flt-1 is poorly tyrosine phosphorylated following ligand binding and expresses only weak kinase activity thereafter (Rahimi, N. 2006). The activation of Flt-1 receptor by VEGF in cells lacking VEGFR-2 does not induce cell proliferation, while activation of the VEGFR-2 receptor by VEGF in cells devoid of Flt-1 results in a mitogenic response (Waltenberger, J. *et al.*, 1994). However, activation of Flt-1 by VEGF does induce cell migration, a response that is also induced as a result of VEGFR-2 activation by VEGF (Yoshida, A *et al.*, 1996). These results indicate that the signal transduction cascades induced by VEGFR-1 and VEGFR-2 are somewhat different. It is not yet completely clear why VEGFR-1 does not induce cell proliferation in response to VEGF and VEGFR-2 does. MAP kinase was not activated by VEGF in cell expressing recombinant VEGFR-1 in two separate studies (Seetharam, L. *et al.*, 1995). So, it is possible that VEGFR-1 does not induce cell proliferation, because it does not activate MAP kinase.

VEGFR-2

VEGFR-2 [in human: KDR (kinase domain region) receptor, in mouse: Flk-1 (fetal liver kinase-1) receptor] is a 200-230 KDa high affinity receptor for VEGF-A, the processed forms of VEGF-C and -D, and VEGF-E (Figure 6). It is expressed in both vascular endothelial and lymphatic endothelial cells; its expression has also been demonstrated in several other cell types such as HSCs (Kato, O. *et al.*, 1995). KDR^{-/-} embryos die *in utero* between days 8.5 and 9.5, exhibiting defects in the

development of endothelial and haematopoietic precursors, indicating that the receptor is crucial for vascular development (Shalaby, F. *et al.*, 1995). VEGF-A binds to the second and third extracellular immunoglobulin-like domains of VEGFR-2 with a Kd of 75-125 pM; this affinity is lower than the affinity of VEGF-A for VEGFR-1, but VEGFR-2 is expressed in higher copy numbers than VEGFR-1 (Waltenberger, J. *et al.*, 1994). VEGFR-2 is considered to be the major mediator of several physiological and pathological effects of VEGF-A on ECs. These include proliferation and survival, migration and permeability. VEGFR-2, like many other receptors, induces proliferation through activation of the classical extracellular regulated kinase pathway, leading to gene transcription (Takahashi, T. *et al.*, 1999b). VEGFR-2 function is modulated through co-receptors such as heparan sulfated proteoglycans, which interact with certain VEGF isoforms and with VEGFR-2 (Gitay-Goren, H. *et al.*, 1992). The functional VEGF-VEGFR-2 complex includes neuropilins (Soker, S. *et al.*, 1998), which are ubiquitous membrane-bound molecules also implicated in axon guidance by binding to the semaphorin family members (Neufeld, G. *et al.*, 2002). Neuropilins might act by stabilizing the VEGF-VEGFR-2 complex. While hypoxia stimulates VEGF expression and upregulates Flt-1, it downregulates VEGFR-2 (Detmar, M. *et al.*, 1997).

VEGFR-3

VEGFR-3 (also known as Flt-4) is a 195 KDa high affinity receptor for VEGF-C and –D. Distinct features of VEGFR-3 includes cleavage during synthesis within the fifth extracellular immunoglobulin loop (Figure 6); the two regulating polypeptides are kept together by a disulfide bridge (Pajusola, K. *et al.*, 1994). There are two VEGFR-3 splice variants in humans, one short and one long. Mouse embryos lacking expression of VEGFR-3 die at embryonal day 9.5 due to deficient vessel remodeling. Larger vessels are disorganized, leading to fluid accumulation and cardiovascular failure (Dumont, D. J. *et al.*, 1998). These effects might be owing to a direct loss of VEGFR-3 function or because of an indirect effect caused by an increased availability of VEGF-C and –D for activation of VEGFR-2 (Hamada, K. *et al.*, 2000). In the adult, VEGFR-3 expression is detected primarily in lymphatic endothelial cells, where its activation induces proliferation, migration and survival.

Neuropilins

Neuropilins (NRP-1 and NRP-2) are two non-kinase VEGF receptors possessing a lower mass than either VEGFR-1 or VEGFR-2 (Gitay-Goren, H. *et al.*, 1992). These receptors are expressed not only on vascular endothelium, but also on many types of normal and tumor cells. They have long been known as receptors for the semaphorins/collapsin family of neuronal guidance mediators (Neufeld, G. *et al.*, 2002 and Eichmann, A. *et al.*, 2005). The neuropilins have a short intracellular domain; gene disruption studies indicate that neuropilin-1 is probably an important regulator of blood vessel development as mouse embryos lacking a functional neuropilin-1 gene die because their cardiovascular system fails to develop properly (Kitsukawa, T. *et al.*, 1997). Neuropilin-1 is a VEGF co-receptor (Figure 6); this assumption is supported by experiments showing that VEGFR-2 binds to VEGF more

efficiently in cells expressing NRP-1 (Soker, S. *et al.*, 1998). Neuropilin-1 is not able to function as a VEGFR-1 co-receptor (Migdal, M. *et al.*, 1998).

Structure and functional analysis of VEGF receptors Flt-1 and KDR

VEGF induces proliferation of ECs through the binding to two receptor tyrosine kinases, Flt-1 and KDR/Flk-1. Both receptors belong to the type III tyrosine kinases and are characterized by seven Ig-like loops within their extracellular domain and a split kinase domain within the cytoplasmic moiety (Fantl, W. *et al.*, 1993). Both VEGF receptors contain several N-glycosylation sites and the apparent molecular weights of the mature proteins suggest that both receptors are extensively glycosylated (de Vries, C. *et al.*, 1992 and Millauer, B. *et al.*, 1993). Since the dimeric structure of VEGF is a prerequisite of receptor activation, it can be speculated that one VEGF molecule bridges two receptors *via* two similar recognition sites (Herren, B. *et al.*, 1993). Characterization of VEGF binding to its receptors by mutational analysis of the ligand supports the assumption that VEGF has two contacts sites for its receptors (Keyt, B. A. *et al.*, 1996). Therefore, domain deletion studies on Flt-1 (Barleon, B. *et al.*, 1997) generating several soluble mutants of the extracellular domains of Flt-1, each consisting of a different stretch of Ig-like loops, have suggested that the recognition site for VEGF is located on the first three Ig-like loops, whereas dimerization is stabilized due to an additional domain located on Ig-like loop four. These studies have also demonstrated that glycosylation is not a prerequisite of high affinity binding of VEGF to Flt-1. Besides, deletion experiments on KDR have shown that only domains two and three are critical for ligand binding. KDR fourth Ig-like loop may also function as a dimerization domain, although there is no experimental data as yet to prove that assumption (Fuh, G. *et al.*, 1998). The receptor binding face of VEGF has been identified by mutagenesis studies (Muller, Y.A. *et al.*, 1997), revealing that the binding epitope for KDR contains two “hot spots”, each of which extends across the dimer interface. Charge-reversal mutagenesis has indicated that some of these same residues are also important for VEGF binding to Flt-1 (Keyt, B. A. *et al.*, 1996). The crystal structure to 1.7Å resolution of the complex between the receptor-binding domain of VEGF (VEGF₈₋₁₀₉) and Flt-1 domain 2 (Flt-1_{D2}) (Wiesmann, C. *et al.*, 1997) shows that an Flt-1 construct consisting of domain 2 binds to VEGF with affinity only about 60 fold weaker than the entire extracellular portion. The crystal structure of the complex is the first example of a cystine-knot growth factor bound to a domain of its receptor. So, the second domain of Flt-1 (Flt-1_{D2}) is necessary and sufficient for high affinity VEGF binding. The 1.7Å resolution crystal structure of Flt-1_{D2} bound to VEGF revealed that this domain is a member of the immunoglobulin superfamily, but has several unusual features, including a region near the N-terminus that bulges away from the domain rather than pairing with the neighboring β-strands (Wiesmann, C. *et al.*, 1997). Some of the residues in this region make contact with VEGF, raising the possibility that this bulge could be a consequence of VEGF binding and might not be present in the absence of ligand. But, in 1999, Starovasnik and co-workers reported the three-dimensional structure of Flt-1_{D2} in its uncomplexed form determined by NMR spectroscopy (Starovasnik, M. A. *et al.*, 1999). The solution structure is very similar to the previously reported VEGF-bound crystal structure and the N-terminal bulge is still present. ¹H-¹⁵N heteronuclear NOEs indicate that this region is flexible in solution. Thus, VEGF-binding is not

accompanied by significant structural change in Flt-1_{D2}, and the unusual structural features of Flt-1_{D2} are an intrinsic property of this domain (Starovasnik, M. A. *et al.*, 1999).

Structures of VEGF-A and PlGF

Structure of VEGF-A in the free form and bound to D2 of VEGFR-1

VEGF-A in the free form

The crystal structure of VEGF-A (residues 8-109, VEGF-A₈₋₁₀₉) shows a homodimer, organized in an antiparallel arrangement with a 2-fold axis perpendicular to the plane of the β -sheets (Figure 7A). The homodimer is covalently linked by 2 intermolecular disulfide bonds between C₅₁ and C₆₀. Each monomer consists of a central irregular antiparallel four-stranded β -sheet with the characteristic cysteine-knot motif. The knot is formed by two intra-molecular disulfide bonds C₅₇-C₁₀₂ and C₆₁-C₁₀₄ which form a ring structure through which a third disulfide bond C₂₆-C₆₈ passes and connects β 1 and the end of loop 2. The cysteine-knot motif is similar to that of the related growth factor PDGF. Each monomer contains three solvent-accessible loop regions connecting the individual β strands (Figure 7B). In addition, an α -helix is present at each N-terminus. While the monomer-monomer interface is predominantly formed by a hydrophobic core, the β -sheets are solvent exposed on both sides (Muller, Y.A. *et al.*, 1997 and Starovasnik, M. A. *et al.*, 1999).

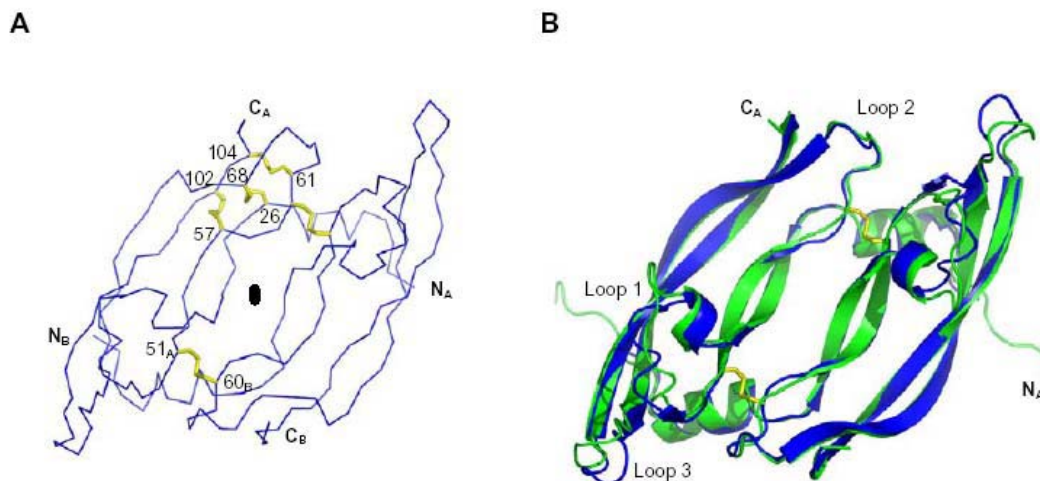


Figure 7_ Representation of VEGF-A (A) and superposition of VEGF-A and PlGF in the free form (B). Crystal structures from VEGF-A (green) and PlGF (blue) were superimposed according to the C α atoms. (A) Disulfide bonds forming the cysteine-knot in monomer A are highlighted in yellow. In addition the 2 intermolecular S-S bridges are shown. (B) Ribbon representation: the individual β -strands are connected by three loops (shown for monomer A of PlGF). While loop 2 adopts a very similar conformation in both proteins, loop 1 and 3 show slight deviations.

VEGF-A in complex with D2 of VEGFR-1

VEGF-A (VEGF₈₋₁₀₉) adopts in the bound state a very similar conformation as in the free form (Figures 8A and 8B). Slight differences are only observed for loop 1 (residues 42-48) and loop 3 (residues 85-89), which are also flexible in the free form (Wiesmann, C. *et al.*, 1997). Comparison of a NMR structure of the unbound D2 (corresponding to residues 129-229) with the crystal structure of the complex has shown that no structural changes are induced upon ligand binding (Starovasnik, M. A. *et al.*, 1999). Each D2 is in contact with both monomers of the ligand. The contact surface is divided into a hydrophobic (~65%) and hydrophilic part (~35%). The only direct polar interaction is a bidentate set of charge-mediated hydrogen bonds between side chains of R₂₂₄ of D2 and D₆₃ of VEGF-A. R₂₂₄ was shown to be critical for high affinity binding (Davis-Smyth, T. *et al.*, 1998). The remaining polar interactions in the interface are mediated by water molecules that bridge between the ligand and the receptor.

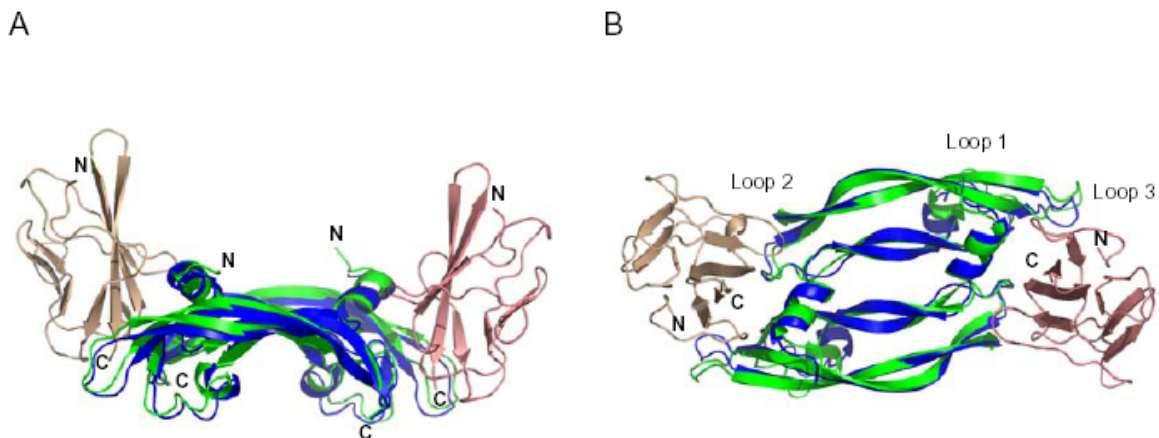


Figure 8_ Superposition of VEGF-A and PIGF with D2 of VEGFR-1

Crystal structures from VEGF-A (blue) and PIGF (green) in complex with D2 (wheat) of VEGFR-1 were superimposed according to the C α atoms. A) side view and B) top view. Indicated in B are the three loops for the upper monomer of the ligands showing that loop 1 and 3 interact with D2 on one site while loop 2 interacts with the opposing D2. Therefore each D2 is in contact with a set of loop 1-3 composed from the two monomers.

Structure of PIGF in the free form and bound to D2 of VEGFR-1

PIGF in the free form

PIGF (PIGF₈₋₁₀₉) and VEGF-A exhibit a remarkable structural similarity. Differences are observed in the N-terminal residues, in loop 1 and loop 3 (Iyer, S. *et al.*, 2001) (see Figure 7).

PIGF in complex with D2 of VEGFR-1

As drawn in Fig. 8A and 8B, the overall binding pattern of PIGF to D2 of Flt-1 resembles that of VEGF-A (Christinger, H. W. *et al.*, 2004). The interface is largely of hydrophobic nature with three direct polar interactions; one is the hydrogen bond formed between the side chain of Q₁₉ of PIGF and the main chain carbonyl of E₁₄₁ of

D2, and two charged interactions occur between D₆₂ of PIGF and R₂₂₄ of D2 from Flt-1. A *bis*-Tris propane molecule from the crystallization buffer is in contact with PIGF and D2 of VEGFR-1 near the interface. Presumably, this molecule greatly stabilizes the crystal packing arrangement. The PIGF dimer is slightly altered when bound to D2, mainly in the regions of loop 1 and loop 3 which results in a more open conformation of the ligand. Because of a dense crystal packing in this area it cannot be excluded that the observed interactions are influenced by packing effects.

VEGF and the induction of pathological angiogenesis: therapeutic implication and perspectives

VEGF plays a crucial role in physiological and pathological angiogenesis, including solid tumor growth and metastasis (Fidler, I. J. *et al.*, 1994 and Folkman, J. 1995) (Figure 9). As the formation of the normal blood vasculature, pathological angiogenesis is a multi-step process that requires ECs division, migration, organization into cords, lumen formation, acquisition of pericytes and degradation of old and synthesis of new basement membrane. In pathological angiogenesis VEGF-A induces the formation of several distinctly different types of new blood vessels with respect to organization, structure and function (Nagy, J. A. *et al.*, 2007). The importance of the function of VEGF suggests that blocking its function is a promising new therapeutic strategy for inhibiting angiogenesis and tumor growth. In the past years hybridization studies have shown that VEGF mRNA is upregulated in many human tumors (Dvorak, H.F. 1995 and Ferrara, N. *et al.*, 1997). Even though tumors do not exhibit an organized structure, from the point of view of angiogenesis a growing tumor may be viewed as a developing new organ. Angiogenesis is as essential for the growing tumor as it is for a developing organ such as the corpus luteum, since the delivery of blood-borne nutrients to the tumor cells is essential for their survival (Hanahan, D. *et al.*, 1996). When VEGF signaling is inhibited, tumor angiogenesis and, consequently, tumor growth are impaired (Kim, K.J. *et al.*, 1993 and Millauer, B. *et al.*, 1994). Besides, as VEGF binds to Flt-1 and KDR/Flk-1, thereby activating signal transduction and regulating physiological and pathological angiogenesis, to find an agent that inhibits binding between VEGF and its receptors may serve as a valuable antiangiogenic and antitumor agent. Many studies reported that antibodies to VEGF exert a potent inhibitory effect on the growth of several tumor cell lines in nude mice (Kim, K.J. *et al.*, 1993). Subsequently, many other tumor cell lines were found to be inhibited *in vivo* by this and other anti-VEGF treatments, including antisense oligonucleotides and antibodies to VEGFR-2 (Ferrara, N. *et al.*, 1997). Several studies have shown that combining anti-VEGF treatments with chemotherapy (Klement, G. *et al.*, 2000) or radiation therapy (Lee, C.G. *et al.*, 2000) results in a greater antitumor effect than either treatment alone. In the past years, clinical trials in cancer patients were carried out with several VEGF inhibitors, including a humanized monoclonal antibody to VEGF (rhuMab VEGF) (Presta, L.G. *et al.*, 1997), an anti-VEGFR-2 antibody (Prewett, M. *et al.*, 1999), small molecules inhibiting VEGFR-2 signal transduction (Wood, J.M. *et al.*, 2000) and a soluble VEGF receptor (Holash, J. 2002). Phase 2 clinical data provided initial evidence that rhuMab VEGF, in combination with conventional chemotherapy, resulted in increase in time to progression and even survival in patients with metastatic colorectal carcinoma (Kabbinavar, F. *et al.*, 2003). Phase 3 studies are currently under way to

confirm and fully assess the benefit of these anti-VEGF treatments in patients with advanced cancer. Another humanized anti-VEGF-A monoclonal antibody is Bevacizumab (trade name Avastin), approved, in February 2004, by the US Food and Drug Administration (FDA) in the United States for the treatment of metastatic colorectal cancer, in combination with chemotherapy regimens. This followed from a phase 3 study showing survival benefits (Hurwitz, H. *et al.*, 2004). The first VEGF receptor tyrosine kinase inhibitor, SU5416, have already been reported; it has produced certain clinical benefits in clinical trials involving patients suffering from advanced malignancies (Stopeck, A. *et al.*, 2002). Besides, Yasuij Ueda and co-workers, using a high throughput screening method, have found a small molecular compound, 5-[N-methyl-N-(4-octadecyloxyphenyl) acetyl] amino-2-methylthiobenzoic acid (VGA1155), that was selected for its potent inhibition of binding of VEGF to its receptors through association with KDR/Flk-1 (Ueda, Y. *et al.*, 2003).

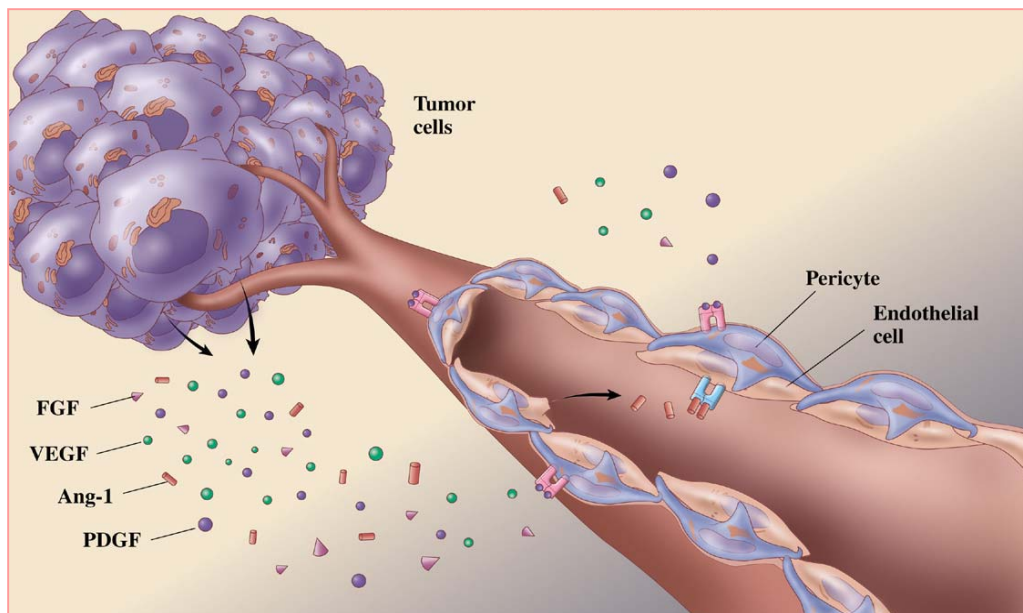


Figure 9_ Endothelial cell survival in pathological angiogenesis: tumor growth.

***De novo* engineered VEGF mimicking peptides**

The analysis of structural and mutagenesis data allowed to identify the residues involved in the binding of VEGF to its receptors. They are distributed over a discontinuous surface that includes residues from the N-terminal helix 17-25. KDR and Flt-1 share the VEGF binding region, in fact, five of the seven most important VEGF binding residues are present in both interfaces (Keyt, B. A. *et al.*, 1996; Muller, Y.A. *et al.*, 1997; Wiesmann, C. *et al.*, 1997). Many approaches have been pursued to modulate the VEGF-receptors interaction, and new molecular entities as peptides have been reported to bind to the extracellular region of the VEGF receptors. A large number of them show an antagonist activity and only few behave as agonists (D'Andrea, L. D. *et al.*, 2008, submitted). Remarkably, the peptides modulating the VEGF-receptors interaction are mainly derived by phage display libraries screening,

and only few examples of rational design approaches have been reported so far (Zilberberg, L. *et al.*, 2003). In our laboratory was designed, by a structure-based approach, a peptide of 15 amino acid residues, QK (Ac-KLTWQELYQLKYKGI-NH₂), reproducing the VEGF 17-25 helix region (D'Andrea, L. D. *et al.*, 2005). It is well known that peptide fragments spanning helices, turns and β -hairpins of natural proteins show little propensity, with very few exceptions, to reproduce their natural secondary structure under physiological conditions (De Grado, W. F. *et al.*, 1999). Nevertheless, the stabilization of suitable conformation in aqueous solutions is a condition to gain the binding of designed peptides to their targets. All data collected on the structural preferences of the QK peptide in aqueous solution strongly indicated that it mainly folds in helical conformation. In particular, the first indication derives from the CD spectrum, which is well confirmed by the H α chemical shift analysis and the NMR structure determination (D'Andrea, L. D. *et al.*, 2005). The basis of the QK helical fold seems to reside on the presence of amino acids with intrinsic helix preference and on the amphipathic nature of the helix. The biological properties of QK were tested performing an *in vitro* angiogenesis assay. In this assay QK induced the formation of newly formed connections in a dose-dependent manner and enhanced the VEGF response. These results demonstrate that QK binds to VEGF receptors *in vitro* and show that it is a potential agonist for angiogenesis. QK shows an unusual thermal stability (D'Andrea, L. D. *et al.*, 2005) and very recently it was showed to be active in gastric ulcer healing in rodents when it is administered either orally or systemically (Dudar G.K. *et al.*, 2008). Although QK was designed to bind to KDR and Flt-1, its agonist-like activity is surprising because receptor dimerization is necessary for receptor activation. QK is a small peptide and probably is unable to induce receptor dimerization by itself. To explain the activity of QK and its additive effects in presence of VEGF, we can speculate that the QK binding possibly induces a conformational change of the receptor that either triggers, in an unknown way, the dimerization or induces the receptor activation through a different uncharacterized mechanism that may not require dimerization. Further structural and biochemical studies are needed to address this issue. Anyway, these data are suggestive that either QK or improved analogues might fulfil the request for a safer pro-angiogenic drug. As therapeutic angiogenesis in cardiovascular conditions such as chronic ischemia or heart failure is sought as a promise of modern biotechnology, potential applications for QK are in the diagnostic field and in therapy of cardiovascular disease. An analogue of QK is MA, a peptide of 15 amino acid residues (Ac-KLTWMELYQLAYKGI-NH₂) synthesized and characterized by NMR in our laboratory. MA-VEGF competition binding assays were carried out by FACS indicating that the peptide is able to bind with specificity to VEGF receptors on ECs surface, inhibiting VEGF anti-apoptotic activity of over 80%, thus showing an antagonist activity with respect to VEGF (Del Gatto, A. PhD thesis, 2005).

The aim of the work

In the last years, much of the basic research in angiogenesis has been focused on detailing the steps involved in blood vessel growth and in identifying molecules that play a key role in regulating this process. This heightened analysis is due in part to the realization that aberrant angiogenesis is involved in relevant pathological conditions. Over the past decade, intensive efforts have been undertaken to inhibit

angiogenesis in cancer, ocular, joint or skin disorders or to develop therapeutic strategies to promote revascularization of ischemic tissues (Carmeliet, P. 2005). Despite some initial setbacks and negative clinical trial results, new angiogenic modulators have been developed in the last years. They mainly fall in three classes: antibodies, peptides and small molecules. Some of these molecules have been approved for treatment of cancer (Avastin), or are in phase 3 of clinical trials (Ferrara, N. 2005). Because of VEGF's predominant role in angiogenesis, inhibition of VEGF seems to be necessary but is probably insufficient to permanently halt this process in many disorders. Considering the anti-tumor therapy, the angiogenic inhibitors are, generally, more safe and less toxic than chemotherapeutic substances, but their exclusive administration as drugs in the treatment of tumors is rare. In fact, a wide range of different growth factors are involved in the stimulation of angiogenesis and the blockage of one factor alone might not be sufficient to inhibit the angiogenesis for a prolonged time period, as tumors could compensate by overproducing other growth factors (Carmeliet, P. 2005). Despite the problems involved, the anti-angiogenic therapy continues to arouse notable interest. In fact, angiogenic inhibitors, if used in conjunction with traditional therapies, have the ability to enhance therapeutic efficacy without significantly raising the risk of toxic side effects. In the process of angiogenesis, vascular endothelial growth factor binds to Flt-1 and KDR, thereby activating signal transduction and regulating physiological and pathological angiogenesis (Neufeld, G. 1999). Actually, of these receptors, are not well known structural data, done exception for the domain 2 of Flt-1 of which, in the literature, is reported the crystal structure complexed with VEGF and PlGF (Wiesmann, C. *et al.*, 1997 and Christinger, H. W. *et al.*, 2004) and the three-dimensional, uncomplexed form determined by NMR spectroscopy (Starovasnik, M. A. *et al.*, 1999). The aim of this PhD thesis is the expression and characterization of the extracellular domains of VEGF receptors, in order to find new compounds of biotechnology interest for modulating the angiogenesis process. Because the angiogenic response strictly depends on VEGF and on functions and signaling properties of its receptors, we centered our efforts on the characterization of the extracellular portion of Flt-1 (VEGFR-1) and KDR (VEGFR-2) receptors. In particular, we expressed some of their extracellular Ig-like domains, focusing the attention on their structural characterization *via* NMR and on their employment in the identification and improvement of new organic or peptide-based molecules targeting the VEGF receptors. In fact, once expressed and purified Flt-1_{D2}, we used the second domain of VEGFR-1 for interaction studies with QK (VEGF agonist) and MA (VEGF antagonist) peptides (D'Andrea, L. D. *et al.*, 2005 and Del Gatto, A. PhD thesis, 2005), in order to better understand their biological behavior in angiogenesis process. Therefore, the recombinant Flt-1_{D2} was employed for the screening of a library of organic molecules by drug discovery analysis, in order to find other new class of VEGF receptor binders.

Materials and Methods

Strains, enzymes and reagents

Reagents used for preparation of buffers and growth media of *Escherichia coli* and the reagents for polyacrylamide gels electrophoresis (Acrylamide, APS, TEMED, SDS, Tris, Glycine) were supplied by Sigma Aldrich, Euroclone, Applichem and ICN Biomedicals. The molecular weight markers for proteins were from Sigma Aldrich. The restriction enzymes and the “modification enzymes” (calf intestine phosphatase, T4 DNA ligase and T4 DNA polynucleotide kinase) were supplied by New England Biolabs (NEB) and the molecular weight markers for nucleic acids were supplied by NEB and Roche. The *Pfu Turbo* polymerase (2.5 U/μL) was supplied by Stratagene, while *Taq* DNA polymerase (5 U/μL) was from NEB. The synthesis of the oligonucleotides was committed at Sigma-Genosys; pETM11 and pETM20 *E. coli* expression plasmids were supplied by Novagen, while the expression vector pPROEXHTa was supplied by Invitrogen. *E. coli* TOP F'10 strain, used for cloning, was supplied by Invitrogen; *E. coli* BL21 *Codon Plus* (DE3) RIL cells, used for overexpression, were supplied by Stratagene. BL21(DE3), BL21(DE3) STAR and JM101 strains, also used for expression, were supplied by Invitrogen while Rosetta GAMI (DE3) were from Novagen. Complete Protease Inhibitor Cocktail Tablets were supplied by Roche and used as a mixture of protease inhibitors, according to manufacturer's instruction. Ethanol, isopropilic alcohol and acetic acid were supplied by J.T. Baker. TFA was from Fluka. Purity and identity of protein samples were assessed by liquid chromatography mass spectrometry (LC-MS) performed on a Thermo Electron Corporation mass spectrometer equipped with an ESI source. The analysis of proteins was carried out on a C₄ column, using a method (referred to as “method A”) developed at 0.2 mL/min with a linear gradient of 0.1% aqueous TFA-0.1%TFA in CH₃CN, from 5% to 70% for 30 min.

Antibiotics

Ampicillin (supplied by Sigma Aldrich as ampicillin sodium salt) and kanamycin (supplied by Sigma Aldrich as kanamycin sulphate) were solubilized in deionized water at a concentration of 1000X, filter sterilized and stored at -20°C until use. Ampicillin was used at a concentration of 100 μg/mL and kanamycin was used at a concentration of 50 μg/mL in both solid and liquid media. Chloramphenicol and tetracycline were solubilized in ethanol 96% and used at a concentration of 33 μg/mL and 12.5 μg/mL, respectively.

E. coli cells transformation techniques

Preparation of *E. coli* TOP F'10 cells and transformation by electroporation

2.5 mL of an overnight culture of *E. coli* TOP F'10 cells were inoculated into 250 mL of LB medium. The cells were grown up to mid-log phase (0.6 OD₆₀₀) at 37°C, stored on ice for 20-30 min and then harvested by centrifugation (6000 rpm, 10 min, 4°C). The pellet was washed in 250 mL of sterile water. After the second centrifugation the cells were washed in 125 mL of sterile water. The third washing was performed in 5 mL 10% glycerol; the cells were then harvested by centrifugation and the pellet was

resuspended in 750 μL of 10% glycerol. Aliquots of 10^{10} cells/mL (40 μL) were mixed with 1 μL of the DNA ligase reaction, incubated for 1 min on ice and transferred into chilled plastic cuvettes with an electrode gap of 0.2 cm (M-Medical). High voltage electroporation (25 μF) was performed with a Bio-Rad Gene Pulser Xcell™ at a field strength of 2.5 kV/cm and 200 Ohm. A shock pulse was applied to competent cells producing pulse length of ~5.0-5.5 ms. Immediately after electroporation cell mixtures were diluted to 1 mL with LB medium and incubated for ~1 h at 37°C under shaking. The cells were then plated onto selective solid medium supplemented with 100 $\mu\text{g}/\text{mL}$ ampicillin or 50 $\mu\text{g}/\text{mL}$ kanamycin to isolate the recombinant clones. Single clones were inoculated in 5 mL LB medium with the same antibiotics and grown overnight at 37°C under shaking. Finally, were harvested by centrifugation (13.000 rpm, 2 min, 4°C) and processed to extract plasmidic DNA by using the *QIAprep Spin Miniprep Kit* or the *QIAGEN plasmid Maxi Kit* (both supplied by Qiagen).

Preparation of *E. coli* BL21 (DE3) competent cells and transformation by heat shock

Single clones of BL21 (DE3) *E. coli* strains, grown at 37°C in LB agar, were inoculated into 2.5 mL of LB medium and incubated overnight at 37°C on a shaker. The cells were inoculated into 250 mL of LB medium and the culture was grown up to mid-log phase (0.6 OD₆₀₀) at 37°C, stored on ice for 20-30 min and then harvested by centrifugation (6000 rpm, 10 min, 4°C). The pellet was washed in 125 mL of cold 50 mM CaCl₂ and stored on ice for 30 min. Successively, the cells were harvested by centrifugation and the pellet resuspended in 16 mL of cold 50 mM CaCl₂. Aliquots of 200 μL of competent cells were mixed with 50 ng of plasmidic DNA and stored on ice for ~30 min. The cells mixtures were transferred at 42°C for 90 sec, on ice for 2 min (heat shock) and then diluted to 1 mL with LB medium. An incubation for ~1 h at 37°C under shaking was performed before plating the cells onto selective solid medium supplemented with the opportune antibiotics, depending on the strain.

Proteins analyses

Determination of the protein concentration

The concentration of the proteins in solution was determined according to the Bradford's method (Bradford, 1976). The Coomassie Brilliant (Bio-Rad) reagent was added to the samples and the absorbance at 595 nm was monitored. A solution of 1 $\mu\text{g}/\mu\text{L}$ of bovine serum albumin (BSA) was used as standard. Protein concentration was also measured by UV spectroscopy, reading the tryptophan absorbance at 280 nm, using a Jasco V-550 UV-VIS spectrophotometer, in an 1 cm quartz cell.

Electrophoretic analysis of proteins (SDS-PAGE)

The electrophoresis on polyacrylamide gel in the presence of SDS (SDS-PAGE) was performed according to Laemmli's protocol (Laemmli, 1970). The samples were denaturized at 100°C for 10 min in 1% SDS (Applichem), 5% β -mercaptoethanol (Sigma), 0.001% bromophenol blue (ICN Biomedicals) and 10% glycerol (Applichem). The samples were then loaded on a 15% or 18% polyacrylamide gel and electrophoresed in 0.025 M Tris-HCl, 0.2 M glycine pH 8.3 and 0.1% SDS. The electrophoresis was performed at 25 mA for ~1.5 hours. The proteins were then revealed by Coomassie Brilliant-Blue (Applichem) staining; the gel was submerged in the staining solution (0.1% Coomassie Brilliant-Blue R250, 25% isopropilic alcohol

and 10% acetic acid) for ~30 min with gentle agitation. The gel was washed in a solution containing 30% ethanol and 10% acetic acid to remove the excess of Coomassie and then stored in 10% acetic acid. Alternatively, the proteins were transferred by electro-blotting from gel to a polyvinylidene fluoride (PVDF) membrane as described in the paragraph "Western blot analysis". For native PAGE the samples were not denaturated at 100°C but loaded on a 10% polyacrylamide gel in 0.001% bromophenol blue and 10% glycerol and electrophoresed in Tris-glycine buffer without SDS. The electrophoresis was performed at 15 mA for ~2 hours, after a gel pre-run of 30 min. The proteins were then revealed by Coomassie Brilliant-Blue staining, as described above.

Bioinformatic tools

Protein sequences were processed using the pI/Mw tool available on the ExPASy Server (<http://www.expasy.ch>), in *proteomics and sequence analysis tools* section. Compute pI/Mw is a tool which allows the computation of the theoretical pI (isoelectric point) and Mw (molecular weight) for a list of UniProt Knowledgebase (Swiss-Prot or TrEMBL) entries or for user entered sequences.

Domains cloning of human KDR and Flt-1 receptors

The genes corresponding to the extracellular domains of KDR and Flt-1 receptors were amplified by PCR from NIH-3T3 cDNA of the entire receptors (kindly provided by Dr. Nicola Normanno).

Cloning of 1-3, 2-3, 1-2 and 2 KDR receptor domains

The amplification of domains 1, 2, 3 of KDR was performed by using the following couples of primers:

kdr_{D1-3} gene (residues 1-335, Fuh *et al.*, 1998)

Forward: 5'- CGGGATCCGAAAGACATACTTACAATTAAGGCTAA -3'

Reverse: 5'- CCGCTCGAGCTATCATCCAAAAGCAACAAAAGGTTTTTCATG-3'

kdr_{D2-3} gene (residues 120-335, Fuh *et al.*, 1998)

Forward: 5'- CGGGATCCGTACAGATCTCCATTTATTGCTTCTGTT -3'

Reverse: 5'- CCGCTCGAGCTATCATCCAAAAGCAACAAAAGGTTTTTCATG -3'

In this case, the *reverse* primer was the same used for the amplification of *kdr_{D1-3}* gene.

kdr_{D1-2} gene (residues 1-222, Fuh *et al.*, 1998)

Forward: 5'- CGGGATCCGAAAGACATACTTACAATTAAGGCTAA -3'

Reverse: 5'- CCGCTCGAGCTATCACCTATAACCCTACAACGACA ACTATGTA -3'

In this case, the *forward* primer was the same used for the amplification of *kdr_{D1-3}* gene. Finally, the PCR reaction necessary to obtain domain 2 of KDR was performed with the following primers:

kdr_{D2} gene (residues 120-222, Fuh *et al.*, 1998)

Forward: 5'- CGGGATCCGTACAGATCTCCATTTATTGCTTCTGTGTT -3'

Reverse: 5'- CCGCTCGAGCTATCACCTATAACCCTACAACGACAACACTATGTA -3'.

The *forward* primers indicated above contained the *Bam*HI restriction site, while the *reverse* primers were designed with the *Xho*I restriction site (underlined in the sequences) positioned downstream to two stop-translation codons (in bold in the sequences). This cloning strategy was used to obtain the gene products fused (at the N-terminal) with the 6xHistidine-tag of the pPROEXHTa expression vector (see below, Figure 10). The pPROEXHTa plasmid is designed to allow inducible, high level intracellular expression of genes; it contains a *tac* promoter for chemical induction, a multiple cloning site (MCS), an internal *lac Iq* gene compatible to any *E. coli* host and a TEV protease recognition site for cleaving the fusion protein.

All amplification reactions were performed in a final volume of 100 μ L, using 50 ng of template DNA. The reaction mixture contained the 2 primers (0.25 μ M each), dNTPs (0.25 mM each) and the *Pfu turbo* polymerase (5U) with its buffer 1x. PCR was performed using an *Eppendorf Mastercycler personal* apparatus, following the procedure indicated below:

- | | |
|-----------------------------|---|
| ✓ Initial denaturation step | 3 min at 95°C |
| ✓ Denaturation (step 2) | 1 min at 95°C |
| ✓ Annealing (step 3) | 1 min at the convenient temperature for each gene amplified |
| ✓ Elongation (step 4) | 1 min at 72°C |
- for 30 cycles, from step 2.

All amplification products were analyzed by 1% agarose (Euroclone) gel electrophoresis performed in TAE buffer (18.6 g/L EDTA, 242 g/L Tris base. Add acetic acid until pH 7.8). PCR products were purified by using the *QIAquick PCR Purification Kit* (Qiagen), and digested with *Bam*HI (20 U/ μ L) and *Xho*I (20 U/ μ L) restriction enzymes. Each amplified fragment (1 μ g) was digested with 3U of restriction enzymes for 2 hours at 37°C in a buffer containing 50 mM NaCl, 10 mM Tris-HCl, 10 mM MgCl₂, 1 mM DTT pH 7.9 supplemented with BSA 100 μ g/mL. Following the digestion, each fragment was cloned into the corresponding sites of the pPROEXHTa expression vector, downstream to the His-tag sequence. To this purpose, the expression vector was previously digested with the same restriction enzymes (3 U/ μ g), and treated with calf intestine phosphatase (CIP, 10U) (NEB) for 30 min at 37°C. CIP enzyme (10 U/ μ L) was then inactivated at 75°C for 10 min. After digestion, PCR amplifications were purified by *QIAquick PCR Purification Kit* (Qiagen), while the *Bam*HI/*Xho*I pPROEXHTa was purified by *QIAquick Gel Extraction Kit* (Qiagen). For ligation reactions was used a 1:3 molar ratio (vector/insert DNA) for shorter fragments and a 1:6 molar ratio for the longer ones. The reactions were performed using 20 U/ μ g DNA of the T4 DNA Ligase (400 U/ μ L), in a final volume of 10 μ L, for 3 hours at RT. The identity of the inserts in the resulting recombinant plasmids was confirmed by DNA sequencing (MWG-Biotech). *E. coli* TOP F'10 strain was used for cloning. *kdr_{D2}* gene was cloned also in pETM11 and pETM20 expression vectors (see Figures 11, 12). The primers used for amplification of the gene in these systems were:

Forward: 5'- GCCATGGCGTACAGATCTCCATTTATTGCT -3'

Reverse: 5'- CCGCTCGAGCTATCACCTATAACCCTACAACGACA ACTATGTA -3'

where the *reverse* primer was the same used for the amplification of *kdr*_{D1-2} gene, while the *forward* primer contained the *Nco*I restriction site. pETM11 and pETM20 expression vectors contain a *T7* promoter for chemical induction and overexpression of recombinant proteins, a multiple cloning site (MCS) and a TEV protease recognition site for cleaving the fusion protein. pETM11 contains a 6xHistidine-tag, while the pETM20 system contains a 6xHistidine-TrxA fusion tag for the increase of the solubility of gene products.

***kdr*_{D2} gene mutagenesis**

The C₁₆₁ residue of domain 2 was mutated in Alanine by using the QuikChange Site Directed Mutagenesis Kit (Stratagene). The primers employed for mutagenesis PCR reaction are reported below:

Forward: 5'- AACGTGTCACTTGCTGCAAGATACCCA -3'

Reverse: 5'- TGGGTATCTTGCAGCAAGTGACACGTT -3'

Codons corresponding to the mutated amino acid are underlined in primers sequences. The recombinant construct pETM11-*kdr*_{D2} was used as template. The PCR reaction was performed, according to the Kit instructions, using an *Eppendorf Mastercycler personal* apparatus, following the procedure indicated below:

- ✓ Initial denaturation step 1 min at 95°C
- ✓ Denaturation (step 2) 50 sec at 95°C
- ✓ Annealing (step 3) 50 sec at 58°C
- ✓ Elongation (step 4) 12 min at 68°C

for 16 cycles from step 2.

XL1-Blue supercompetent cells (supplied by the mutagenesis Kit) were used for the transformation of the circular, nicked dsDNA (the methylated, non-mutated, parental DNA from mutagenesis PCR was first digested, for 2 hours at 37°C, with the restriction enzyme *Dpn*I-10 U/μL). The identity of the mutagenic insert was confirmed by DNA sequencing.

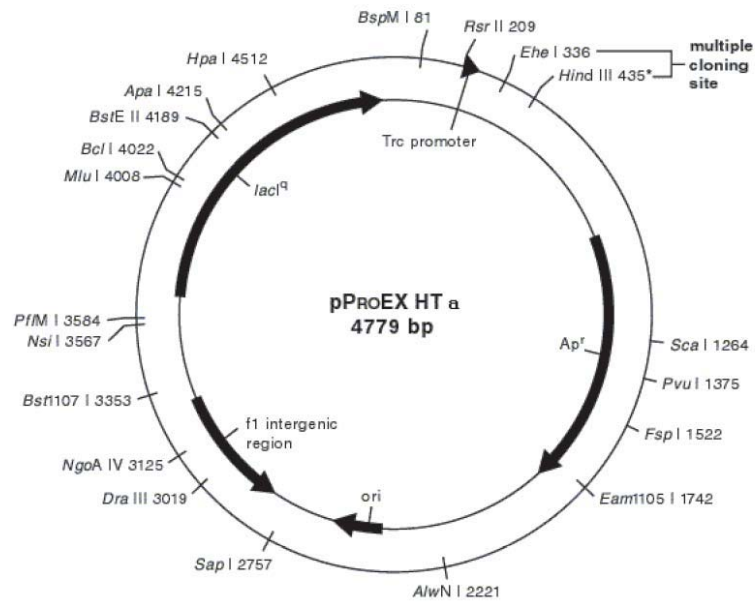


Fig.10_ Structural organization of pPROEXHTa expression vector (Invitrogen).

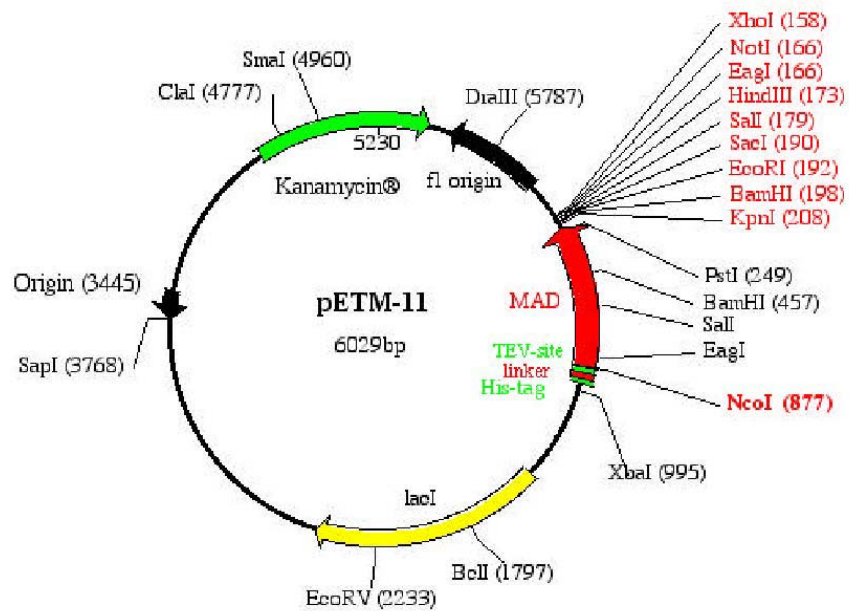


Fig.11_ Structural organization of pETM11 expression vector (Novagen).

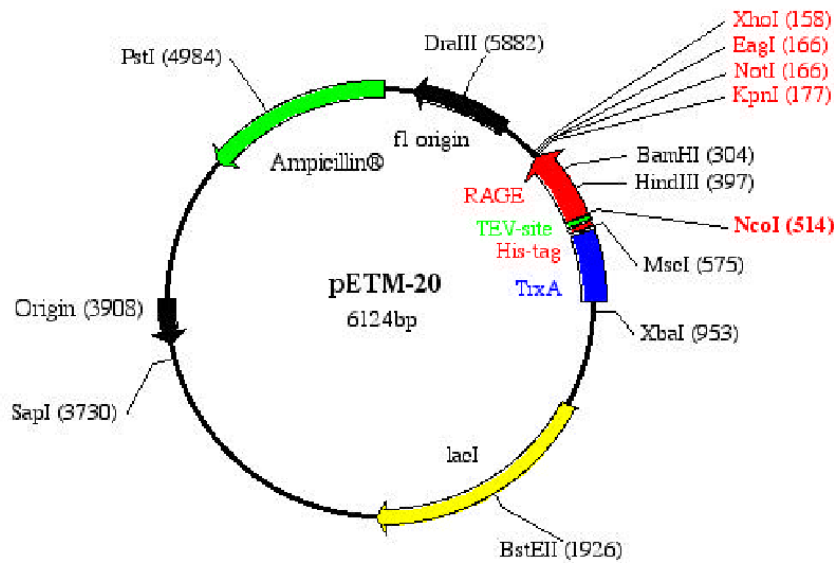


Fig.12_ Structural organization of pETM20 expression vector (Novagen).

Cloning of 1-4, 2-4, 2-3 and 2 Flt-1 receptor domains

Domains 1, 2, 3, 4 of Flt-1 receptor gene were amplified by PCR using the following couples of primers:

*flt-1*_{D1-4} gene (residues 27-428, Wiesmann *et al.*, 1998)

Forward: 5'- GCCATGGCGTCAAAATTAAGATCCTGAA -3'

Reverse: 5'- GTGCTCGAGCTATCAGGGTTTCACATTGACAAT -3'

*flt-1*_{D2-4} gene (residues 129-428, Wiesmann *et al.*, 1998)

Forward: 5'- GCCATGGCGAGTGATACAGGTAGACCTTTC -3'

Reverse: 5'- GTGCTCGAGCTATCAGGGTTTCACATTGACAAT -3'

*flt-1*_{D2-3} gene (residues 129-334, Wiesmann *et al.*, 1998)

Forward: 5'- GCCATGGCGAGTGATACAGGTAGACCTTTC -3'

Reverse: 5'- GTGCTCGAGCTATCAGATGAATGCTTTATCATA -3'

*flt-1*_{D2} gene (residues 129-229, Wiesmann *et al.*, 1998)

Forward: 5'- GCCATGGCGAGTGATACAGGTAGACCTTTC -3'

Reverse: 5'- GTGCTCGAGCTATCAGATTGTATTGGTTTGTTCG -3'.

The *forward* primers indicated above contained the *NcoI* restriction site, while the *reverse* primers were designed with the *XhoI* restriction site (underlined in the sequences). All amplification reactions of the genes were performed as described above, in a final volume of 100 μ L, using 50 ng of template DNA. The reaction mixture contained the 2 primers (10 μ M each), dNTPs (0.25 mM each) and the *Pfu turbo* polymerase (5U) with its buffer 1x. PCR was performed using the same

apparatus, following the procedure indicated above for KDR receptor domains. *flt-1_{D2}* gene was also cloned in the pETM20 expression vector using the same primers employed in the cloning of the gene in pETM11. PCR products were purified and digested following the same procedure described above for *kdr* genes.

Expression and purification of recombinant KDR and Flt-1 extracellular domains

Expression

After a first screening of small expression cultures, performed using different strains, temperatures and IPTG concentration, all the recombinant constructs obtained with cloning of Ig-like KDR and Flt-1 receptors domains in pPROEXHTa, pETM11 and pETM20 were transferred into *E. coli* BL21 *Codon Plus* (DE3) RIL cells. In fact, in all used conditions and strains, the proteins of interest were expressed in inclusion bodies, so we selected *E. coli* BL21 *Codon Plus* (DE3) RIL cells that assured a better expression of all proteins. Single clones of RIL strain, previously transformed with each recombinant expression vector and grown at 37°C on LB agar containing antibiotics, were inoculated in 10 mL of LB medium, containing the same antibiotics. The overnight cultures were inoculated into 1L of prewarmed LB medium supplemented with antibiotics: 100 µg/mL ampicillin (for pPROEXHTa and pETM20 recombinant vectors) or 50 µg/mL kanamycin (for pETM11 recombinant vectors) and 33 µg/mL chloramphenicol. Cultures were grown at 37°C under shaking until they reached the mid-log phase (0.7/0.8 OD₆₀₀) then, they were induced with 0.7 mM IPTG (Inalco). After 3-4 hours the cells were harvested by centrifugation (6000 rpm, 15 min, 4°C). Cell pellets were resuspended in 50 mM Tris-HCl, pH 8 containing protease inhibitors, to avoid proteins degradation, and the suspension was sonicated for 6 min, by using a Misonix Sonicator 3000 apparatus with a micro tip probe and an impulse output of 1.5/2 (=9/12 Watt). Bacterial lysates were then centrifuged (15000 rpm, 30 min, 4°C) and the supernatant (soluble fraction) and the pellet, obtained from each sample, were loaded on a 15% or 18% polyacrylamide gel.

Batch purification of 6xHis-tagged proteins under denaturing conditions

The expression of each recombinant plasmid produced insoluble proteins, so they were solubilized from inclusion bodies using a lysis buffer containing 50 mM Tris-HCl, pH 8, 10 mM imidazole, 8 M urea. The cleared lysate containing the His-tagged proteins in 8 M urea was added to 50% Ni²⁺-NTA agarose slurry resin (Qiagen) for the affinity chromatography purification. The binding capacity of Ni²⁺-NTA resins is between 5-10 mg/mL for 6xHis-tagged proteins. Before loading the lysate, the resin was extensively washed with water and finally equilibrated in the lysis buffer. The lysate was then loaded in presence of 10 mM imidazole and 100 mM NaCl to avoid non-specific binding of *E. coli* contaminants and the column was gently shaken for 45 min-1h. Then, the flow-through (F.T.), containing all unbound proteins, was collected and the resin was washed three times with the lysis buffer containing 100 mM NaCl, and finally the His-tagged proteins were eluted with high concentrations of imidazole (250/300 mM). All the proteins expressing KDR extracellular domains and Flt-1_{D1-4}, Flt-1_{D2-4}, Flt-1_{D2-3} were eluted and then refolded by step dialysis to remove urea. Only Flt-1_{D2} was subjected to an "on column" refolding protocol. Once loaded the lysate, collected the flow-through and wash fractions, the bound protein was refolded by equilibrating the column in buffers with decreasing concentrations of urea. All

fractions eluted from the resin (flow-through, washes and elutions) were analyzed on SDS–PAGE gels and stained with Coomassie Brilliant Blue R-250. Protein samples were dialyzed by using Spectra/Por membranes with the appropriate MWCO.

Expression and refolding of ¹⁵N-labeled recombinant Flt-1_{D2} for NMR studies

A single clone of JM101 strain was cultured for 3 h at 37°C in 5 mL of LB medium without antibiotics. The cells were then inoculated in M9 medium (see composition in tables 2 and 3), containing ¹⁵NH₄Cl (1g/L) as the sole nitrogen source, and grown overnight at 37°C. The harvested cells were lysed with 37% HCl (100°C for 8h) to obtain a mixture of single ¹⁵N labeled amino acids then used to enrich M9 medium for the expression of Flt-1_{D2} in *E. coli* BL21 *Codon Plus* (DE3) RIL strain previously transformed with pETM11-*flt-1*_{D2} recombinant expression vector. The expression, refolding and protein purification were performed as described for the unlabeled protein.

M9 salt solution 10X	100 mL
100 mM MgSO ₄	10 mL
10 mM CaCl ₂	10 mL
100 mM thiamine-HCl	10 mL
20% glucose	10 mL
sterile ddH ₂ O	860 mL
Total volume	1 L

Table 2: M9 medium composition. 100 mM MgSO₄, 10 mM CaCl₂, 100 mM thiamine-HCl and 20% glucose were filter sterilized before use.

Na ₂ HPO ₄	6 g
KH ₂ PO ₄	3 g
NaCl	0.5 g
¹⁵ NH ₄ Cl	1 g
ddH ₂ O to	100 mL
Total volume	100 mL

Table 3: M9 salt solution 10X composition. Autoclave before use.

Western blot analysis

After gel electrophoresis, proteins were transferred to a polyvinylidene fluoride (PVDF) membrane (Immobilon-P, Transfer Membrane, Millipore) in Transferring Buffer (25 mM Tris-HCl, pH 8.0, 190 mM Glycine and 10% methilic alcohol) at 4°C overnight, using a 25 V electric field. The PVDF membrane was submerged in methilic alcohol for 2 min before using, to eliminate the hydrophobic properties, washed in H₂O for 5 min and equilibrated in Transferring Buffer for 5 min. After

overnight electro-blotting, membrane was stained with Ponceau Red to verify proteins transferring and incubated in the blocking solution (5% BSA in PBS buffer, containing 0.05% Tween 20) at room temperature for 1 hour. It was washed with PBS buffer (137 mM NaCl, 2.7 mM KCl, 10 mM Na₂HPO₄, 2 mM KH₂PO₄ pH 7.4), containing 0.05% Tween 20, and incubated with mouse anti-His monoclonal antibody (supplied by Sigma Aldrich) dilution (1:6000) at room temperature for 1 hour. Successively, membrane was washed with PBS buffer and incubated on a shaker, for 1 hour at room temperature, with horseradish peroxidase-conjugated anti-mouse antibody (supplied by Pierce) dilution (1:10000) as the secondary antibody. Membrane was finally washed with PBS buffer. The detection of immunopositive species by enzyme-linked chemiluminescence (enhanced chemiluminescence: ECL) was performed according to the manufacturer's instructions (Super Signal[®] West Pico Chemiluminescent Substrate, Pierce), using a Chemi doc XRS apparatus (Bio-Rad).

TEV digestion of 6xHis-tagged proteins

All 6xHis-tagged proteins, after purification by affinity chromatography and on column/step dialysis refolding, were dialyzed overnight against TEV buffer (50 mM Tris-HCl, pH 7.0/8.0 in redox buffer containing 3 mM glutathione/0.3 mM oxidized glutathione) at 20°C. To protein substrates was added TEV protease, using a molar ratio (protease:substrate) of 1:35 and the cleavage was allowed to proceed overnight at 20°C. Cleaved products were analyzed by 18% polyacrylamide gel electrophoresis performed in Laemmli buffer, then, mixture was loaded onto a Ni²⁺-NTA affinity column equilibrated in binding buffer (the same employed for digestion reaction) containing 10 mM imidazole; the proteins without His-tag were collected in the flow-through, while His-tag and TEV protease remained bound to the column. TEV protease was expressed and purified in our laboratory, after transforming the BL21 *pLysisS* cells (Invitrogen) with the pET24a-TEV recombinant vector kindly provided by Dr. Nina Dathan. Purity and identity of Flt-1_{D2} before and after the cleavage by TEV protease were assessed by liquid chromatography mass spectrometry (LC-MS), using a Phenomenex Jupiter C₄ column (250x2.00 mm, 5 μm, 300 Å) and the method **A** described in “stains, enzymes and reagents” paragraph.

Flt-1_{D2} alkylation by Iodoacetamide and trypsin digestion

Cleaved and purified Flt-1_{D2} was dialyzed overnight, at 20°C, against 50 mM Tris-HCl, pH 7.0 containing NaCl 100 mM and concentrated until 0.3 mM by using the Amicon Ultra system (5000 MWCO, Millipore). Then, the protein was alkylated by iodoacetamide to estimate the oxidation state of the cysteines present in its sequence. In fact, Flt-1_{D2}, as attested by structural data, has two cysteine residues involved in the formation of a disulfide bridge (Wiesmann, C. *et al.*, 1997). Flt-1_{D2} was diluted until 10 μM in AMBIC buffer 100 mM, pH 8.0; then, iodoacetamide, dissolved in AMBIC buffer 100 mM, pH 8.0 to a final concentration of 55 mM, was added for the alkylation reaction. Sample was allowed to mix by vortexing and incubated for 30 min at RT, in the dark. As positive control, Flt-1_{D2} was first reduced with DTT 10 mM and then alkylated by iodoacetamide. The reduction reaction was allowed to proceed 45 min at 60°C in a heating block. Purity and identity of both alkylated and reduced-alkylated proteins were assessed by LC-MS, using a Phenomenex Jupiter C₄ column (250x2.00 mm, 5 μm, 300 Å) and the method **A** described in “stains, enzymes and reagents” paragraph. To estimate the globular state of Flt-1_{D2}, was performed a

trypsin digestion in 50 mM Tris-HCl, pH 7.5 containing 20 mM CaCl₂, adding trypsin with a molar ratio trypsin:Flt-1_{D2} of 1:100. The reaction was allowed to proceed at 37°C and was analyzed at different times (45, 90 min) by LC-MS, using the same column and method described above.

Flt-1_{D2} CD analysis

Flt-1_{D2} far-UV circular dichroism spectra were obtained using a Jasco J-715 spectropolarimeter, equipped with a PTC-423S/15 Peltier temperature controller, using a 0.1mm quartz cell in the far UV range 190-260 nm. Spectra were acquired using a band width of 1 nm, a response of 8 sec, a data pitch of 0.2 nm and a scanning speed of 10 nm/min. Each spectrum was the average of three scans with the background of the buffer solution subtracted. Spectra were performed at 20°C at a protein concentration of 15 μM, in 20 mM phosphate buffer at pH 7. CD data were expressed as mean residue ellipticity (θ). Spectra processing was obtained by using the Spectra Manager software, while the analysis of the secondary structure content of the proteins was performed following the programs Continll (Provencher, S. W. *et al.*, 1981), Selcon3 (Sreerama, N. *et al.*, 2000) and CDSSTR (Manavalan, P. *et al.*, 1987) of the CDPro program pack (<http://lamar.colostate.edu/~sreeram/CDPro/>) and one of the most widely used neural network program: CDNN (Bohm, G. *et al.*, 1992). An additional method named Cluster was employed for determination of tertiary structure class of examined proteins (Venyaminov, S. *et al.*, 1994).

Flt-1_{D2} thermal unfolding was performed at 15 μM protein concentration in 20 mM phosphate buffer, pH 7.0, using the same Jasco apparatus and the temperature/wavelength scan measurement program of the Spectra Manager software. The temperature was increased from 10°C to 100°C at a rate of 30°C/h. The CD signals were acquired at 1°C intervals at the indicated wavelength (214 nm).

Flt-1_{D2}-VEGF binding competition assay on ECs by Fluorescence Activated Cell Sorting (FACS)

The assay was performed on HUVEC cells by using the *Fluorokine Biotinylated Human VEGF Kit* supplied by R&D System. HUVEC cells were cultured in EBM (Endothelial basal medium) enriched with 2% FCS (Fetal Calf Serum), 0.5 ng/mL VEGF, 22.5 μg/mL heparin, 0.1 ng/mL EGF, 1 ng/mL bFGF, 1 μg/mL hydrocortisone, 50 ng/mL amphotericin B, 50 μg/mL gentamicyn to obtain the EGM (Endothelial Growth Medium). Both HUVEC cells and the components added to obtain the EGM were supplied by Cambrex. The cells were kept with 5% CO₂ at a temperature of 37°C. All the experiments (two) were conducted using sub-confluent cells cultures (between 5°-6° passages). Then, the cells were treated with *Cell Dissociation Solution Non-enzymatic* (Sigma) to remove them from flasks (25 cm²) without damaging the membrane receptors. According to the kit instructions, one cells sample was incubated with VEGF-biotin (positive control), another cells sample was treated with an aspecific biotinylated protein supplied by the kit (negative control); one other sample was pre-incubated with human IgG, then treated with VEGF-biotin in presence of anti-human VEGF IgG to block the binding of VEGF to cell surface membrane (specificity control). The last cells sample was treated with VEGF-biotin pre-incubated with Flt-1_{D2} (using a VEGF-biotin:Flt-1_{D2} molar ratio of 1:20). After one hour incubation at 4°C all the samples were incubated with provided FITC-avidin for 30 min, at 4°C, in the dark; then were washed with the supplied buffer and analyzed

to the citofluorimeter. The signals of fluorescence were acquired at a wavelength of 488 nm (in logarithmic scale) and analyzed with Cell Quest software (Facscalibur Becton Dickinson).

NMR Spectroscopy

Preparation of NMR samples

NMR measurements were performed on a Varian Unity Inova 600 MHz spectrometer equipped with a cold-probe, using either unlabeled (300 μ M) or uniformly ^{15}N labeled (220 μ M) Flt-1_{D2} protein, in 90% H₂O/10% D₂O (v/v), containing 50 mM Tris-HCl and 100 mM NaCl, pH 7.

Peptide-protein interactions

Chemical Shift Mapping

Peptide-protein interactions were performed using QK and MA peptides and were monitored by identifying perturbations in 2D [^1H , ^{15}N] HSQC spectra. ^{15}N -Flt-1_{D2} was titrated increasing QK and MA peptides concentrations. 2D [^1H , ^{15}N] HSQC spectra were acquired with 32 transients per t_1 value. Presaturation of water was employed during a recycle delay of 1.5 s. 1K complex points were acquired in t_2 , with an acquisition time of 102.5 ms, while 128 complex points were acquired in t_1 with an acquisition time of 64 ms.

To determine the *per residue* chemical shift perturbation upon binding and account for differences in spectral widths between ^{15}N and ^1H resonances, weighted average chemical shift differences, $\Delta\text{av}(\text{HN})$, were calculated for the amide ^{15}N and ^1H resonances, using equation:

$$\Delta\text{av}(\text{HN}) = [\Delta H^2 + (\Delta N/2)^2]^{1/2}$$

where ΔH and ΔN are the differences between free and bound chemical shifts. The weighted average chemical shift differences were mapped to the Flt-1_{D2} NMR structure (1QSV.pdb) using MOLMOL graphics program.

Saturation Transfer Difference

Spectra of the unlabeled Flt-1_{D2}/peptide complex were recorded with 2048 scans and selective saturation of the protein resonances at 12 ppm and -3 ppm. Time dependence of the saturation transfer was investigated using an optimized saturation times ranging from 0.2 to 4.0 s. STD NMR spectra were acquired using a series of equally spaced 50 ms Gaussian-shaped pulses for selective saturation, with 1 ms delay between the pulses. Subtraction of the protein FID resonance was performed by phase cycling.

Results

Domains cloning of human KDR and Flt-1 receptors

Cloning of 1-3, 2-3, 1-2 and 2 KDR receptor domains

One step PCR subcloning technique was used to generate bacterial expression vectors containing the sequences encoding an N-terminal His-Tag, a TEV cleavage site and the extracellular domains 1-3, 2-3, 1-2 and 2 of VEGFR-2 (KDR). First, sequences D1-3 (residues 1-335, Fuh *et al.*, 1998), D2-3 (residues 120-335, Fuh *et al.*, 1998), D1-2 (residues 1-222, Fuh *et al.*, 1998) and D2 (residues 120-222, Fuh *et al.*, 1998) were amplified by PCR from NIH-3T3 cDNA of the entire receptor using the primers designed on the basis of the sequence of the same domains (see Materials and Methods section). This cloning strategy was used to obtain the gene products fused (at the N-terminal) with the 6xHistidine-tag of pPROEXHTa expression vector. Single products were amplified by PCR, purified and digested with *Bam*HI-*Xho*I restriction enzymes. In Figure 13 are showed the products purified after digestion.

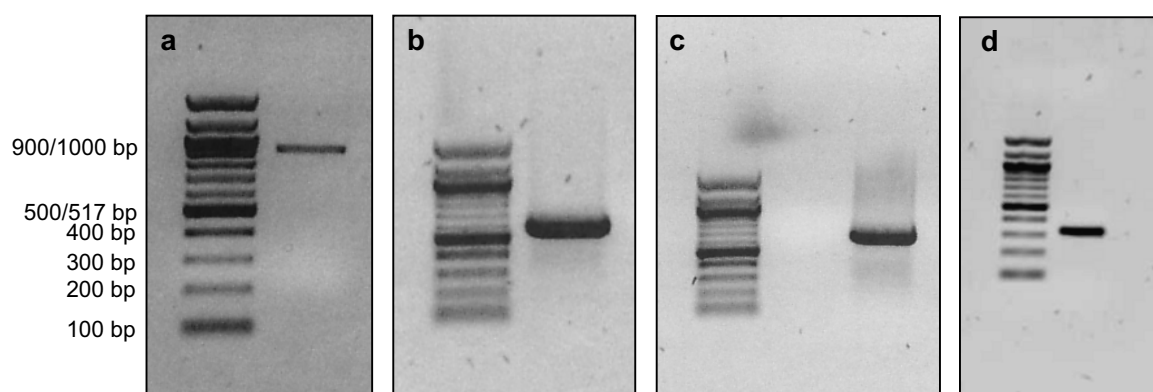


Figure 13 1% agarose-gel analysis of KDR domains PCR products. In a, b, c and d are reported, respectively, the *Bam*HI/*Xho*I digested *kdr*_{D1-2-3} (911 bp), *kdr*_{D1-2} (570 bp), *kdr*_{D2-3} (647 bp), *kdr*_{D2} (330 bp) genes amplified from NIH-3T3 KDR receptor cDNA. DNA molecular weight marker is the Ladder 100 bp.

pPROEXHTa expression vector was digested with the same enzymes, purified using the *QIAquick Gel Extraction Kit* and analyzed by electrophoresis on a 1% agarose gel (Figure 14a). *kdr*_{D2} gene was cloned also in pETM11 and pETM20 expression vectors. In this case, both vectors (Figure 14 b-c) and PCR fragment corresponding to the second domain of VEGFR-2 (Figure 15) were digested with *Nco*I/*Xho*I restriction enzymes.

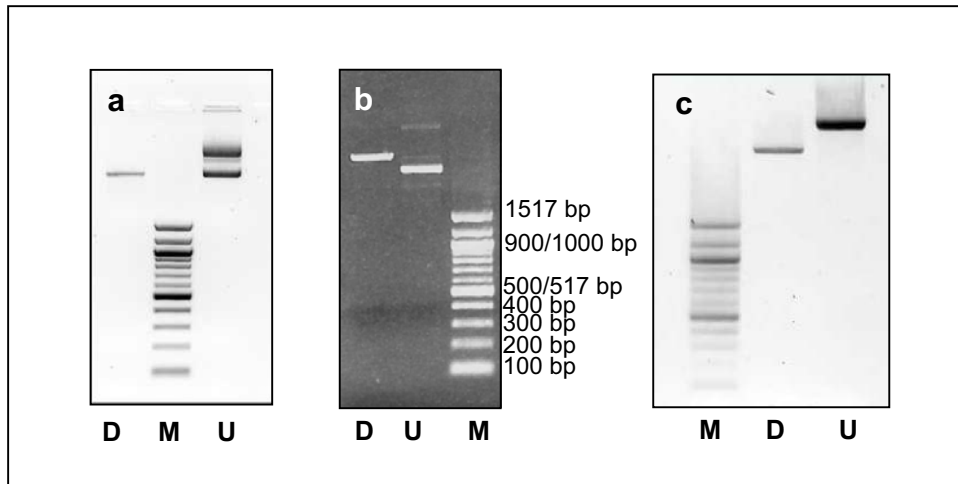


Figure 14 a-b-c 1% agarose-gel analysis of the digested vectors. In **b** lane labelled with “D” indicates the pPROEXHTa expression vector digested with *Bam*H1/*Xho*1 restriction enzymes, while in **a** and **c** the *Nco*I/*Xho*I digested pETM20 and pETM11, respectively. Lanes marked with “U” indicate undigested vectors. M is the DNA molecular weight marker (Ladder 100 bp).

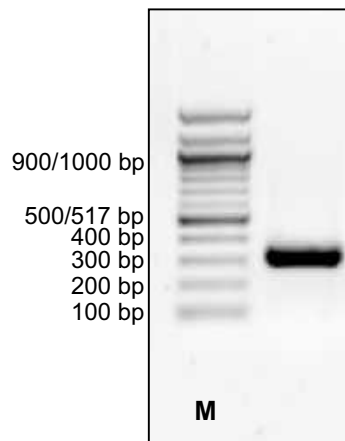


Figure 15 1% agarose-gel analysis of the *kdr_{D2}* gene PCR product amplified from NIH-3T3 receptor cDNA and digested with *Nco*I/*Xho*I endonucleases. M, Ladder 100 bp.

All amplicates obtained from PCR reactions were ligated into the corresponding expression vectors; then, each recombinant construct resulted from cloning, was transformed in TOP F'10 cells by electroporation. Plasmidic DNA was extracted from overnight cultures and purified using the *QIAprep Spin Miniprep Kit*. The identity of the inserts was tested with a PCR screening (Figures 16, 17) and confirmed by DNA sequencing.

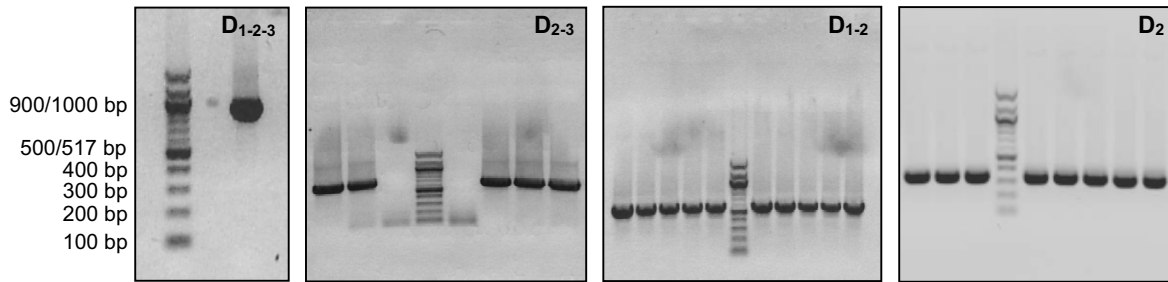


Figure 16_ 1% agarose-gel analysis of the PCR screening of recombinant KDR domains. In figure are showed the PCR products resulted from recombinant plasmids after cloning of *kdr*_{D1-2-3}, *kdr*_{D2-3}, *kdr*_{D1-2} and *kdr*_{D2} genes in pPROEXHTa expression vector. All amplification products were obtained using the putative recombinant vectors as templates and the same primers of cloning PCR reactions. In Figure is reported the Ladder 100 bp.

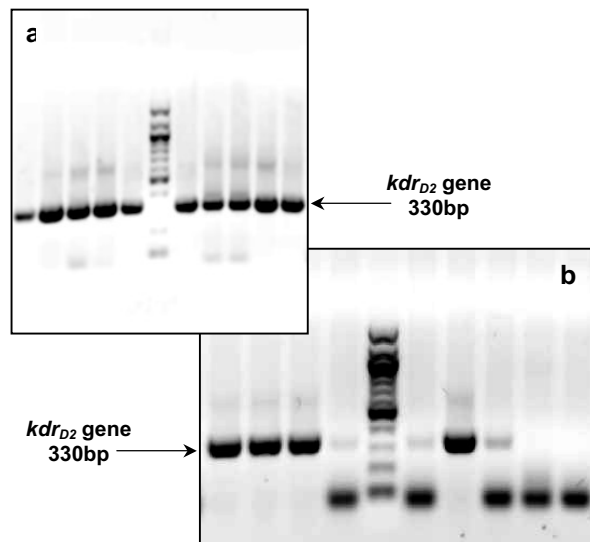


Figure 17_ 1% agarose-gel analysis of the PCR screening products amplified from recombinant pETM11-*kdr*_{D2} (a) and pETM20-*kdr*_{D2} (b) expression vectors. In both gels is reported the Ladder 100bp.

Cloning of 1-4, 2-4, 2-3 and 2 Flt-1 receptor domains

VEGFR-1 (Flt-1) domains 1-4 (residues 27-428, Wiesmann *et al.*, 1998), 2-4 (residues 129-428, Wiesmann *et al.*, 1998), 2-3 (residues 129-334, Wiesmann *et al.*, 1998) and 2 (residues 129-229, Wiesmann *et al.*, 1998) were amplified by polymerase chain reaction from NIH-3T3 cDNA of the entire receptor. Products obtained from PCR were ligated into the bacterial expression vector pETM11; domain 2 was also cloned into the pETM20 expression vector. Thus, the expression plasmids encoded Flt-1 domains fused, respectively, to an N-terminal 6xHis-tag sequence and to an N-terminal 6xHis/TrxA-tag.

Each polymerase chain reaction amplified, with high yields, only the desired product; all products were then digested with *Nco*I-*Xho*I restriction enzymes, purified and separated on a 1% agarose gel (Figure 18).

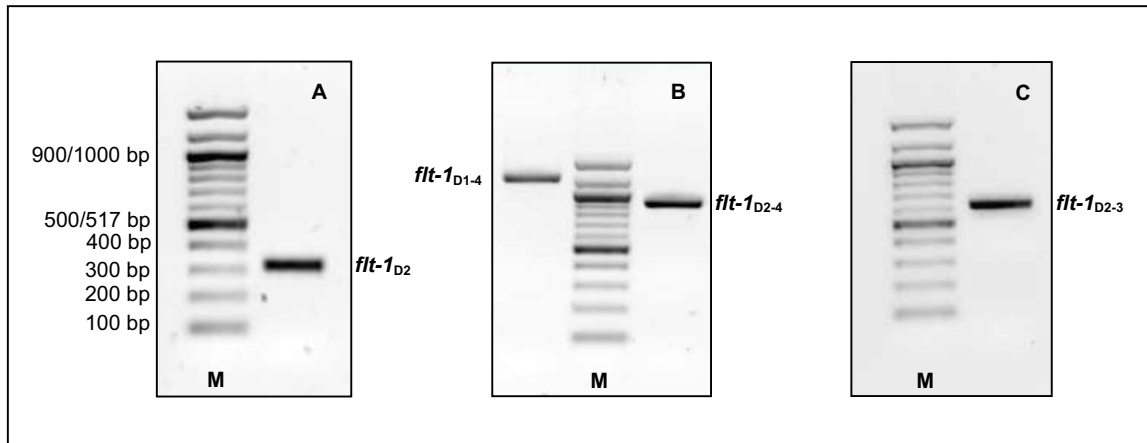


Figure 18_ 1% agarose-gel analysis of VEGFR-1 domains PCR products. In A, B and C are reported, respectively, the *NcoI/XhoI* digested *flt-1_{D2}* (320 bp), *flt-1_{D1-4}* (1202 bp), *flt-1_{D2-4}* (897 bp), *flt-1_{D2-3}* (627 bp) genes amplified from NIH-3T3 Flt-1 receptor cDNA. M, DNA molecular weight marker (Ladder 100 bp).

After cloning, each recombinant construct was transformed in TOP F'10 cells by electroporation; then, plasmidic DNA was extracted from overnight cultures and purified. The identity of the inserts in each resulting recombinant plasmid was tested with a PCR screening (Figures 19, 20) and confirmed by DNA sequencing.

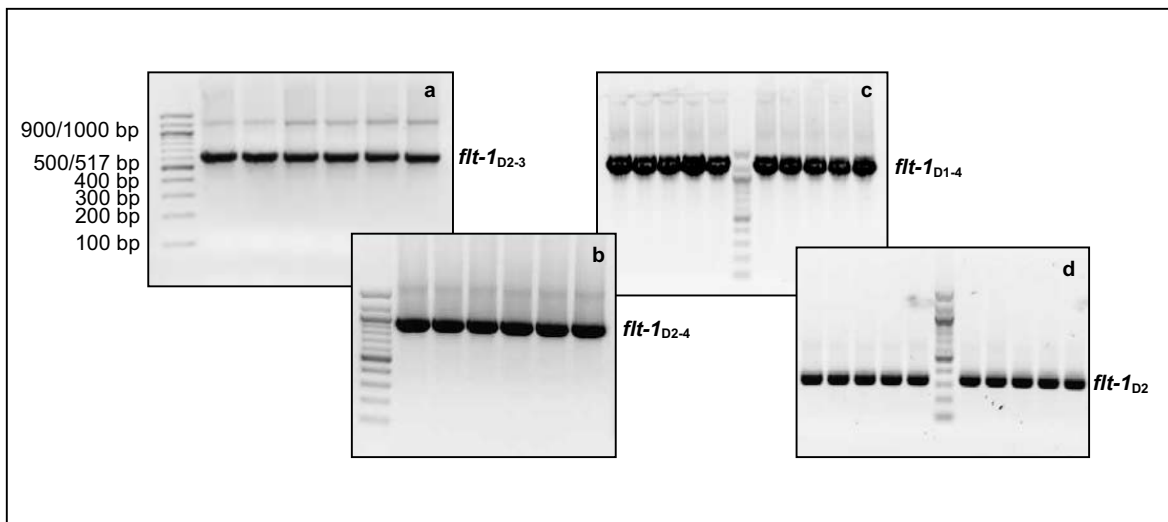


Figure 19_ 1% agarose-gel analysis of the products resulted from PCR screening of the recombinant plasmids obtained after cloning of the genes *flt-1_{D2-3}* (a), *flt-1_{D2-4}* (b), *flt-1_{D1-4}* (c) and *flt-1_{D2}* (d) in pETM11 expression vector. All amplification products were obtained using the putative recombinant vectors as templates and the same primers of cloning PCR reactions. The marker loaded with the samples is the Ladder 100 bp.

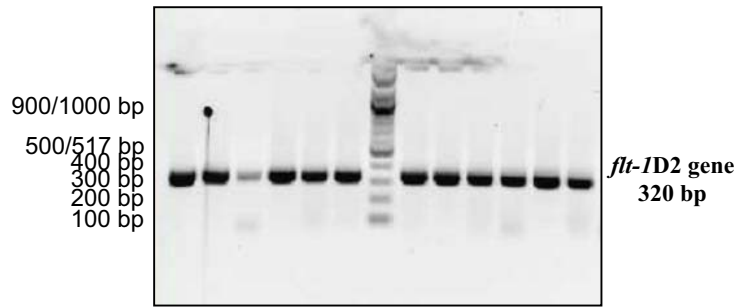


Figure 20 PCR screening agarose-gel analysis. The products were amplified by polymerase chain reaction from the recombinant plasmids obtained after cloning of *flt-1_{D2}* gene in pETM20 expression vector. In figure is reported the Ladder 100 bp.

Expression and purification of recombinant human KDR and Flt-1 extracellular domains

Expression of 1-3, 2-3, 1-2 and 2 KDR receptor domains

The recombinant pPROEXHTa and pETM11 expression vectors containing VEGFR-1 and VEGFR-2 extracellular domains were verified by DNA sequencing and utilized to transform bacterial cells, in order to express the corresponding proteins. For the expression of all recombinant proteins was performed a screening by using different strains and different growing conditions (temperature and IPTG concentration). The host strain chosen for the expression of all recombinant proteins was the BL21 *Codon Plus* (DE3) RIL strain, done exception for KDR_{D1-2} and KDR_{D1-3} that were expressed in Rosetta Gami (DE3) competent cells. BL21 *Codon Plus* (DE3) RIL competent cells, as Rosetta (DE3), are efficient for the high-expression of eukaryotic proteins in *E. coli* since they are engineered to contain extra copies of the genes that encode the tRNAs that most frequently limit translation of heterologous proteins in *E. coli*. In fact, these strains supply tRNAs for AGG, AGA, AUA, CUA, CCC and GGA on a compatible chloramphenicol-resistant plasmid. Rosetta Gami (DE3) strain combines the enhanced expression of eukaryotic proteins with the enhanced disulfide bond formation resulting from *trxB/gor* mutations that are selectable on kanamycin (15 µg/mL) and tetracycline (12.5 µg/mL), respectively. As the proteins corresponding to domains 1-2 and 1-3 of human KDR contain, respectively, 7 and 9 cysteine residues in addition to rare codons, Rosetta Gami (DE3) strain was chosen to create in cell milder reduction conditions, thus facilitating expression and fold of these proteins. Rosetta Gami (DE3) competent cells, previously transformed with pPROEXHTa-*kdr*_{D1-2} and pPROEXHTa-*kdr*_{D1-3} recombinant expression vectors and selected on solid medium, were induced overnight with 0.7 mM IPTG at 37°C and at 22°C when cell cultures reached an OD_{600nm} of 0.8. Non-induced samples were kept before adding IPTG. The cells were harvested and the pellets were resuspended in 25 mL of 50 mM Tris-HCl, pH 7. Suspensions were sonicated and then centrifuged at 15.000 rpm at 4°C for 30 min. Analysis by SDS-PAGE of bacterial lysates showed the presence of the protein KDR_{D1-3} in IPTG-induced cells, precisely in crude extract pellet (expressed at 37°C and resuspended in 50 mM Tris-HCl, pH=7) (Figure 21, lane 3), with a molecular weight of about 36 KDa, as expected for the protein corresponding to domains 1-3. Instead, for KDR_{D1-2} was not possible to observe any

induced protein with the expected molecular weight (about 24 KDa), in any tested condition (Figure 22). Protein concentration of each sample loaded on the gel was determined according to the Bradford's method.

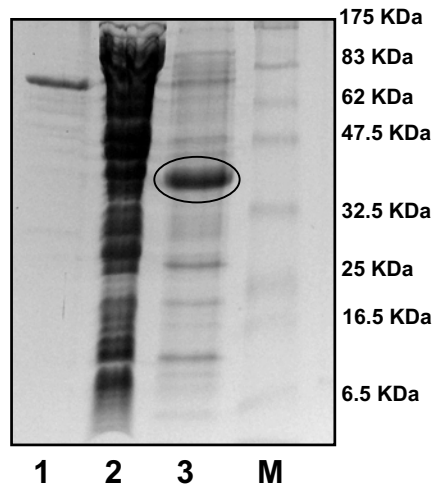


Figure 21_ Analysis by SDS-PAGE of recombinant KDR_{D1-3} expressed overnight in Rosetta Gami (DE3) strain at 37°C. In the first lane is reported the BSA standard (1.48 µg/µl), in lane 2 *E. coli* crude extract supernatant in 50 mM Tris-HCl, pH 7 and in lane 3 *E. coli* crude extract pellet in the same buffer. In the circle is shown the induced KDR_{D1-3} . M, Biorad molecular weight marker.

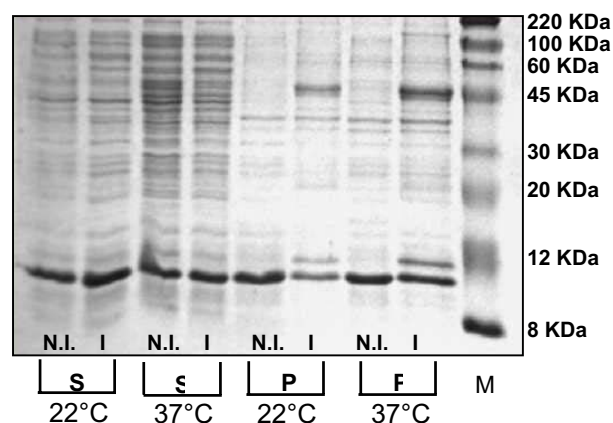


Figure 22_ SDS-PAGE analysis of KDR_{D1-2} expression in Rosetta Gami (DE3) strain at 22°C and 37°C overnight. N.I., non induced samples in Tris-HCl 50 mM pH 7; I, induced samples in Tris-HCl 50 mM pH 7. S, supernatant; P, pellet. M, Sigma pre-stained molecular weight marker. No induced protein band, with the expected molecular weight, is observed on the gel.

BL21 *Codon Plus* (DE3) RIL cells were transformed with pPROEXHTa- kdr_{D2-3} and pPROEXHTa- kdr_{D2} . Both proteins were expressed in inclusion bodies, in fact, analysis by SDS-PAGE of bacterial lysates obtained after sonicating the cells

showed the presence of KDR_{D2-3} and KDR_{D2} in crude extract pellets resuspended in 50 mM Tris-HCl, pH 8 (Figures 23, 24). The protein content of each sample was measured using the Bradford's method with bovine serum albumin as the standard.

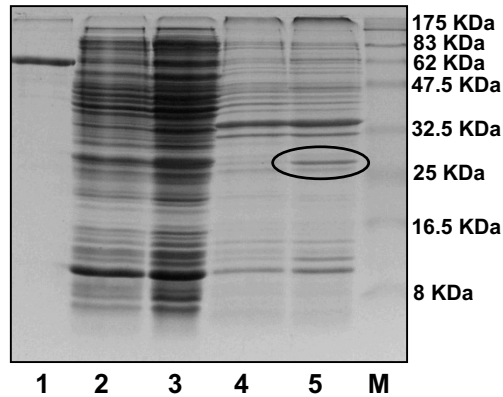


Figure 23_ SDS-PAGE analysis of KDR_{D2-3} (26.8 KDa) expression at 37°C, in BL21 *Codon Plus* (DE3) RIL strain. The gel shows the induced and not induced samples; in the first lane is reported the BSA standard (1.48 µg/µl), in lanes 2 and 3 *E. coli* crude extract supernatants (not induced and induced, respectively) in 50 mM Tris-HCl, pH 8; in lanes 4 and 5 *E. coli* crude extract pellets (not induced and induced, respectively) in 50 mM Tris-HCl, pH 8. In the oval there is the induced KDR_{D2-3}. M, NEB pre-stained molecular weight marker.

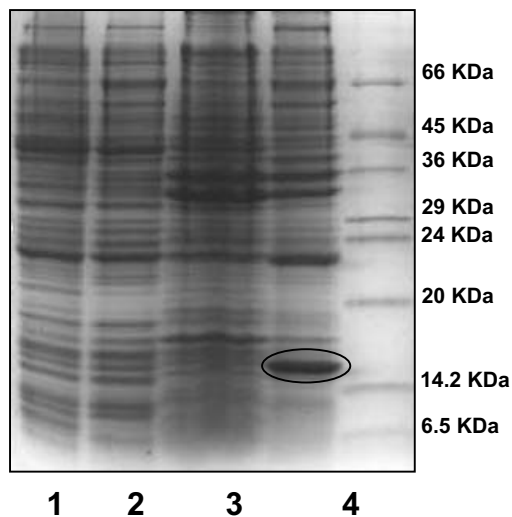


Figure 24_ SDS-PAGE analysis of KDR_{D2} (14.5 KDa) expression at 37°C, in BL21 *Codon Plus* (DE3) RIL strain. The gel shows the induced and not induced samples. In the first and second lanes are reported *E. coli* crude extract supernatants (not induced and induced, respectively) in 50 mM Tris-HCl, pH 8; in lanes 3 and 4 *E. coli* crude extract pellets (not induced and induced, respectively) in the same buffer. In the oval is circled the induced KDR_{D2}. M, Sigma molecular weight marker.

The inclusion body pellet of KDR_{D2} was solubilized in 20 mL 8 M urea, 10 mM imidazole, 0.15 M NaCl, 50 mM Tris-HCl, pH 8. The denatured protein in Tris-HCl-urea buffer was loaded onto a Ni²⁺-NTA agarose resin, previously equilibrated with the same buffer, and the His-tagged protein was in batch purified by affinity chromatography. Fractions eluted from the resin were collected and analyzed by 15% SDS-PAGE gel. In Figure 25 is showed the affinity chromatography elution profile.

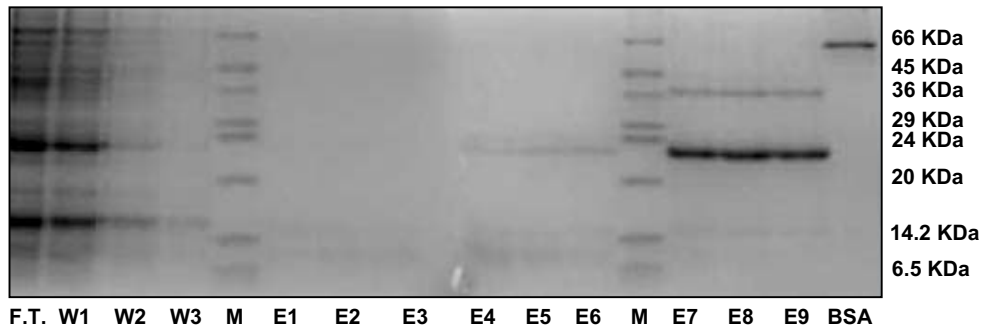


Figure 25_ Affinity chromatography profile of the His-tagged KDR_{D2} purified on a Ni²⁺-NTA resin. F.T., unbound proteins eluted from resin. W1-W3, wash of the resin with Tris-HCl-urea buffer containing 20 mM imidazole. E1-E9, fractions eluted from resin with higher concentration of imidazole: E1-E3 are the fractions eluted with 50 mM imidazole; E4-E6 with 100 mM imidazole and E7-E9 with 250 mM imidazole. M, Sigma molecular weight marker. KDR_{D2} was eluted in F.T. and, in part, in wash fractions.

As observed on the gel, the protein corresponding to the second domain of VEGFR-2, despite loaded in urea 8 M, did not bind to the resin and probably eluted in F.T.. In fact, no coomassie-stained band was visible in elutions in correspondence of the expected molecular weight (14.5 KDa), but a band with an apparent expected molecular weight was found in F.T.. To assure the presence of KDR_{D2} in the unbound protein fraction, 100 µg of F.T. were separated by electrophoresis on a 15% polyacrylamide SDS-PAGE and transferred from gel to a polyvinylidene difluoride (PVDF) membrane by electro-blotting. Detected immunopositive species were visualized using a Chemi doc XRS apparatus and are showed in Figure 26. On the gel, then electro-blotted, was loaded, near the pre-stained marker, a His-tagged protein purified by affinity chromatography as positive control. This protein has a molecular weight of 11 KDa and is showed in lane 2 of Figure 26.

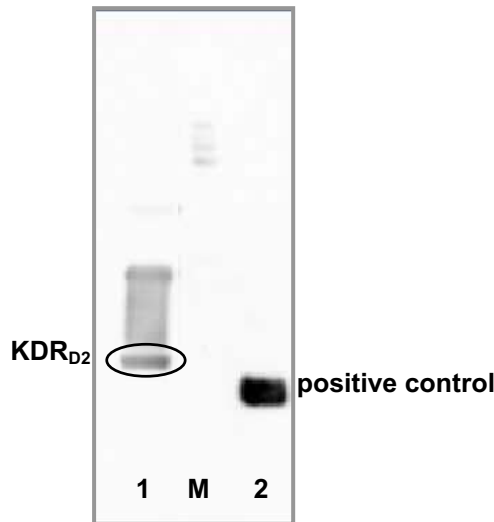


Figure 26_ Western analysis of KDR_{D2} . The first lane of the blot was found to contain a protein that migrates with the expected molecular weight (in the oval). In lane 2 there is the positive control constituted by a His-tagged protein with a molecular weight of 11 KDa. Both species were recognized by an anti-His antibody. M, NEB pre-stained marker.

Western blotting analysis showed the presence of the His-tagged KDR_{D2} in F.T., but did not explain the unusual behavior of the protein. The second domain of VEGFR-2 was successively cloned in pETM11 and pETM20 expression vectors, but the recombinant protein was expressed in inclusion bodies and did not bind to the resin again (data not shown). So, its sequence was mutated and cloned again in pETM11.

***kdr*_{D2} gene mutagenesis**

As *in vitro* site-directed mutagenesis is an available technique for studying protein structure-function relationship and gene expression, we used this approach to change one of the three residues of cysteine (C_{161}) of the second domain of KDR receptor in Alanine. Our aim was to obtain a protein capable to bind to the Ni^{2+} -NTA resin and to be purified by affinity chromatography as the second domain of VEGFR-1 that has only two cysteine residues in its sequence (see below). According to the procedure suggested by the *Quik Change Site Directed Mutagenesis Kit*, we utilized a supercoiled double-stranded DNA (dsDNA) vector with the insert of interest and two synthetic oligonucleotide primers contained the desired mutation. In our case, was used the pETM11-*kdr*_{D2} plasmid and the oligonucleotide primers, each complementary to opposite strands of the vector, contained the mutation for an alanine in the middle. The primers were extended during temperature cycling; their incorporation generated a mutated plasmid containing staggered nicks. In fact, as we can see in Figure 27, PCR mutagenesis product (*mut*) is shifted on the agarose gel with respect to the control represented by the non mutated construct pETM11-*kdr*_{D2} (*wt*), as attended for a nicked dsDNA plasmid. Following PCR reaction, the product was treated with *DpnI*, an endonuclease specific for methylated and hemimethylated DNA, used to digest the parental DNA template and to select for mutation-containing

synthesized DNA. In fact, DNA isolated from almost all *E. coli* strains is *dam* methylated and therefore susceptible to *DpnI* digestion. The nicked vector containing the desired mutation was then transformed into XL1-Blue supercompetent cells. The identity of the mutagenic insert was confirmed by DNA sequencing.

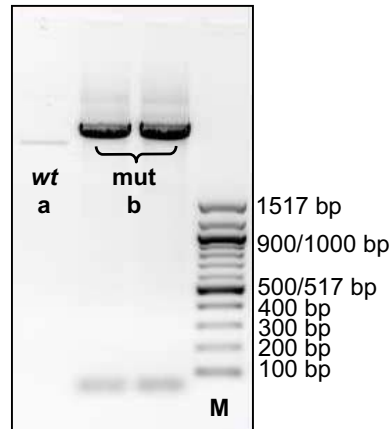


Figure 27_ 1% agarose gel analysis of mutated *kdr_{D2}* gene. The products derived from PCR mutagenesis were visualized by ethidium bromide fluorescence. The reaction (performed in double) was loaded on the gel (b) with the control pETM11-*kdr_{D2}* (a). M, Ladder 100 bp.

Mutated *KDR_{D2}* was expressed in BL21 *Codon Plus* (DE3) RIL at 22°C and at 37°C. Once again, the protein was expressed in crude extract pellet induced with IPTG, solubilized from inclusion bodies and eluted in the unbound proteins fraction when loaded on Ni²⁺-NTA resin for affinity purification (data not shown).

The other recombinant proteins expressing domains 1-3 and 2-3 of VEGFR-2, instead, were solubilized from inclusion bodies, purified by affinity chromatography on Ni²⁺-NTA resin and refolded by step dialysis. Refolding was performed against buffers containing 6, 4, 3, 2, 1, and 0 M urea successively, and each dialysis was carried out at 20°C for 8 h against 10 volumes of the dialysis buffer containing 3 mM glutathione/0.3 mM oxidized glutathione, in order to facilitate protein disulfide bond formation. Despite the creation of more less reducing conditions, with the last steps of refolding some protein for both samples precipitated, probably due to their aggregation or misfolding. Thus, the amount of *KDR_{D1-3}* and *KDR_{D2-3}* recovered after TEV protease cleavage, performed to remove the His-tag sequence from the N-terminal of the proteins, was insufficient for structural characterization.

Expression of 1-4, 2-4 and 2-3 Flt-1 receptor domains

For bacterial expression, the recombinant pETM11 containing 1-4, 2-4 and 2-3 VEGFR-1 extracellular domains were verified by DNA sequencing and transformed into *E. coli* BL21 *Codon Plus* (DE3) RIL cells carrying an inducible T7 RNA polymerase gene, in order to express high yields of the corresponding proteins. Bacterial cultures of 1L of LB medium containing 50 µg/mL kanamycin and 33 µg/mL chloramphenicol were grown in shaking flasks at 37°C to an *A*_{600nm} of 0.8. IPTG was

added to a final concentration of 0.7 mM and the cultures were grown for another 3 h. From each culture was kept a non induced sample, before adding IPTG. Analyses by SDS-PAGE of bacterial lysates obtained after sonicating the cells showed the presence of all interest proteins in IPTG-induced crude extract pellet fractions (Figures 28, 29, 30).

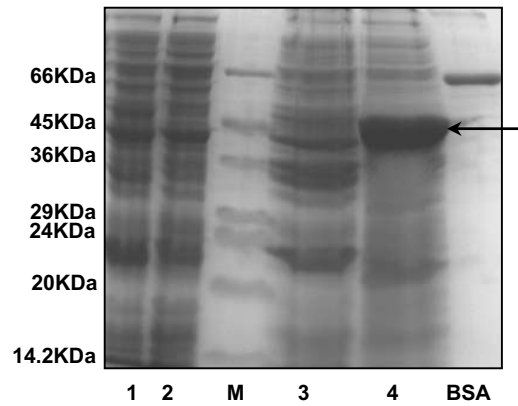


Figure 28_ SDS-PAGE analysis of Flt-1_{D1-4} (48.7 KDa) expressed in *E. coli* BL21 *Codon Plus* (DE3) RIL strain at 37°C. Gel shows the induced and not induced samples. In the first and second lanes are reported *E. coli* crude extract supernatants (not induced and induced, respectively) in 50 mM Tris-HCl, pH 8; in lanes 3 and 4 *E. coli* crude extract pellets (not induced and induced, respectively) in the same buffer. Black arrow indicates the induced protein. M, Sigma molecular weight marker.

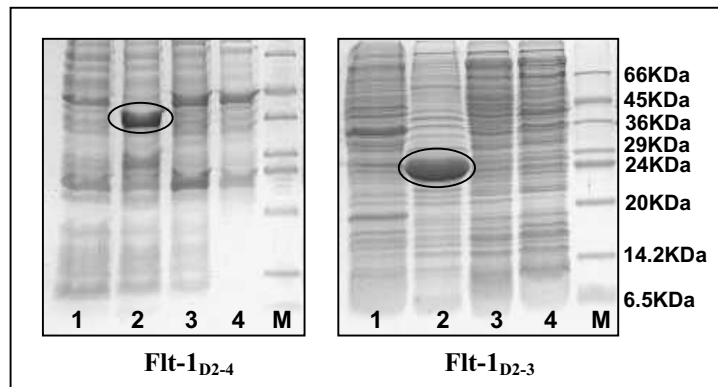


Figure 29_ SDS-PAGE analysis of expressed Flt-1_{D2-4} and Flt-1_{D2-3} (respectively 37.4 and 26.8 KDa). Gels show the induced and not induced samples. In the first and second lanes of both gels are reported *E. coli* crude extract pellets (not induced and induced, respectively) in Tris-HCl 50 mM, pH 8; in lanes 3 and 4 *E. coli* crude extract supernatants (not induced and induced, respectively) in the same buffer. In the ovals are reported the induced proteins. M, Sigma molecular weight marker.

Expression, refolding and purification of 2 Ig-like Flt-1 receptor domain cloned into the pETM11 expression vector

pETM11-*flt-1*_{D2} was verified by DNA sequencing and transformed into *E. coli* BL21 Codon Plus (DE3) RIL. Significant amounts of Flt-1_{D2} (60mg/L) were obtained upon induction by IPTG, but, also in this case, the protein accumulated in the form of inclusion bodies. The induced protein, in fact, was visible in crude extract pellet fraction (Figure 30, Lane 4).

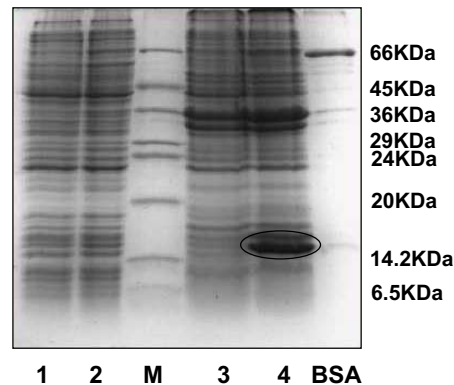


Figure 30_ SDS-PAGE analysis of Flt-1_{D2} (14.8 KDa) expressed in BL21 Codon Plus (DE3) RIL at 37°C. Gel shows the induced and not induced samples. In the first and second lanes are reported *E. coli* crude extract supernatants (not induced and induced, respectively) in 50 mM Tris-HCl, pH 8; in lanes 3 and 4 *E. coli* crude extract pellets (not induced and induced, respectively) in the same buffer. In the oval is reported the induced protein. M, Sigma molecular weight marker.

Obtaining recombinant protein in the form of inclusion bodies has its own advantages and disadvantages. The isolation steps for inclusion bodies are relatively simple, but the refolding becomes more complicated. In fact, in the refolding process, various factors such as protein concentration, denaturant, ionic strength, pH, temperature play an important role in determining protein refolding yields. Thus, the refolding process of Flt-1_{D2} has been optimized through adjusting these conditions to prevent auto-degradation and aggregation of the protein and performing an “on column refolding”. The idea was to refold the protein still bound to the resin and then elute it by increasing concentration of imidazole. The inclusion body pellet of Flt-1_{D2} was solubilized in 20 mL 8 M urea, 10 mM imidazole, 0.15 M NaCl, 50 mM Tris-HCl, pH 8 and the lysate was loaded on a Ni²⁺-NTA agarose resin equilibrated previously with the same buffer. Once collected the flow-through and wash fractions, the bound protein was refolded by equilibrating the column in buffers containing decreasing concentration of urea. The protein was refolded in following six steps using buffers containing 6, 4, 3, 2, 1, and 0 M urea successively, and each step was carried out at 20°C for 3 h with 20 column volumes. After refolding, Flt-1_{D2} was eluted in 50 mM Tris-HCl, pH 8 containing high concentrations of imidazole (50, 100 and 250 mM). Elution profile of the protein is showed in Figure 31.

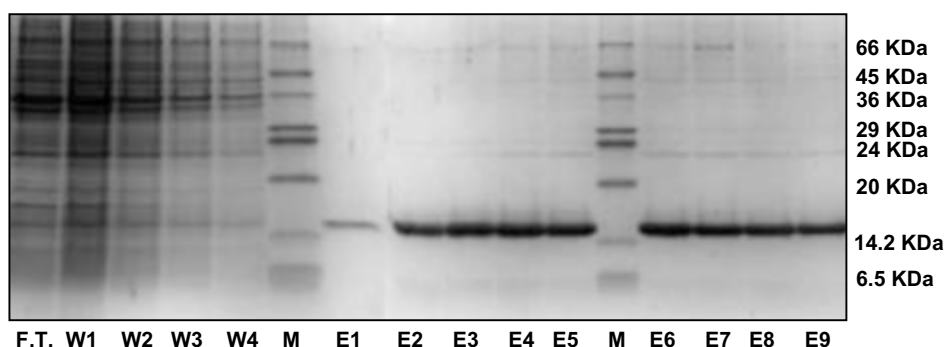


Figure 31_ Affinity chromatography profile of the His-tagged Flt-1_{D2} purified on Ni²⁺-NTA resin after “on column refolding”. F.T., unbound proteins eluted from resin. W1-W4, wash of the resin with Tris-HCl-urea buffer (50 mM Tris-HCl, 8 M urea, 0.15 M NaCl) containing 20 mM imidazole. E1-E9, fractions eluted from resin in 50 mM Tris-HCl, pH 8 with higher concentration of imidazole: E1-E3 are the fractions eluted with 50 mM imidazole; E4-E6 with 100 mM imidazole and E7-E9 with 250 mM imidazole. M, Sigma molecular weight marker.

TEV digestion and native-PAGE analysis of Flt-1_{D2}

Fractions eluted with 50, 100 and 250 mM imidazole from Ni²⁺-NTA resin were pooled (20 mL) and dialyzed against Tris-HCl 50 mM, pH 7, in order to remove imidazole and prepare the protein to the TEV cleavage. Dialysis was carried out at 20°C overnight against 2 L of the dialysis buffer. The N-terminal His-tag was removed from the dialyzed Flt-1_{D2} by recombinant TEV protease. Glutathione (3mM reduced/0.3 mM oxidized) was added to the partially purified protein just before addition of TEV protease. Cleavage reaction was performed adding TEV to protein substrate in a molar ratio of 1:35 and allowed to proceed overnight at 20°C. The His-tagged TEV was expressed in BL21 *pLysisS* cells (transformed with pET24a-TEV recombinant expression vector, kindly provided by Dr. Nina Dathan) and purified in our laboratory by affinity chromatography, using denaturing conditions. Eluted TEV was refolded by one step overnight dialysis and then stored at -80°C before being used to digest protein substrates. TEV-cleaved Flt-1_{D2} was analyzed by 18% polyacrylamide gel electrophoresis (Figure 32).

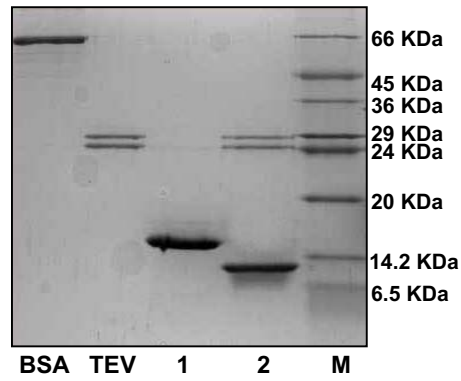


Figure 32_ SDS-PAGE analysis of the cleaved Flt-1_{D2}. Lane 1, negative control constituted by the uncut protein; lane 2, cleaved Flt-1_{D2}. M, Sigma molecular weight marker.

Then, mixture obtained after TEV cleavage was subjected to a second step of affinity purification on Ni²⁺-NTA resin and finally concentrated until 0.3 mM by using the Amicon Ultra system with a molecular weight cut off of 5000. Flt-1_{D2} concentration was estimated according to the Bradford's method and by UV spectroscopy, reading the tryptophan absorbance at 280 nm, and verified by SDS-PAGE analysis. As observed on the gel, the protein of interest resulted as a homogeneous product (Figure 33).

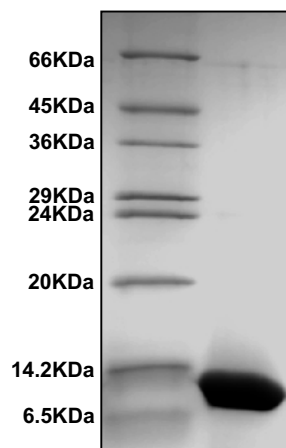


Figure 33_ SDS-PAGE analysis of Flt-1_{D2} after concentration in Amicon Ultra. As visualized by comassie-staining, the protein was purified homogeneously. Near Flt-1_{D2} was loaded Sigma molecular weight marker.

An aliquot of Flt-1_{D2} was loaded on native-PAGE for an analysis of its conformation in absence of denaturing detergents and reducing agents. For native PAGE the sample was not denaturated at 100°C but loaded on a 10% polyacrylamide gel in 0.001% bromophenol blue and 10% glycerol and electrophoresed in Tris-glycine buffer without SDS. As shown in Figure 34, the protein was able to migrate into the gel showing a single coomassie-stained band and suggesting its monomeric conformation.

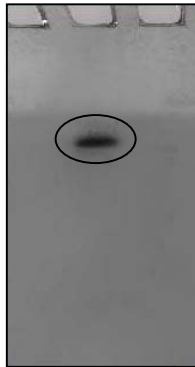


Figure 34 Native-PAGE analysis of Flt-1_{D2} cleaved by TEV and purified. As shown, coomassie-stained protein band entered the gel, without remaining into the well.

In order to obtain the second domain of VEGFR-1 in a soluble form, *flt-1_{D2}* gene was cloned in pETM20 expression vector. This cloning strategy allows the expression of the protein of interest with an N-terminal tag constituted by TrxA, a very soluble protein in most of cases able to solubilize its fusion partner.

In spite of this, the recombinant Flt-1_{D2} was again expressed in inclusion bodies (data not shown).

LC-MS analyses of Flt-1_{D2} after TEV cleavage, alkylation and trypsin digestion

Purity and identity of Flt-1_{D2} before and after TEV protease cleavage were assessed by liquid chromatography mass spectrometry. The analysis of proteins was carried out on a C₄ column, using the method **A** described in “Strains, enzymes and reagents” section of Materials and Methods. In Figure 35 are reported the chromatogram and mass spectrum of the His-tagged protein purified by affinity chromatography after “on column refolding”, while in Figure 36 are showed the chromatogram and mass spectrum of the untagged protein. The molecular weights calculated from the experimental data were in accordance with theoretical ones, for both proteins. Successively, the protein was employed in experiments of alkylation by iodoacetamide, in order to determine the oxidation state of its two cysteine residues. In fact, as previously described, these two cysteine residues are involved in the

formation of a disulfide bridge (Wiesmann, C. *et al.*, 1997). Flt-1_{D2} was alkylated with 55 mM iodoacetamide in 100 mM AMBIC, pH 8 and the reaction was kept in the dark for 30 min. As reaction control, the protein was first reduced with 10 mM DTT (45 min at 37°C), then alkylated by iodoacetamide. The alkylation reaction was checked by LC-MS and in Figure 37 and Figure 38 are reported the chromatograms and mass spectra of the alkylated and alkylated/reduced proteins, respectively. In non reducing conditions no alkylated adducts were found, while, in presence of DTT, the main product presented a mass increment of 116 Da consisted with alkylation of the two cysteine residues. Finally, the second domain of Flt-1 receptor was subjected to a trypsin digestion, in order to estimate the globular state of the protein. The reaction was allowed to proceed at 37°C in 50 mM Tris-HCl, pH 7.5 containing 20 mM CaCl₂. Trypsin was added to the mix in a molar ratio enzyme:Flt-1_{D2} of 1:100. The reaction was analyzed by LC-MS at different times (45 min and 90 min) and showed a stable conformation of the protein that was not drastically digested by trypsin, as attended for a compact immunoglobulin-like domain. In fact, LC chromatogram and mass spectrum of Flt-1_{D2} after reaction, were similar to these of non digested protein (data not shown).

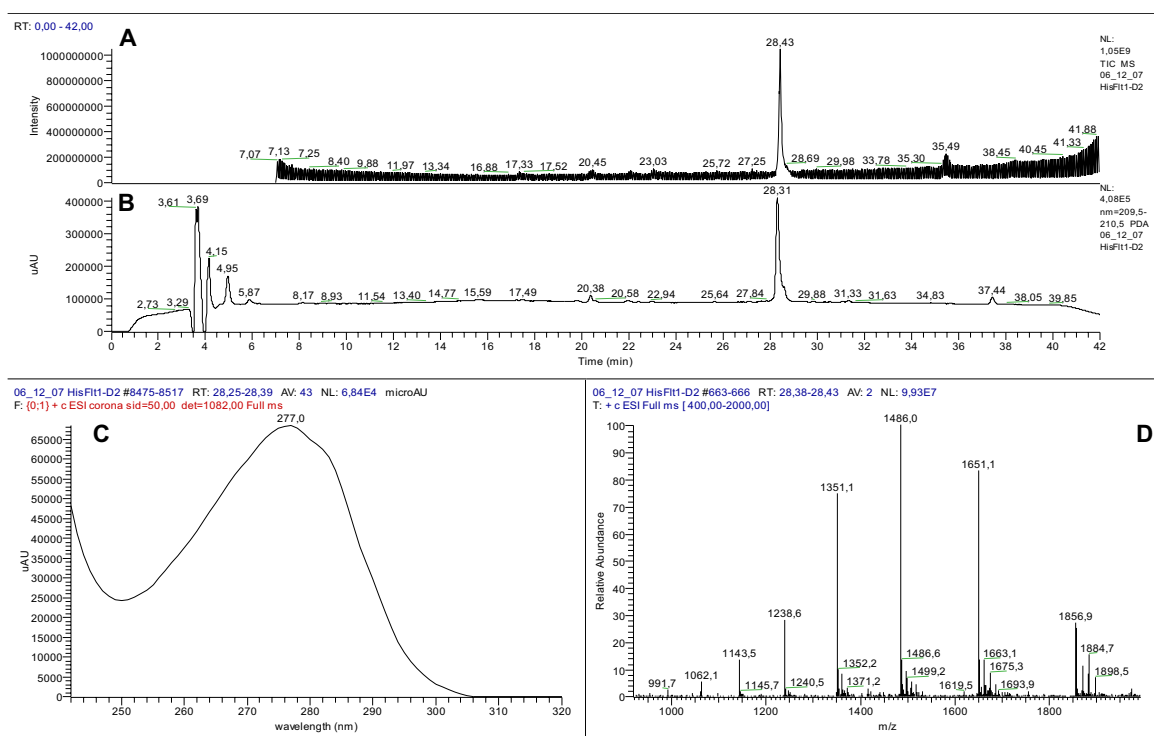


Figure 35_ LC-MS analysis of the His-tagged Flt-1_{D2}. A, chromatogram profile revealed by Total Ion Count; B, chromatogram profile revealed by absorbance at 210 nm; C, UV spectrum of the peak at 28.3 min; D, ESI spectrum of the peak at 28.4 min. Deconvolution analysis of Flt-1_{D2} charged states (reported in box D) corresponds to a mass of 14850.8 Da that is in agreement with the theoretical one.

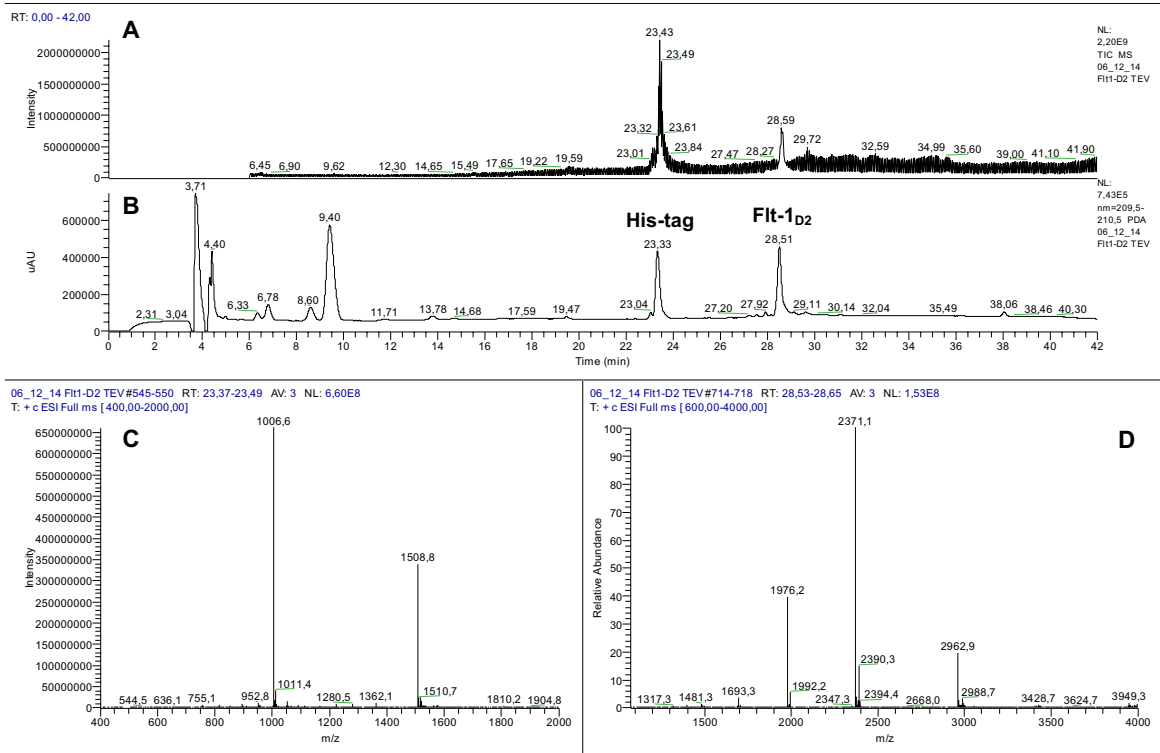


Figure 36 LC-MS analysis of Flt-1_{D2} after TEV cleavage. A, chromatogram profile revealed by Total Ion Count; B, chromatogram profile revealed by absorbance at 210 nm; C and D, ESI spectra of the peaks at 23.33 and 28.51 min, respectively. Deconvolution analysis of Flt-1_{D2} charged states (reported in box D) corresponds to a mass of 11850.6 Da that is in agreement with the theoretical one.

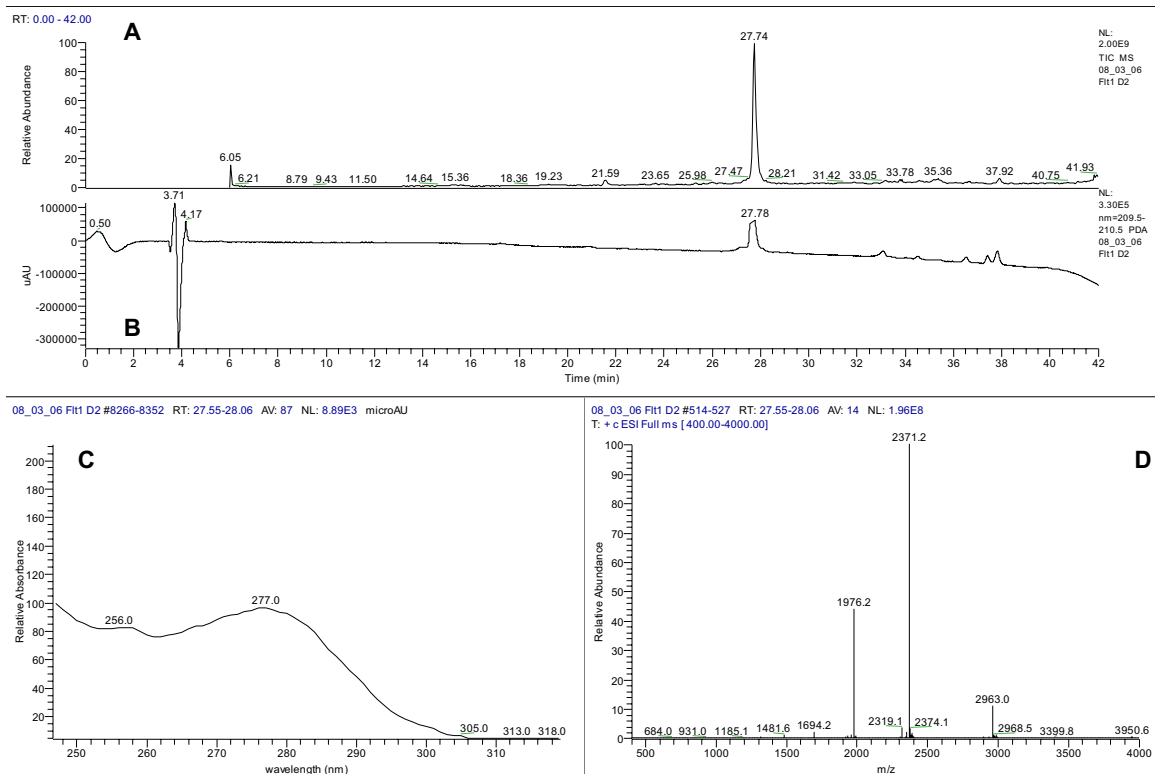


Figure 37_ LC-MS of the alkylated Flt-1_{D2}. A, chromatogram profile revealed by Total Ion Count; B, chromatogram profile revealed by absorbance at 210 nm; C, UV spectrum of the peak at 27.78 min; D, ESI spectrum of the peak at 27.74 min. It is the same obtained for the untreated protein (Fig. 36, box D).

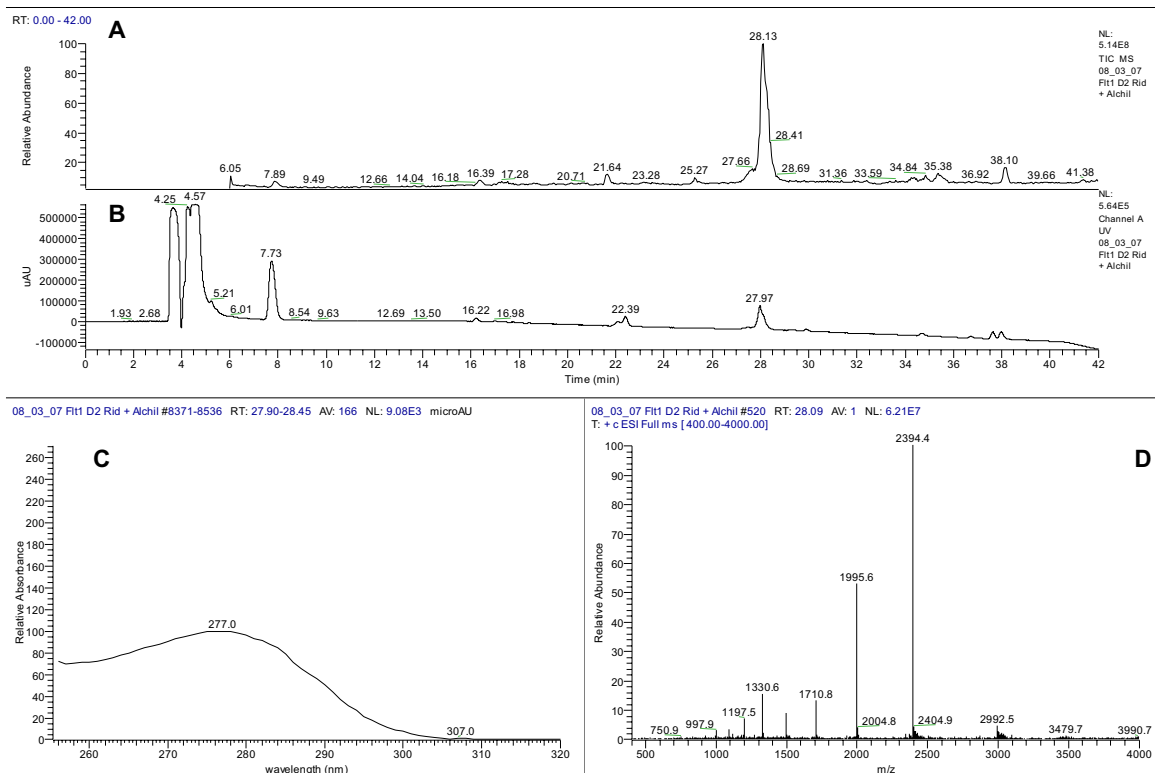


Figure 38_ LC-MS of reduced/alkylated Flt-1_{D2}. A, chromatogram profile revealed by Total Ion Count; B, chromatogram profile revealed by absorbance at 210 nm; C, UV spectrum of the peak at 27.97 min; D, ESI spectrum of the peak at 28.13 min. Deconvolution analysis of the charged states reported in box D corresponds to a mass of 11966.2 Da that is in agreement with the theoretical one, testifying that two alchilic groups (58 Da each) were added to the protein after alkylation.

Flt-1_{D2} VEGF-binding competition assay by Fluorescence Activated Cell Sorting (FACS)

The ability of Flt-1_{D2} to bind to VEGF was assessed, indirectly, by an *in vitro* competition assay performed on HUVEC cells. Flt-1_{D2} was used as a competitor of the interaction between a biotin-conjugated VEGF and its receptors present on HUVEC membrane. The cells were incubated with VEGF-biotin that binds to the receptors on membrane surface, in absence or in presence of Flt1_{D2}. The amount of VEGF-biotin bound to the cell surface was revealed with FITC-avidin, measuring the intensity of fluorescence, through cytofluorometry analysis.

The signal indicating the binding of VEGF-biotin to receptors on the surface of HUVEC cells (green curve in Figure 39) significantly decreases in presence of Flt-1_{D2} (yellow curve). The specificity of the signal was confirmed by blocking the VEGF with an anti-human VEGF antibody (blue curve), in fact, the intensity of fluorescence decreased similarly in both experiments. This experiment indicates that the recombinant receptor domain is able to bind to VEGF and competes with the cell membrane receptors in their binding the growth factor.

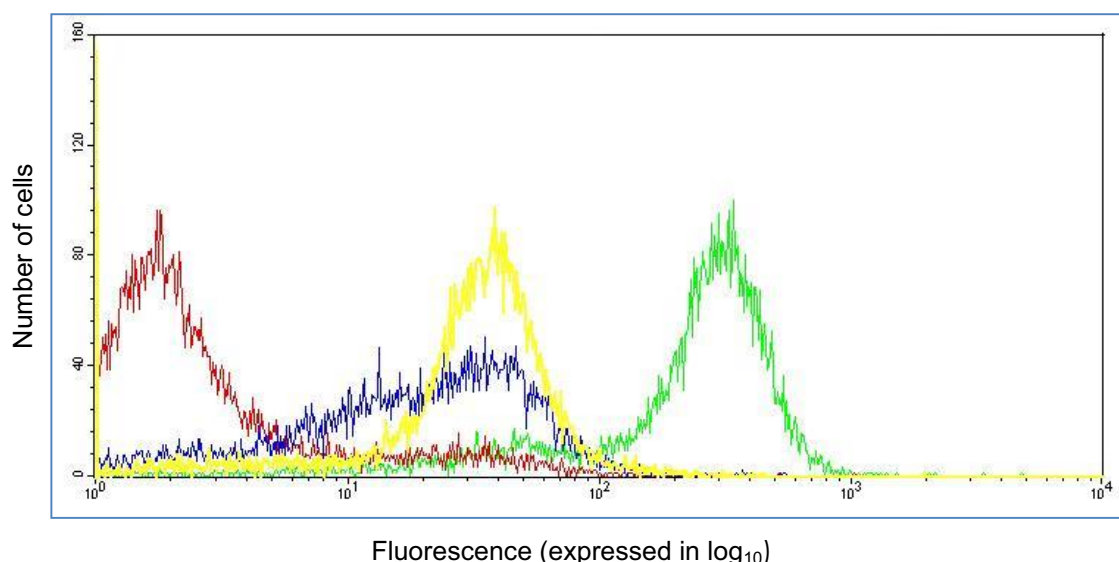


Figure 39 Analysis of the binding of VEGF-biotin to receptors on HUVEC cell membrane. The **red** curve represents the cells incubated with a not specific biotinylated protein + FITC-avidin (negative control); the **green** curve shows the cells treated with VEGF-biotin + FITC-avidin (positive control); the **blue** curve represents the cells incubated with VEGF-biotin + FITC-avidin in the presence of anti-human VEGF IgG that blocks VEGF, and the **yellow** curve indicates the cells incubated with VEGF-biotin + FITC-avidin in the presence of Flt-1_{D2}.

Expression, refolding and purification of ¹⁵N-Flt-1_{D2}

E. coli JM101 cells were inoculated in M9 medium, containing 1g/L ¹⁵NH₄Cl as the sole nitrogen source, and grown overnight at 37°C. The harvested cells were lysed with 37% HCl and the mixture of single ¹⁵N labeled amino acids was used to enrich M9 medium for the expression of Flt-1_{D2} in BL21 *Codon Plus* (DE3) strain previously transformed with pETM11-*flt-1*_{D2} recombinant expression vector. Refolding and purification of the labeled Flt-1_{D2} (referred to as ¹⁵N-Flt-1_{D2}) were successfully performed using the same conditions described for the unlabeled protein. The yield of ¹⁵N-Flt-1_{D2} was comparable to that obtained for the unlabeled protein. The homogeneous product was concentrated until 0.22 mM and employed, together with the unlabeled protein, in protein-peptide NMR interaction studies.

CD spectroscopic analysis

CD spectroscopic analyses were performed on both labeled and unlabeled proteins. Proteins were tested at a concentration of 15 μM in 20 mM phosphate buffer, pH 7.0 and spectra were recorded at 20°C in the range 190-260 nm. The overall far-UV CD spectrum of Flt-1_{D2} at neutral pH is shown in Figure 40. It indicates that the protein has high β-sheet content, with two negative bands at about 198 nm and 214 nm, suggesting that the protein assumes the correct fold expected for an immunoglobulin-like domain and in agreement with data reported in the literature (Wiesmann, C. *et al.*, 1997 and Starovasnik, M. A. *et al.*, 1999).

To perform heat-denaturation experiments, the proteins under test were dissolved in 20 mM phosphate buffer, pH 7.0 at a concentration of 15 μM. Thermal unfolding curve of Flt-1_{D2} is shown in Figure 41. The curve shows a sigmoidal behavior, with a single transition and a T_m of about 60°C, indicating that a two-state unfolding

process occurred for the protein. Moreover, thermal unfolding was found to be reversible when temperature was lowered again to 10°C (data not shown).

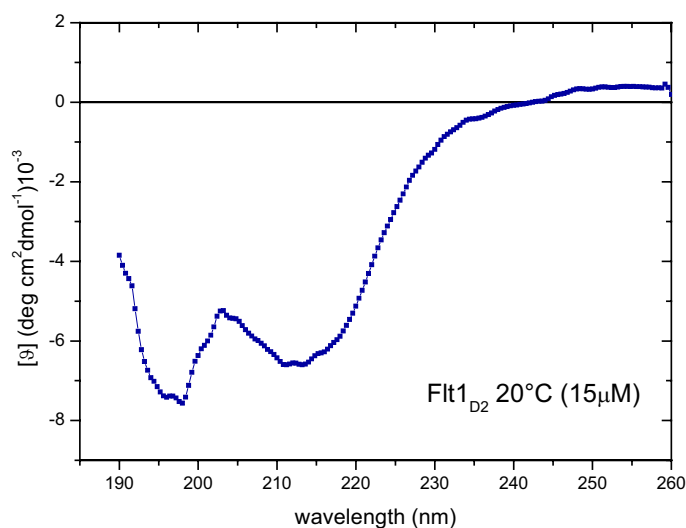


Figure 40_ Far-UV CD spectrum of Flt1_{D2} recorded at 20°C, diluting the protein in phosphate buffer 20 mM, pH 7.

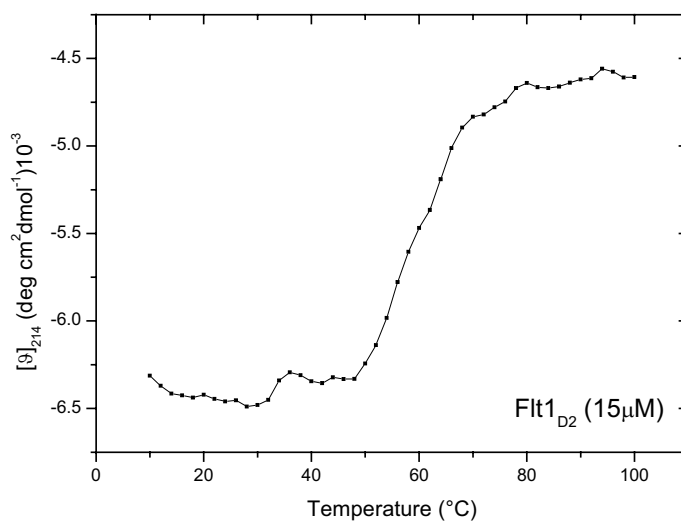


Figure 41_ CD spectrum of Flt1_{D2} thermal unfolding analysis. The protein was tested in phosphate buffer 20 mM, pH 7 at 214 nm, increasing the temperature from 10°C to 100°C. Estimated T_m was about 60°C.

Proteins secondary structure content

In order to assess the secondary structure of Flt-1_{D2} proteins, we performed far-UV CD analyses using different methods to analyze CD spectra and estimate their secondary structure content. Circular dichroism is, in fact, an excellent tool for rapid determination of the secondary structure and folding properties of proteins. The

analysis of the secondary structure composition was performed on Flt-1_{D2} following the programs Continll, Selcon3 and CDSSTR of the CDPro software package and one of the most widely used neural networks program: CDNN. An additional method, Cluster, was employed for determination of tertiary structure class. CDPro programs were run using different sets of model proteins, as illustrated in Table 4. All these analyses indicate that Flt-1_{D2} adopts prevalently a β -sheet structure (Tables 4-7). These data are consisted with the analysis by the program Cluster, that determined an *all beta* tertiary structure class for Flt-1_{D2}, and in agreement with the DSSP (Kabsch, W. *et al.* 1983) analysis performed on X-Ray and NMR structures of the protein (Table 7).

Ref. Prot. Set.	Program	% PP2	% Helix	% Sheet	% Turn	% Unrd
SP22X	Continll	11.2	3.8	28.4	12.3	44.3
	Selcon3	12	7.9	24.2	12	42.6
	CDSSTR	10.4	4.6	27.6	13.5	43.1
SP37A	Continll	9.6	3.5	25.5	11.6	49.8
	Selcon3	10.2	5.2	24.1	12.6	50.3
	CDSSTR	8.5	1.7	27	13.4	48.9
SP29	Continll		4.4	38.3	21.5	35.8
	Selcon3	n.d.	7.2	36.8	21.7	36.4
	CDSSTR		4.2	36.9	24	34.9
SDP48	Continll		3.2	33.9	18.7	44.2
	Selcon3	n.d.	4.4	32.7	19.7	41.6
	CDSSTR		3.7	33.9	19.7	42.9

Table 4_ Predictions of Flt-1_{D2} secondary structure resulting from the use of different sets of proteins derived from different source and combined to create a large reference set of CD spectra. In this table are reported the predictions derived from the use of Continll, Selcon3 and CDSSTR programs with SP22X, SP37A, SP29 and SDP48 sets consisting in reference CD spectra of 22, 37, 29 and 48 proteins, respectively. The first three sets comprise soluble proteins, the latter also denatured proteins. SP29 and SP22X work in the wavelength range 178-260 nm, while SP37A and SDP48 in ranges 185-240 nm and 190-240 nm, respectively.

CDNN, employed in the analysis of Flt-1_{D2} CD spectra, is a program of artificial intelligence used to analyze data of interest and determine helix, β -structure, and turns contents of them, reminding the information previously acquired from the analysis of known proteins. A neural network is, in fact, first trained using a set of known proteins, so that the input of the CD at each wavelength results in the output of the correct secondary structure. The trained network is then used to analyze

unknown proteins. Below, in Tables 5 and 6, are reported the results obtaining from Flt-1_{D2} CDNN analysis, starting from two sets of globular reference proteins consisting in 23 and 33 elements, respectively.

Table 5_ CDNN 2.1 (Spectra basis 23)

	180-260 nm	185-260 nm	190-260 nm	195-260 nm	200-260 nm	205-260 nm	210-260 nm
Helix	n.d.	n.d.	13,1%	12,5%	12,1%	12,3%	11,0%
Antiparallel	n.d.	n.d.	39,8%	40,6%	42,7%	41,9%	44,7%
Parallel	n.d.	n.d.	4,4%	5,2%	5,5%	5,5%	5,3%
Beta-Turn	n.d.	n.d.	20,9%	21,2%	21,7%	21,8%	22,1%
Rndm. Coil	n.d.	n.d.	32,8%	33,8%	36,3%	37,1%	35,5%
Total Sum	-	-	111,0%	113,4%	118,3%	118,6%	118,6%

Table 6_ CDNN 2.1 (Spectra basis 33)

	180-260 nm	185-260 nm	190-260 nm	195-260 nm	200-260 nm	205-260 nm	210-260 nm
Helix	n.d.	n.d.	6,8%	8,0%	8,2%	6,5%	7,0%
Antiparallel	n.d.	n.d.	35,0%	33,3%	34,5%	34,5%	35,6%
Parallel	n.d.	n.d.	3,4%	4,7%	5,3%	5,4%	5,4%
Beta-Turn	n.d.	n.d.	19,7%	20,6%	21,2%	20,2%	19,4%
Rndm. Coil	n.d.	n.d.	35,2%	35,9%	36,9%	35,2%	35,3%
Total Sum	-	-	100,1%	102,6%	106,2%	101,7%	102,7%

Starting from X-Ray and NMR structures of the second domain of Flt-1_{D2} (Wiesmann, C. *et al.*, 1997 and Starovasnik, M. A. *et al.*, 1999), the program DSSP calculated another set of values to describe the secondary structure content of the protein. The DSSP program was designed to standardize secondary structure assignments. DSSP is a database of secondary structure assignment for all proteins entries in the Protein Data Bank (PDB). In this case, we obtained a similar percentage of β -sheet content for both crystal and in solution structures (Table 7), in agreement with data collected on the refolded Flt-1_{D2} by running CDPro and CDNN programs.

Table 7

Program	% Alpha	% Beta	% Random
DSSP-NMRFlt-1 _{D2}	5	41	54
DSSP-XRayFlt-1 _{D2}	3	47	50

NMR Characterization of Flt-1_{D2}

The NMR characterization of Flt-1_{D2} and the interaction studies with peptides and library were performed in collaboration with Prof. Roberto Fattorusso and Dr. Donatella Diana (Dipartimento di Scienze Ambientali, Seconda Università di Napoli, Caserta).

All the analyses performed on the recombinant second domain of VEGFR-1 expressed in BL21 *Codon Plus* (DE3) RIL were indicative of the correct fold assumed by the protein after the “on column refolding”. In Figure 42 is showed the one-dimensional ¹H spectrum of Flt-1_{D2}, while in Figure 43 its 2D [¹H, ¹H] NOESY spectrum. Both mono- and bi-dimensional spectra are the most conclusive evidence that Flt1_{D2} adopts a globular conformation, showing good chemical shift dispersion and several intra- and inter-residue NOEs, according to data yet reported in the literature (Starovasnik, M. A. *et al.*, 1999). In Figure 44 is reported the ¹H/¹⁵N-HSQC spectrum of ¹⁵N-Flt1_{D2} that shows a good chemical shift dispersion in amide region (6.5-9.5 ppm), suggesting that the protein folds into a unique well defined structure.

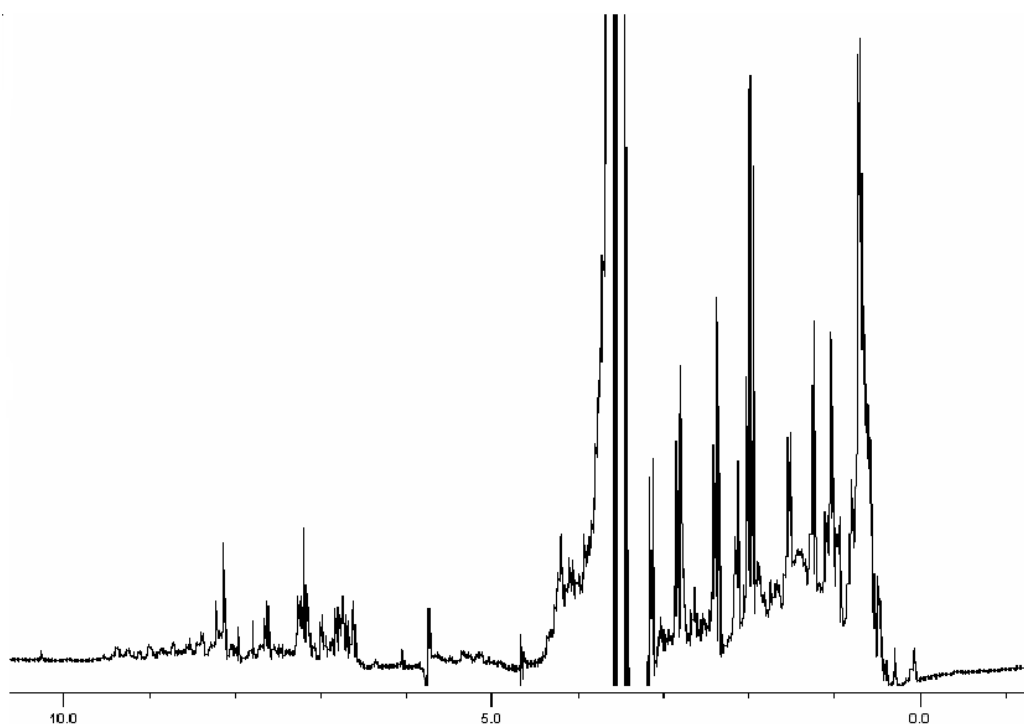


Figure 42_ One-dimensional ¹H-NMR spectrum of Flt-1_{D2} protein, acquired at 298 K in H₂O/D₂O mixture at pH 7.0.

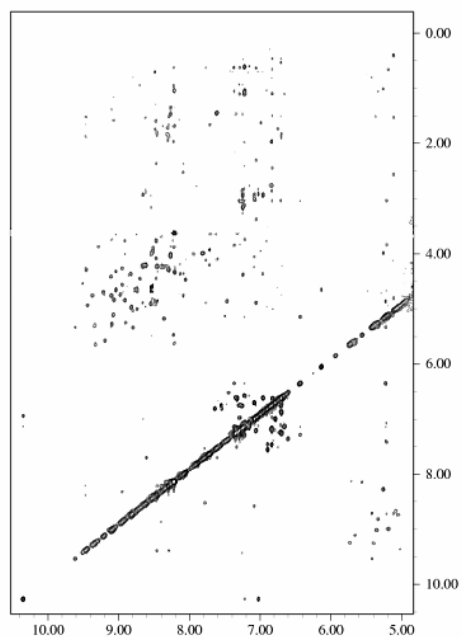


Figure 43_ A section of the 2D [^1H , ^1H] NOESY spectrum (100 ms mixing period) recorded at 298 K and 600 MHz is shown.

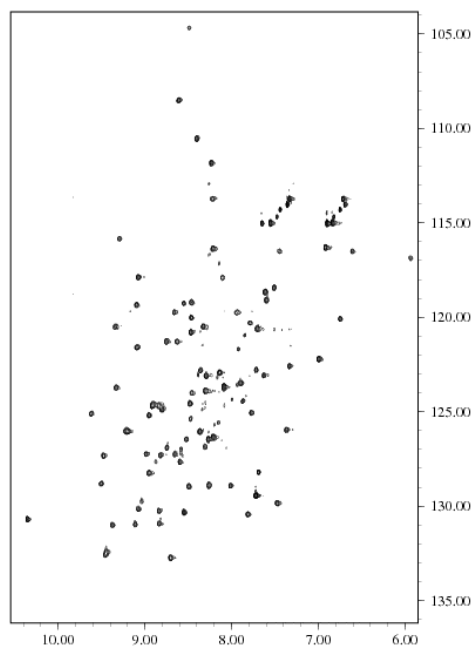


Figure 44_ $^1\text{H}/^{15}\text{N}$ -HSQC spectrum of ^{15}N -Flt-1_{D2} protein recorded at 25°C with a spectral width of 2066 Hz.

NMR analysis of peptide-protein interaction

Despite their conformational similarity, QK and MA peptides show a different biological activity, since the first has an agonist-like activity (D'Andrea, L. D. *et al.*, 2005), while the second shows an interesting antagonist behavior compared with VEGF (Del Gatto, A. PhD thesis, 2005). QK and MA were employed in binding studies with Flt-1_{D2} aimed to investigate the nature of this interaction and to better understand their behavior from a molecular point of view.

Identification of the binding site on Flt-1_{D2} via Chemical Shift Mapping

To map the binding site of Flt-1_{D2}, were used NMR titration experiments, monitoring the interaction between QK peptide and the protein. Upon progressive additions of QK to the free ¹⁵N-Flt-1_{D2} (Table 8), were observed continuous changes in ¹H and ¹⁵N chemical shifts for several signals of ¹⁵N-Flt-1_{D2} in 2D [¹H, ¹⁵N] HSQC spectra. These chemical shifts changes indicated the formation of the complex ¹⁵N-Flt-1_{D2}/QK in intermediate and in fast exchange on the NMR scale. Flt-1_{D2} residues with the most significant changes in ¹H and ¹⁵N chemical shifts ($\Delta\delta > 0.04$ ppm) upon formation of the complex were mapped onto the NMR solution structure of Flt-1_{D2} and are located in the strand βf (E₂₀₁, I₂₀₂, G₂₀₃, L₂₀₄, T₂₀₅), the strand βg (L₂₁₅, Y₂₁₆, K₂₁₇, R₂₁₉, Y₂₂₀, L₂₂₁), the loop between the strand $\beta a'$ and βb (K₁₇₀, F₁₇₂, P₁₇₃, L₁₇₄) and the region spanning the amino acid sequence Y₁₃₉, S₁₄₀, E₁₄₁, I₁₄₂, E₁₄₄, as showed in Figure 45.

¹⁵ N-Flt-1 _{D2} (μ M)	[QK] (μ M)	¹⁵ N-Flt-1 _{D2} :QK Ratio
220	0	1:0
220	55	1:0.25
220	100	1:0.50
220	165	1:0.75
220	220	1:1
220	440	1:2
220	660	1:3

Table 8 _ Concentrations of ¹⁵N-Flt-1_{D2} protein and QK peptide used in the titration experiments. In the table is also reported the molar ratio protein:peptide determined for each concentration of both species.

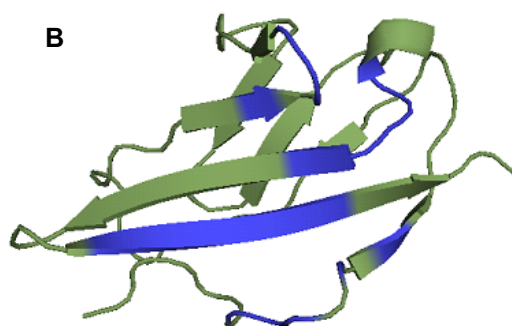
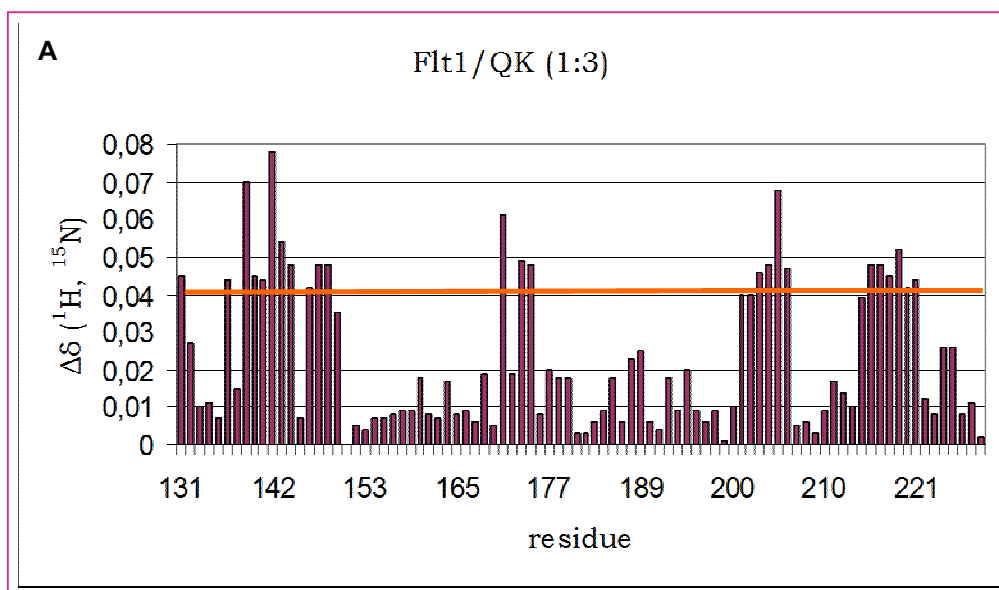


Figure 45_ Panel A, histogram of the variations of the chemical shifts ($\Delta\delta$ ppm) observed in 2D [^1H , ^{15}N] HSQC spectra of the free Flt-1 $_{\text{D}2}$ and in presence of 3 equivalents of QK peptide. Panel B, the ribbon model of the NMR structure of Flt-1 $_{\text{D}2}$ (1QSV.pdb). The amino acids that undergo significant chemical shift changes upon formation of Flt-1 $_{\text{D}2}$ /QK complex were mapped in blue onto the ribbon model.

Next, similar experiments were carried out for MA peptide. As observed for the ^{15}N -Flt-1 $_{\text{D}2}$ /QK complex, progressive additions of MA to the sample containing the ^{15}N -labeled Flt-1 $_{\text{D}2}$ (Table 9) resulted in significant chemical shift changes ($\Delta\delta > 0.07$ ppm) for several signals in 2D [^1H , ^{15}N] HSQC spectra of the free ^{15}N -Flt-1 $_{\text{D}2}$. Again, this indicates formation of a complex ^{15}N -Flt-1 $_{\text{D}2}$ /MA.

$[^{15}\text{N-FIt-1}_{\text{D}_2}]$ (μM)	[MA] (μM)	$^{15}\text{N-FIt-1}_{\text{D}_2}:\text{MA}$ Ratio
220	0	1:0
220	55	1:0.25
220	100	1:0.50
220	165	1:0.75
220	220	1:1
220	440	1:2

Table 9_ Concentrations of $^{15}\text{N-FIt-1}_{\text{D}_2}$ protein and MA peptide used in the titration experiments. In the table is also reported the molar ratio protein:peptide determined for each concentration of both species.

When mapped onto the solution structure of the free FIt-1_{D2}, the residues of the refolded protein, upon formation of the complex with MA peptide, displayed significant chemical shift changes. They are located on a discontinuous surface defined by strands βb (L₁₆₉, K₁₇₀, P₁₇₂), βf (E₂₀₈, A₂₀₉), βg (V₂₁₁, L₂₁₅, K₂₁₇, N₂₁₉), and on a flexible region localized at the N-terminus (R₁₃₃, P₁₃₅, Y₁₃₉, S₁₄₀), as shown in Figure 46.

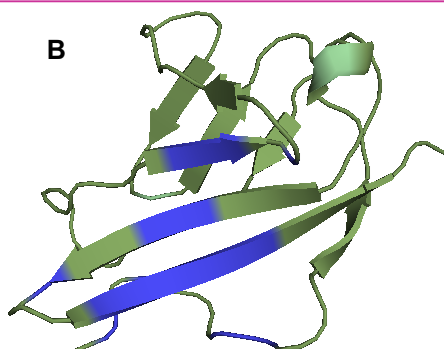
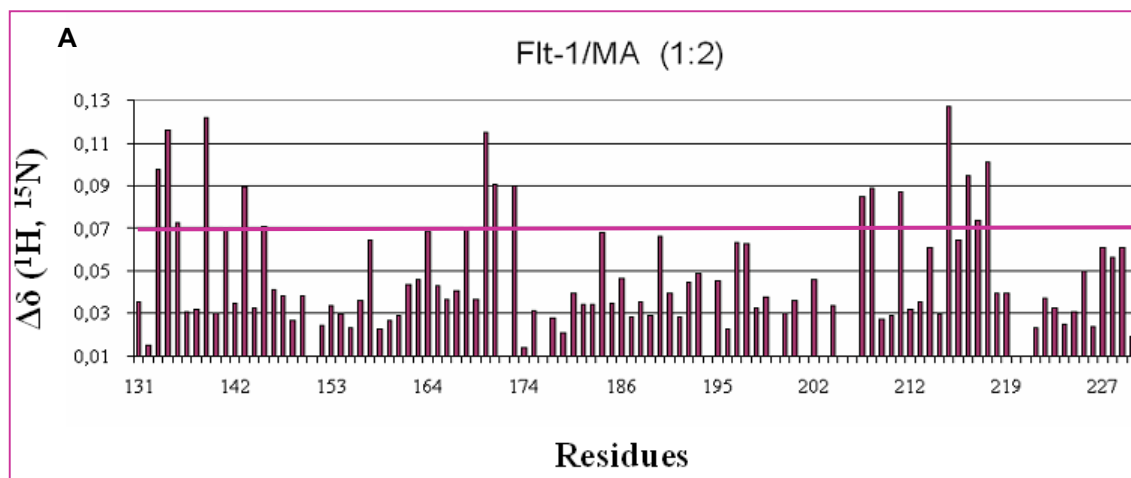


Figure 46_ Panel A, histogram of the variations in chemical shifts ($\Delta\delta$ ppm) observed in 2D [^1H , ^{15}N] HSQC spectra of the free FIt-1_{D2} and in presence of 2 equivalent of MA peptide. Panel B, the ribbon model of the NMR structure of FIt-1_{D2} (1QSV.pdb). The amino acids that undergo significant chemical shift changes upon formation of FIt-1_{D2}/MA complex were mapped in blue onto the ribbon model.

Epitope Mapping of QK and MA peptides bound to Flt-1_{D2} via Saturation Transfer Difference

To provide additional information regarding the interaction between peptides and Flt-1_{D2}, at atomic resolution, STD (*Saturation Transfer Difference*) NMR experiments were performed. Without the unlabeled protein, STD spectra did not contain ligand signals because saturation transfer does not occur. The sample containing Flt-1_{D2} protein was the only one to show saturation transfer from the protein to their ligands in STD spectra.

STD NMR studies provided peptide's binding epitope for both QK and MA and were used to classify the residues relevant for the interaction with Flt-1_{D2}. STD spectra were recorded studying the unlabeled Flt-1_{D2}/peptide complex and, in the case of QK, clearly demonstrate the involvement of the aromatic region protons of the residues such as W₄, Y₈, Y₁₂. For the side chain of Q₅ and Q₉ the signal of NεH protons has similar large intensities (Figure 47).

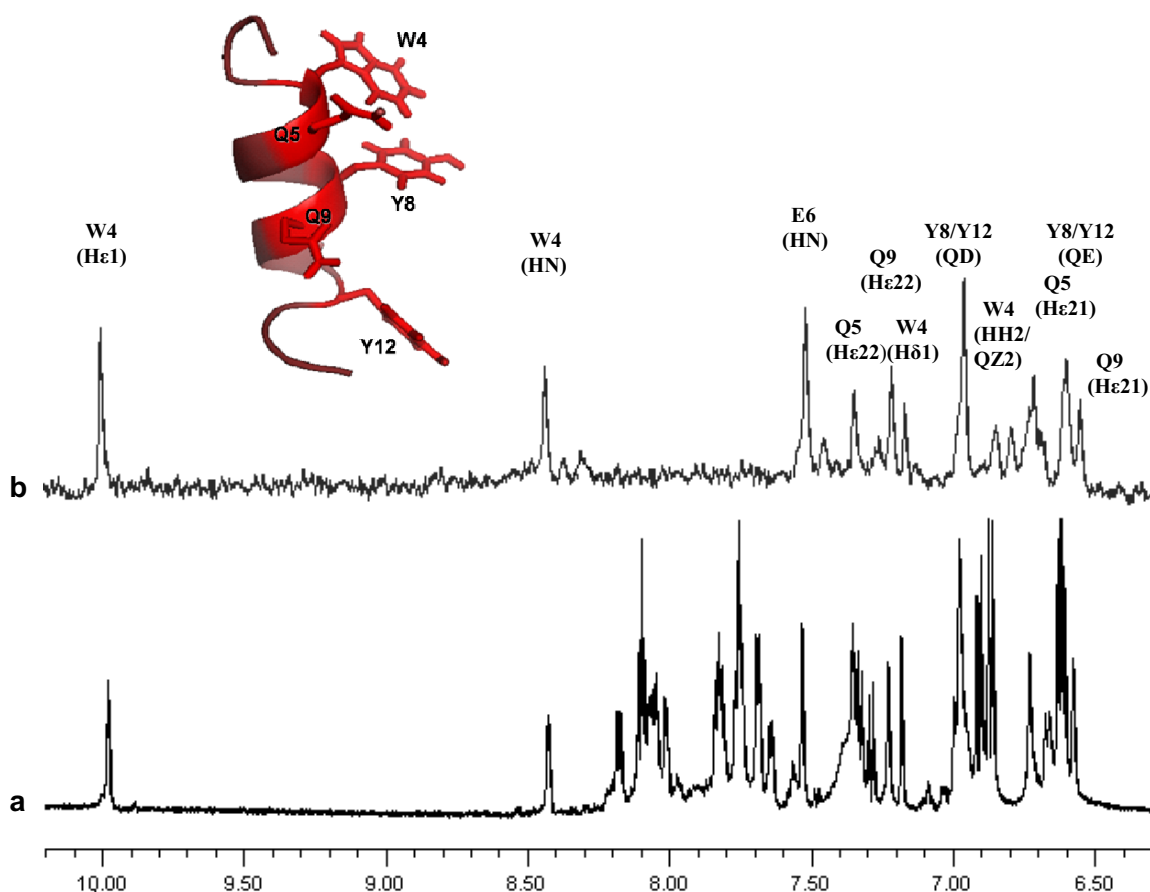


Figure 47_ a) expansion of the amide and aromatic region of ¹H NMR spectrum of QK alone. b) expansion of the region containing resonances of the amide and aromatic protons of STD spectrum for a QK:Flt-1_{D2} ratio of 1:20. In red is shown the backbone of the QK representative structure; side chain of the interacting residues with the Flt1_{D2} are shown.

For MA peptide, the strongest interactions are attributed to the aromatic protons of W₄, Y₈ and Y₁₂ and to NεH protons of the residue Q₉. Expansions of the region containing resonances of the amide and aromatic region are shown in Figure 48.

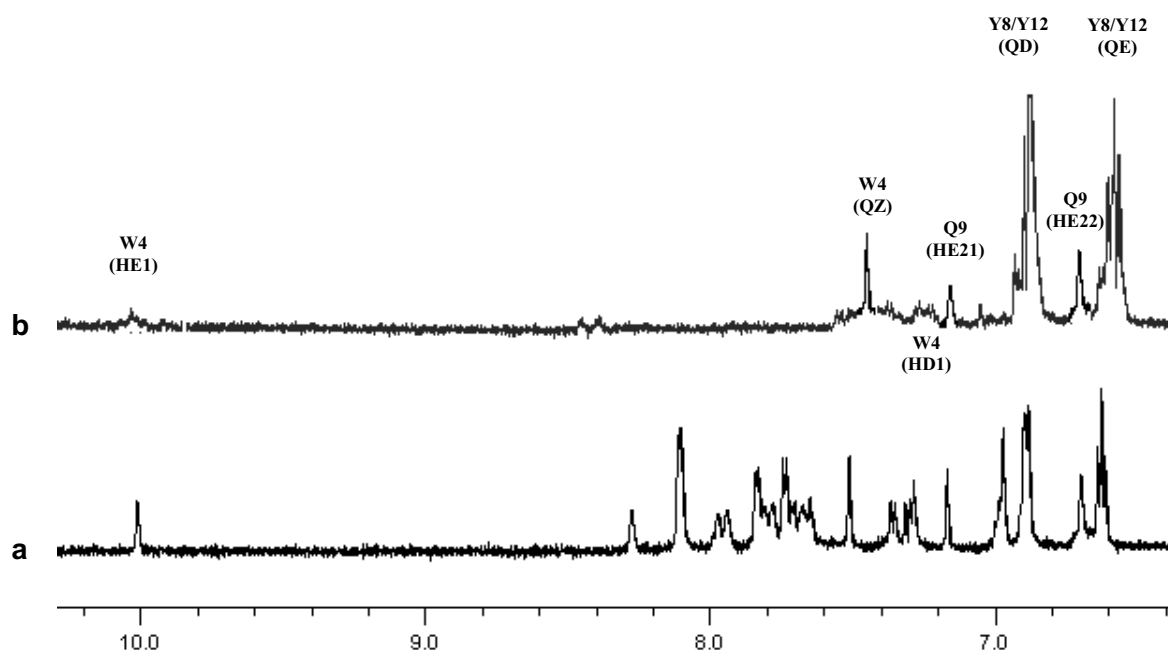


Figure 48 a) expansion of the amide and aromatic region of ¹H NMR spectrum of MA alone. b) expansion of the region containing resonances of the amide and aromatic protons of STD spectrum for a MA:Flt-1_{D2} ratio of 1:20.

Flt-1_{D2} was also employed in the screening of a small organic molecules library, but data obtained are preliminary. Seven compounds (3% of the library) were selected after two screening cycles, but the work is in progress to improve these molecules.

Discussion

In recent years the study of the mechanisms of angiogenesis and the research of new molecules able to modulate this process have been among the most well funded fields of the medical research. A strong clinical interest has emerged in developing anti-angiogenesis agents as therapeutic strategies for inhibiting tumor growth and metastasis, as well as a variety of other pathologies. Progresses towards a therapeutic treatment culminated, in 2004, in the approval of the first antiangiogenic agents for gastrointestinal cancer (Hurwitz, H. *et al.*, 2004). On the other hand, therapeutic angiogenesis, consisting in promoting new vessel growth to treat disorders, such as ischemia, is an exciting frontier of cardiovascular medicine.

The aim of this work is the expression of the extracellular domains of VEGF receptors KDR and Flt-1, in order to characterize them *via* NMR studies. Structural data on the extracellular portion of the receptors are, in fact, still very limited. The only structural data about Flt-1 receptor regards the domain 2 of the extracellular region that has been described in the free form (Starovanik, M. A. *et al.*, 1999), bound to VEGF (Wiesmann, C. *et al.*, 1997) or PlGF (Christinger, H. W. *et al.*, 2004). So far, no structural data have been reported for Flt-4 and the extracellular domains of KDR. Instead, KDR intracellular kinase domain has been described (McTigue, M. A. *et al.*, 1999). A partial characterization of NRP-1 and NRP-2 receptors has been performed (Pellet-Many, C. *et al.*, 2008) and, very recently, the complex between VEGF and the extracellular Flt-1 domain has been observed by electron microscopy (Ruch, C. *et al.* 2007). Hence, to extend the structural information about VEGF receptors is a very attractive goal. Besides, our intention is to test the binding capacity of the recombinant domains in interaction experiments with small synthetic peptides to understand the molecular bases of the interaction between VEGF receptors and its selected agonists/antagonists. This represents, in fact, an important step towards the designing of therapeutic approaches aimed at the treatment or prevention of angiogenic diseases. Finally, our aim is to employ the recombinant domains in drug discovery studies by targeting phage or small organic molecules libraries since, to date, no small organic molecules have been identified to target VEGF receptors in their extracellular portion.

Flt-1 and KDR extracellular domains have been cloned successfully in several expression systems and expressed in *Escherichia coli*. *E. coli* is a very suitable host for the over-expression of heterologous proteins whose activity does not request post-translational modifications and allows achieving greater efficiency, reproducibility and convenience than mammalian cells. VEGF receptors contain several putative N-glycosylation sites and the mature proteins are extensively glycosylated, but this post-translational modification is not a prerequisite of high affinity binding of receptors to VEGF (Barleon, B. *et al.*, 1997). Besides, in spite of mammalian cells, it is possible to grow *E. coli* strains in minimum medium, in order to express labeled proteins for characterization studies, without affecting physiology of bacterial cells. In addition, most of the commercially available receptors are Fc-IgG chimeras, resulting impossible to study *via* NMR because of their dimension and costs. Instead, the bacterial expression systems designed for the expression in *E. coli* enable to produce the recombinant proteins fused to a convenient tag which can be removed.

Thus, the different constructs introduced in bacterial host cells allowed, for most of them, achieving high yields of recombinant receptors domains. In some cases, however, the limiting step was just the expression, as, for example, for KDR_{D1-2}.

Despite different cloning strategies and the optimization of their expression conditions, the first two domains of KDR receptor have never been expressed. The domain 2, instead, was expressed, but was not possible to purify it, because, either under native or denaturing conditions and, in spite of its N-terminal 6xHis-tag, it did not bind to the Ni²⁺-NTA resin. In addition, even if for each recombinant construct have been tested several conditions to optimize the expression of proteins of interest and try to get them in soluble form, no domain of both receptors was soluble expressed, but all proteins were extracted with denaturing agents from inclusion bodies and refolded. On the other hand, refolding was not always successfully and the difficulty to obtain a refolded protein from inclusion bodies in sufficient amount made so far impossible further structural and functional studies for their characterization. These negative results make clear how difficult is to express these proteins and reflect the absence, in the literature, of extensive structural information on KDR and Flt-1 extracellular domains.

Instead, it was developed an experimental protocol for refolding and purification of the second domain of VEGF Flt-1 receptor. The structure of Flt-1_{D2} has been solved either by X-Ray (complexed with VEGF) (Wiesmann, C. *et al.* 1997) or by NMR studies (Starovasnik, MA *et al.* 1999). In both cases, the protein was cloned and expressed in *E. coli* as inclusion bodies and refolded. Despite these available protocols, we were not able to purify the protein as a homogeneous product. In fact, according to Wiesmann *et al.*, the construct comprising residues 129-229 was expressed as an insoluble protein in *E. coli* and inclusion bodies were treated with 6 M urea in 20 mM Tris-HCl, pH 7.5. Flt-1_{D2} was then refolded in two step dialysis by diluting the above solution in 6 M urea to 0.05 mg/mL. But in the last step Flt-1_{D2} precipitated. On the other hand, Starovasnik *et al.* proposed first the purification of the protein by affinity chromatography under denaturing conditions, then by reversed-phase HPLC, in order to separate the *folded* Flt-1_{D2} from the *unfolded* form (Starovasnik, M. A. *et al.*, 1999). Consequently, the case would have requested an additional refolding step, but, also this method failed. Our protocol consists of the expression of the recombinant 6xHis-tagged Flt-1_{D2} in *E. coli* BL21 *Codon Plus* (DE3) strain. The protein, expressed as inclusion bodies, is refolded by an “on column refolding” protocol which resulted determinant for succeeding in the production to homogeneity of the second domain of VEGF Flt-1 receptor. The protein was, in fact, first refolded, still bound to the resin Ni²⁺-NTA, and then eluted in Tris buffer containing high concentration of imidazole. This strategy allowed making refolding in relatively shorter time than step dialysis and with less amount of urea. Besides, only two purification steps of affinity chromatography occurred, after which the homogeneous Flt-1_{D2} was concentrated to 3.5 mg/mL. Hence, the final product was analyzed to investigate its conformational and functional properties using a multidisciplinary approach.

Protein Alkylation was performed to analyze the oxidation state of its two cysteine residues on both reduced and not reduced samples and showed that, in non reducing conditions, no alkylated adducts were found, while, in presence of DTT, the main product presented the two cysteine residues alkylated with an increment of 58 Da for each thiol group derived from reduction reaction. This experiment shows that in the refolded Flt-1_{D2} the two cysteine residues are involved in the formation of a disulfide bridge, as expected from literature data (Wiesmann, C. *et al.*, 1997). Besides, the partial digestion with trypsin demonstrated the compact structure of the Ig-like domain, suggesting again the correct fold of the refolded protein.

Conformation preference of the recombinant Flt-1_{D2} was inspected by circular dichroism analyses. The content in secondary structure derived from the CD spectra analysis was in agreement with X-Ray data reported for Flt-1_{D2} (Wiesmann, C. *et al.*, 1997), prevalently folded in a β -sheet structure. Thermal unfolding analysis showed a sigmoidal curve, with a single transition (T_m of about 60°C), indicating that a two-state unfolding process occurred. Moreover, thermal unfolding was reversible.

In addition, the functionality of Flt-1_{D2} was assessed with a competition assay performed on HUVEC cells. The experiment verified the capability of the Flt-1 second domain to bind to VEGF, interfering with the interaction VEGF/receptors on HUVEC membrane.

The results were fully confirmed by NMR studies conducted on both ¹⁵N-labeled and unlabeled proteins. Protonic mono- and bi-dimensional spectra of the unlabeled protein show the same strong signal dispersion of chemical shifts reported in the literature (Starovasnik, MA *et al.* 1999). The ¹H/¹⁵N-HSQC spectrum of the uniformly ¹⁵N-labeled sample indicates that the global fold of the refolded Flt-1_{D2} is very similar in that reported by Starovasnik and in the crystalline state complexed to VEGF (Wiesmann, C. *et al.*, 1997). We used the protein in order to understand the molecular bases of the interaction with two rationally designed peptides: QK and MA (D'Andrea, L. D. *et al.*, 2005 and Del Gatto, A. PhD thesis, 2005). This would be the start point for the optimization and stabilization of that features which these molecules need to be used as good modulators in angiogenesis.

QK and MA differ in their sequence for only two amino acid residues, but the first acts as an agonist of VEGF (D'Andrea, L. D. *et al.*, 2005), while MA is a VEGF antagonist (Del Gatto, A. PhD thesis, 2005). In the literature are reported evidences that QK competes with VEGF for a binding site on endothelial cells expressing both KDR and Flt-1 receptors (D'Andrea, L. D. *et al.*, 2005). The peptide binds to and activates both receptors similarly to VEGF and its agonist-like behavior is confirmed by *in vitro* and *in vivo* cell proliferation experiments. Although QK was designed to bind to KDR and Flt-1, its agonist-like activity is surprising because receptor dimerization is necessary for receptor activation and QK is a small peptide, probably unable to induce receptor dimerization by itself. Maybe, QK binding induces a conformational change of the receptor that either triggers, in an unknown way, the dimerization or induces the receptor activation through a different, previously uncharacterized mechanism that may not require dimerization. To address this issue, further structural and biochemical studies are needed.

The interaction with peptides occurred following two approaches: one based on ligand observation, through Saturation Transfer Difference experiments, the other on observation of the protein, with Chemical Shift Mapping analysis.

The interaction studies with QK peptide identified the binding site on protein surface through analysis of chemical shift perturbations of ¹⁵N-Flt-1_{D2}. For this purpose were recorded 2D [¹⁵N, ¹H] HSQC spectra of the protein, adding increasing amounts of peptide.

From variations in chemical shifts induced by QK on ¹⁵N-Flt-1_{D2}, significant changes in the fast exchange regime, in respect to the time scale of NMR, are identified for the strand β f (E₂₀₁, I₂₀₂, G₂₀₃, L₂₀₄, T₂₀₅), the strand β g (L₂₁₅, Y₂₁₆, K₂₁₇, R₂₁₉, Y₂₂₀, L₂₂₁), the loop between strand β a' and β b (K₁₇₀, F₁₇₂, P₁₇₃, L₁₇₄) and the region comprising residues Y₁₃₉, S₁₄₀, E₁₄₁, I₁₄₂, E₁₄₄.

On the other hand, STD experiments have identified peptide's binding epitope, confirming the involvement of side chains of amino acids W₄, Q₅, Y₈, Q₉, Y₁₂ in interacting with the receptor.

Similar experiments were carried out for MA peptide. Progressive additions of MA to the sample containing the ^{15}N -labeled Flt-1_{D2} result in significant chemical shift changes for several signals in the [^1H , ^{15}N] HSQC spectra of the free ^{15}N -Flt-1_{D2}, indicating, again, the formation of a complex ^{15}N -Flt-1_{D2}/MA. When mapped onto the solution structure of the free Flt-1_{D2}, the residues displaying significant chemical shift changes are mapped on a discontinuous surface defined by strands βb (L₁₆₉, K₁₇₀, P₁₇₂), βf (E₂₀₈, A₂₀₉), βg (V₂₁₁, L₂₁₅, K₂₁₇, N₂₁₉), and on a flexible region localized at the N-terminus (R₁₃₃, P₁₃₅, Y₁₃₉, S₁₄₀). For MA peptide, the strongest interactions are attributed to the aromatic protons of W₄, Y₈ and Y₁₂ and to N ϵ H protons of the residue Q₉.

Although peptides binding epitopes are clearly overlapping, NMR data indicate that QK and MA bind Flt-1_{D2} in distinct ways. In fact, on protein surface, QK induces chemical shift changes that are not observed in the case of the interaction with MA. On the basis of the chemical shift analysis, QK interacts with Flt-1_{D2} through β -strands βg and $\beta a'$ and βc - $\beta c'$ loop region, whereas MA interacts more extensively with the residues located on the strands βc and βf . However, it is evident that both peptides bind to a region of Flt-1_{D2} protein known to contain the contact surface for VEGF. This region comprises highly positively charged residues, suggesting that ionic interactions play an important role in the binding, as well as hydrophobic interactions.

On the other hand, STD NMR studies of QK and MA peptides in the presence of Flt-1_{D2} show that the aromatic protons of the residues Trp₄, Tyr₈ and Tyr₁₂ interact with the receptor. In addition, the HN side chain of the residues Gln₅ (only for QK) and Gln₉ are recognized, whereas the HN backbone amide protons are less implicated.

The second domain of Flt-1 receptor was also used in the screening of a library of small organic molecules, in order to find new compounds of biotechnology interest for modulating the angiogenesis process. Seven compounds (3% of the library) were selected after two screening cycles, but the work is in progress to improve these molecules.

In conclusion, in this work we cloned and expressed different portions of the extracellular region of KDR and Flt-1 receptors. Only the second domain of Flt-1 receptor was refolded and purified using effective and reliable conditions to produce the protein at NMR concentration, developing an experimental protocol for the "on column refolding" resulted fast, cheap and efficient for our purpose. The protein, even when ^{15}N -labelled expressed, was obtained as a homogeneous product (3.5 mg/mL), without adding VEGF or other cofactors that in the literature are reported to facilitate its concentration (Wiesmann, C. *et al.* 1999). Its proper folding was verified by nuclear magnetic resonance, biochemical and functional analyses. The protein was used in NMR interaction studies with two bioactive peptides and in a drug discovery analysis with the screening of a library of organic compounds. Our next perspective is to deepen the interaction studies with peptides, in order to obtain the dissociation constants of their binding to the second domain of Flt-1 receptor and try to explain their agonist or antagonist activity from a molecular point of view. Regarding the screening of the library, the obtainment of seven compounds to be improved is a very satisfactory result. To date, there are no small organic molecules able to target VEGF receptors in their extracellular portion and to identify new low molecular weight compounds able to act in this way, modulating the interaction between VEGF and its receptors, could be very exciting.

Finally, our intention is to express and refold the other domains of VEGF receptors, in order to characterize them by NMR studies.

References

- Abraham, J. A. et al.** Human basic fibroblast growth factor: nucleotide sequence, genomic organization and expression in mammalian cells. *Cold Spring Harb. Symp. Quant. Biol.* **51** Pt1, 657-668 (1986a).
- Abraham, J. A. et al.** Nucleotide sequence of a bovine clone encoding the angiogenic protein, basic fibroblast growth factor. *Science* **233**, 545-548 (1986b).
- Ago, H. et al.** Crystal structure of basic fibroblast growth factor at 1,6 Å resolution. *J. Biochem.* **110**, 360-363 (1991).
- Aiello, L. P. et al.** Suppression of retinal neovascularization *in vivo* by inhibition of vascular endothelial growth factor (VEGF) using soluble VEGF-receptor chimeric proteins. *Proc. Natl. Acad. Sci. USA* **92**, 10457-10461 (1995).
- Alvarez, R. H. et al.** Biology of platelet-derived growth factor and its involvement in disease. *Mayo. Clin. Proc.* **81**, 1241-1257 (2006).
- Andrae, J. et al.** Role of platelet-derived growth factors in physiology and medicine. *Genes Dev.* **22**, 1276-1312 (2008).
- Asahara, T. et al., and Isner, J.M.** Isolation of putative progenitor endothelial cells for angiogenesis. *Science* **275**, 964-967 (1997).
- Asahara, T. et al.** Tie-2 receptor ligands , angiopoietin-1 and angiopoietin-2, modulate VEGF-induced postnatal neovascularization. *Circ. Res.* **83**, 233-240 (1998).
- Barillari, G. et al.** The basic residues of placenta growth factor type 2 retrieve sequestered angiogenic factors into a soluble form. Implications for tumor angiogenesis. *Am. J. Pathol.* **152**, 1161-1166 (1998).
- Barleon, B. et al.** Mapping of the sites for ligand binding and receptor dimerization at the extracellular domain of the vascular endothelial growth factor receptor Flt-1. *J. Biol. Chem.* **272**, 10382-10388 (1997).
- Bates, D. O. & Curry, F.E.** Vascular endothelial growth factor increases microvascular permeability via a Ca(2+)-dependent pathway. *Am. J. Physiol.* **273**, H687-H694 (1997).
- Beck, L., Jr and D'Amore, P.** Vascular development: cellular and molecular regulation. *FASEB J.* **11**, 365-373 (1997).
- Bennett, S. P. et al.** Growth factors in the treatment of diabetic foot ulcers. *Br. J. Surg.* **90**, 133-146 (2003).
- Bergers, G. et al.** Effects of angiogenesis inhibitors on multistage carcinogenesis in mice. *Science* **284**, 808-812 (1999).
- Boehm, T. et al.** Antiangiogenic therapy of experimental cancer does not induce acquired drug resistance. *Nature* **390**, 404-407 (1997).
- Bohm, G. et al.** Quantitative analysis of protein far-UV CD spectra by neural networks. *Protein Eng.* **5**, 191-195 (1992).
- Bradford, M.** A rapid and sensitive method for the quantitation of microgram quantities of protein utilizing the principle of protein dye-binding. *Anal. Biochem.* **72**, 248-254 (1976).
- Brooks, P. C. et al., and Cheresh D.A.** Integrin $\alpha_v\beta_3$ antagonists promote tumor regression by inducing apoptosis of angiogenic blood vessels. *Cell* **79**, 1157-1164 (1994).
- Brown, L. F. et al.,** Vascular permeability factor/ vascular endothelial growth factor: a multifunctional angiogenic cytokine. *EXS* **79**, 233-269 (1997).

Carmeliet, P. et al. Abnormal blood vessel development and lethality in embryos lacking a single VEGF allele. *Nature* **380**, 435-439 (1996).

Carmeliet, P. Mechanisms of angiogenesis and arteriogenesis. *Nat. Med.* **6**, 389-395 (2000a).

Carmeliet, P. VEGF gene therapy: stimulating angiogenesis or angioma-genesis? *Nat. Med.* **6**, 1102-1103 (2000b).

Carmeliet, P. et al. Synergism between vascular endothelial growth factor contributes to angiogenesis and plasma extravasation in pathological conditions. *Nat. Med.* **7**, 575-583 (2001).

Carmeliet, P. Angiogenesis in health and disease. *Nat. Med.* **9**, 653-660 (2003).

Carmeliet, P. Angiogenesis in life, disease and medicine. *Nature* **438**, 932-936 (2005).

Chaffer, C. L. et al. Aberrant fibroblast growth factor receptor signaling in bladder and other cancers. *Differentiation* **75**, 831-842 (2007).

Christinger, H. W. et al. The crystal structure of PlGF in complex with domain 2 of VEGFR-1. *J. Biol. Chem.* **279**, 10382-10388 (2004).

Claffey, K. P. and Robinson G.S. Regulation of VEGF/VPF expression in tumor cells: consequences for tumor growth and metastasis. *Canc. Metast. Rev.* **15**, 165-176 (1996).

D'Andrea, L. D. et al. Targeting angiogenesis: structural characterization and biological properties of a *de novo* engineered VEGF mimicking peptide. *PNAS* **102**, 14215-14220 (2005).

Dameron, K. M. et al. Control of angiogenesis in fibroblasts by p53 regulation of thrombospondin-1. *Science* **265**, 1582-1584 (1994).

Davis, S. et al., and Yancopoulos, G.D. Isolation of angiopoietin-1, a ligand for the Tie-2 receptor, by secretion-trap expression cloning. *Cell* **87**, 1161-1169 (1996).

Davis, S. and Yancopoulos, G.D. The angiopoietins : Yin and Yang in angiogenesis. *Curr.Top. Microbiol. Immunol.* **237**, 173-185 (1999).

Davis-Smyth, T., Presta, L. G. & Ferrara, N. Mapping the charged residues in the second immunoglobulin-like domain of the vascular endothelial growth factor/placenta growth factor receptor Flt-1 required for binding and structural stability. *J. Biol. Chem.* **273**, 3216-3222 (1998).

DeGrado, W. F. et al. De novo design and structural characterization of proteins and metalloproteins. *Annu. Rev. Biochem.* **68**, 779-819 (1999).

Detmar, M. et al. Hypoxia regulates the expression of vascular permeability factor/vascular endothelial growth factor (VPF/VEGF) and its receptors in human skin. *J. Invest. Dermatol.* **108**, 263-268 (1997).

de Vries, C. et al. The fms-like tyrosine kinase, a receptor for vascular endothelial growth factor. *Science* **255**, 989-991 (1992).

Dnanabal, M. et al. Endostatin induces endothelial cell apoptosis. *J. Biol. Chem.* **274**, 11721-11726 (1999).

Dudar, G.K. et al. A Vascular Endothelial Growth Factor Mimetic Accelerates Gastric Ulcer Healing in an iNOS-Dependent Manner. *Am. J. Physiol. Gastrointest. Liver Physiol.* **295**, 374-381 (2008).

Dvorak, H. F., Brown, L.F., Detmar, M. & Dvorak, A.M. Vascular permeability factor/vascular endothelial growth factor, microvascular hyperpermeability, and angiogenesis. *Am. J. Pathol.* **146**, 1029-1039 (1995).

Dvorak, H. F. How tumors make bad blood vessels and stroma. *Am. J. Pathol.* **162**, 1747-1757 (2003).

Dvorak, H. F. Vascular permeability factor/ vascular endothelial growth factor (VPF/ VEGF, VEGF-A). *Microvascular research* **1**, 97-103 (2006).

Dumont, D. J. et al. Dominant-negative and targeted null mutations in the endothelial receptor tyrosine kinase, tek, reveal a critical role in vasculogenesis of the embryo. *Genes Dev.* **8**, 1897-1909 (1994).

Dumont, D. J. et al. Cardiovascular failure in mouse embryos deficient in VEGF receptor 3. *Science* **282**, 946-949 (1998).

Eichmann, A. et al. Guidance of vascular and neural network formation. *Curr. Opin. Neurobiol.* **15**, 108-115 (2005).

Eliceiri, B.P. and Cheresh, D.A. The role of $\alpha_v\beta_3$ integrins during angiogenesis. *Mol. Med.* **4**, 741-750 (1998).

Eriksson, A. E. et al. Three-dimensional structure of human basic fibroblast growth factor. *Proc. Natl. Acad. Sci. USA* **88**, 3441-3445 (1991).

Fantl, W. et al. Signaling by receptor tyrosine kinases. *Annu. Rev. Biochem.* **62**, 453-481 (1993).

Ferrara, N. et al. Molecular and biological properties of the vascular endothelial growth factor family of proteins. *Endocr. Rev.* **13**, 18-32 (1992).

Ferrara, N. et al. Heterozygous embryonic lethality induced by targeted inactivation of the VEGF gene. *Nature* **380**, 439-442 (1996).

Ferrara, N. & Davis-Smyth, T. The biology of vascular endothelial growth factor. *Endocr. Rev.* **18**, 4-25 (1997).

Ferrara, N. & Alitalo, K. Clinical applications of angiogenic growth factors and their inhibitors. *Nat. Med.* **5**, 1359-1364 (1999).

Ferrara, N. VEGF: an update on biological and therapeutic effects. *Curr. Opin. Biotechnol.* **11**, 617-624 (2000).

Ferrara, N. Role of Vascular endothelial growth factor in physiologic and pathologic angiogenesis: therapeutic implications. *Semin. Oncol.* **29**, 10-14 (2002).

Ferrara, N. et al. The biology of VEGF and its receptors. *Nat. Med.* **9**, 669-676 (2003).

Ferrara, N. et al. Angiogenesis as a therapeutic target. *Nature* **438**, 967-974 (2005).

Fidler, I. J. et al. The implications of angiogenesis for the biology and therapy of cancer metastasis. *Cell* **79**, 185-188 (1994).

Folkman, J. and D'Amore, P. Blood vessel formation: what is its molecular basis? *Cell* **87**, 1153-1155 (1996).

Folkman, J. Angiogenesis in cancer, reumatoid and other diseases. *Nat. Med.* **1**, 27-31 (1995).

Fong, G.H., Rossant, J., Gertsenstein, M. & Breitman, M.L. Role of the Flt-1 receptor tyrosine kinase in regulating the assembly of vascular endothelium. *Nature* **376**, 66-70 (1995).

Fong, G. H., Zhang, L., Bryce, D.M. & Peng, J. Increased hemangioblast commitment, not vascular disorganization, is the primary defect in flt-1 knock-out mice. *Development* **126**, 3015-3025 (1999).

Fredriksson, L. et al. The PDGF family: four gene products form five dimeric isoforms. *Cytokine Growth Factor Rev.* **15**, 197-204 (2004a).

Fredriksson, L. et al. Tissue plasminogen activator is a potent activator of PDGF-CC. *EMBO J.* **23**, 3793-3802 (2004).

Fuh, G. et al. Requirements for binding and signaling of the kinase domain receptor for vascular endothelial growth factor. *J. Biol. Chem.* **273**, 11197-11204 (1998).

Fukumura, D. et al. Hypoxia and acidosis independently up-regulate vascular endothelial growth factor transcription in brain tumors *in vivo*. *Canc. Res.* **61**, 6020-6024 (2001).

George DJ, Kaelin WG Jr. The von Hippel-Lindau protein, vascular endothelial growth factor, and kidney cancer. *N. Engl. J. Med.* **349**, 419-421(2003).

Gerber, H.P., Condorelli, F., Park, J. & Ferrara, N. Differential transcriptional regulation of the two VEGF receptor genes. Flt-1, but not Flk-1/KDR, is up-regulated by hypoxia. *J. Biol. Chem.* **272**, 23659-23667 (1997).

Gerber, H.P., Dixit, V. & Ferrara, N. Vascular endothelial growth factor induces expression of the antiapoptotic proteins Bcl-2 and A1 in vascular endothelial cells. *J. Biol. Chem.* **273**, 13313-13316 (1998a).

Gerber, H. P. et al. VEGF regulates endothelial cell survival by the PI3-kinase/Akt signal transduction pathway. Requirement for Flk-1/KDR activation. *J. Biol. Chem.* **273**, 30366-30343 (1998b).

Gitay-Goren, H. et al. The binding of vascular endothelial growth factor to its receptors is dependent on cell surface-associated heparin-like molecules. *J. Biol. Chem.* **267**, 6093-6098 (1992).

Goldman, C. K. et al. Paracrine expression of a native soluble form of the vascular endothelial growth factor receptor inhibits tumor growth, metastasis and mortality rate. *Proc. Natl. Acad. Sci. USA* **95**, 8795-8800 (1998).

Grunstein, J. et al. Isoforms of vascular endothelial growth factor act in a coordinate fashion to recruit and expand tumor vasculature. *Mol. Cell Biol.* **20**, 7282-7291 (2000).

Hamada, K. et al. VEGF-C signaling pathways through VEGFR-2 and VEGFR-3 in vasculogenesis and hematopoiesis. *Blood* **96**, 3793-3800 (2000).

Hanahan, D. and Folkman, J. Patterns and emerging mechanisms of the angiogenic switch during tumorigenesis. *Cell* **86**, 353-364 (1996).

Hanahan, D. Signaling vascular morphogenesis and maintenance. *Science* **277**, 48-50 (1997).

Heldin, C. H. et al. Mechanism of action and *in vivo* role of platelet-derived growth factor. *Physiol. Rev.* **79**, 1283-1316 (1999).

Herren, B. et al. Dimerization of extracellular domains of platelet-derived growth factor receptors. A revised model of receptor-ligand interactions. *J. Biol. Chem.* **268**, 15088-15095 (1993).

Holash, J. VEGF-Trap: a VEGF blocker with potent antitumor effects. *Proc. Natl. Acad. Sci. USA* **99**, 11393-11398 (2002).

Holmgren, L., O' Reilly, M.S. and Folkman, J. Dormancy of micrometastasis: balanced proliferation and apoptosis in the presence of angiogenesis suppression. *Nat. Med.* **1**, 149-153 (1995).

Hurwitz, H. et al. Bevacizumab plus irinotecan, fluorouracil and leucovorin for metastatic colorectal cancer. *N. Engl. J. Med.* **350**, 2335-2342 (2004).

Hynes, R. O. A reevaluation of integrins as regulators of angiogenesis. *Nat. Med.* **8**, 918-921 (2002).

Ivan, M. et al. HIF α targeted for VHL-mediated destruction by proline hydroxylation: implications for O₂ sensing. *Science* **292**, 464-468 (2001).

Iyer, S. et al. The crystal structure of human placenta growth factor-1 (PlGF-1), an angiogenic protein, at 2.0 Å resolution. *J. Biol. Chem.* **276**, 12153-12161 (2001).

Jussila, L. and Alitalo, K. Vascular growth factors and lymphangiogenesis. *Physiol. Rev.* **82**, 673-700 (2002).

Kabbinavar, F. et al. Phase II, randomized trial comparing bevacizumab plus fluorouracil (FU)/leucovorin (LV) with FU/LV alone in patients with metastatic colorectal cancer. *J. Clin. Oncol.* **21**, 60-65 (2003).

Kabsch, W. et al. Dictionary of protein secondary structure: pattern recognition of hydrogen-bonded and geometrical features. *Biopolymers* **22**, 2577-2637 (1983).

Karkkainen, M. J., Makinen, T. & Alitalo, K. Lymphatic endothelium: a new frontier of metastasis research. *Nat. Cell Biol.* **4**, E2-E5 (2002).

Katoh, O. et al. Expression of the vascular endothelial growth factor (VEGF) gene receptor, KDR, in hematopoietic cells and inhibitory effect of VEGF on apoptotic cell death caused by ionizing radiation. *Cancer Res.* **55**, 5687-5692 (1995).

Kelly, J. D. et al. Platelet-derived growth factor stimulates PDGF receptor subunit dimerization and intersubunit trans-phosphorylation. *J. Biol. Chem.* **266**, 8987-8992 (1991)..

Kendall, R. L. et al. Identification of a natural soluble form of the vascular endothelial growth factor receptor, Flt-1 and its heterodimerization with KDR. *Biochem. Biophys. Res. Commun.* **226**, 324-328 (1996).

Keyt, B. A. et al. Identification of vascular endothelial growth factor determinants for binding KDR and Flt-1 receptors. *J. Biol. Chem.* **271**, 5638-5646 (1996).

Kim, K.J. et al. Inhibition of vascular endothelial growth factor-induced angiogenesis suppresses tumor growth *in vivo*. *Nature* **362**, 841-844 (1993).

Kitsukawa, T. et al. Neuropilin-semaphorin III/D-mediated chemorepulsive signals play a crucial role in peripheral nerve projection in mice. *Neuron* **19**, 995-1005 (1997).

Klagsbrun, M. and D'Amore, P. Regulators of angiogenesis. *Annu. Rev. Physiol.* **53**, 217-239 (1991a).

Klagsbrun, M. et al. A dual receptor system is required for basic fibroblast growth factor activity. *Cell* **67**, 229-231 (1991b).

Klement, G. et al. Continuous low-dose therapy with vinblastine and VEGF receptor-2 antibody induces sustained tumor regression without overt toxicity. *J. Clin. Invest.* **105**, R15-R24 (2000).

Laemmli, U. Cleavage of structural proteins during the assembly of the head of bacteriophage T4. *Nature* **227**, 680-685 (1970).

Lee, C. G. et al. Anti-vascular endothelial growth factor treatment augments tumor radiation response under normoxic or hypoxic conditions. *Cancer Res.* **60**, 5565-5570 (2000).

Lee, C.G. et al. Vascular endothelial growth factor (VEGF) induces remodeling and enhances TH2-mediated sensitization and inflammation in the lung. *Nat. Med.* **10**, 1095-1103 (2004).

Lee, P. N. et al. Purification and complementary DNA cloning of a receptor for basic fibroblast growth factor. *Science* **245**, 57-60 (1989).

Leung, D. W., Cachianes, G., Kuang, W.J., Goeddel, D.V. & Ferrara, N. Vascular endothelial growth factor is a secreted angiogenic mitogen. *Science* **246**, 1306-1309 (1989).

Levy, A. P. et al. Regulation of vascular endothelial growth factor by hypoxia and its modulation by the von Hippel-Lindau tumor suppressor gene. *Kidney Int.* **51**, 575-578 (1997).

Lindahl, P. et al. Pericyte loss and microaneurysm formation in PDGF-B –deficient mice. *Science*, **277**, 242-245 (1997).

Luttun, A. et al. Revascularization of ischemic tissues by PlGF treatment and inhibition of tumor angiogenesis, arthritis and atherosclerosis by anti-Flt-1. *Nat, Med.* **8**, 831-840 (2002).

Lyttle, D. J. et al. Homologs of vascular endothelial growth factor are encoded by the poxvirus orf virus. *Virology* **68**, 84-92 (1994).

Maes, C. et al. Impaired angiogenesis and endochondral bone formation in mice lacking the vascular endothelial growth factor isoforms VEGF164 and VEGF188. *Mech. Dev.* **111**, 61-73 (2002).

Maisonpierre, P. C. et al., and Yancopoulos, G.D. Angiopoietin-2, a natural antagonist for Tie-2 that disrupts *in vivo* angiogenesis. *Science* **277**, 55-60 (1997).

Manavalan, P. et al. Variable selection method improves the prediction of protein secondary structure from CD spectra. *Anal. Biochem.* **167**, 76-85 (1987).

Mansukhani, A. et al. Characterization of the murine BEK fibroblast growth factor (FGF) receptor: activation by three members of the FGF family and requirement for heparin. *Proc. Natl. Acad. Sci. USA* **89**, 3305-3309 (1992).

Matsui T. et al. Isolation of a novel receptor cDNA establishes the existence of two PDGF receptor genes. *Science* **243**, 800-804 (1989).

Matsumoto, T. & Claesson-Welsh, L. VEGF receptor signal transduction. *Sci. STKE* **2001**, RE21(2001).

McTigue, M. A. et al. Crystal structure of the kinase domain of human vascular endothelial growth factor receptor 2: a key enzyme in angiogenesis. *Structure* **7**, 319-330 (1999).

Mercer, A. A. et al. Vascular endothelial growth factors encoded by Orf virus show surprising sequence variation but have a conserved, functionally relevant structure. *J. Gen. Virol.* **83**, 2845-2855 (2002).

Merelo, J. J. et al. Proteinotopic Feature Maps. *Neurocomputing* **6**, 443-454 (1994).

Migdal, M. et al. Neuropilin-1 is a placenta growth factor-2 receptor. *J. Biol. Chem.* **273**, 22272-22278 (1998).

Millauer, B. et al. High affinity VEGF binding and developmental expression suggest Flk-1 as a major regulator of vasculogenesis and angiogenesis. *Cell* **72**, 835-846 (1993).

Millauer, B. et al. Glioblastoma growth inhibited *in vivo* by a dominant-negative Flk-1 mutant. *Nature* **367**, 576-579 (1994).

Moreira, I. S. et al. VEGF inhibition-a critical review. *Anti-Cancer agents in medicinal chemistry.* **7**, 223-245 (2007).

Moses, M. A. The regulation of neovascularization by matrix metalloproteinases and their inhibitors. *Stem Cells* **15**, 180-189 (1997).

Moses, M. A. et al., and Langer, R. Troponin I is present human cartilage and inhibits angiogenesis. *Proc. Natl. Acad. Sci. USA* **96**, 2645-2650 (1999).

Mukhopadhyay, D. and Datta, K. Multiple regulatory pathways of vascular permeability factor/vascular endothelial growth factor (VPF/VEGF) expression in tumors. *Semin. Canc. Biol.* **14**, 123-130 (2004).

Muller, Y. A. et al. Vascular endothelial growth factor: crystal structure and functional mapping of the kinase domain receptor binding site. *Proc. Natl. Acad. Sci. USA* **94**, 7192-7197 (1997).

Nagy, J. A. et al. Vascular permeability factor/vascular endothelial growth factor induces lymphangiogenesis as well as angiogenesis. *J. Exp. Med.* **196**, 1497-1506 (2002).

Nagy, J. A. et al. VEGF-A and the induction of pathological angiogenesis. *Annu. Rev. Pathol. Mech. Dis.* **2**, 251-275 (2007).

Neufeld, G., Cohen, T., Gengrinovitch, S. & Poltorak, Z. Vascular endothelial growth factor (VEGF) and its receptors. *FASEB J.* **13**, 9-22 (1999).

Neufeld, G. et al. The neuropilins: multifunctional semaphorin and VEGF receptors that modulate axon guidance and angiogenesis. *Trends Cardiovasc. Med.* **12**, 13-19 (2002).

Nguyen, M., Folkman, J. and Biscoff, J. 1-Deoxymannojirimycin inhibits capillary tube formation *in vitro*. Analysis of N-linked oligosaccharides in bovine capillary endothelial cells. *J. Biol. Chem.* **267**, 26157-25165 (1992).

O' Reilly, M. S. et al., and Folkman, J. Angiostatin: a novel angiogenesis inhibitor that mediates the suppression of metastasis by a Lewis lung carcinoma. *Cell* **79**, 315-328 (1994).

O' Reilly, M.S. et al., and Folkman, J. Endostatin: an endogenous inhibitor of angiogenesis and tumor growth. *Cell* **88**, 277-285 (1997).

Olofsson, B. et al. Vascular endothelial growth factor B (VEGFB) binds to VEGF receptor-1 and regulates plasminogen activator activity in endothelial cells. *Proc. Natl. Acad. Sci. USA* **95**, 11709-11714 (1998).

Ornitz, D. M. et al. Ligand specificity and heparin dependence of fibroblast growth factor receptors 1 and 3. *J. Biol. Chem.* **267**, 16305-16311 (1992).

Ornitz, D. M. et al. Fibroblast growth factors. *Genome Biol.* **2**, Review S3005 (2001).

Pajusola, K. et al. Signaling properties of Flt-4, a proteolytically processed receptor tyrosine kinase related to two VEGF receptors. *Oncogene* **9**, 3545-3555 (1994).

Pan, B. et al. Solution structure of a phage-derived peptide antagonist in complex with vascular endothelial growth factor. *J. Mol. Biol.* **316**, 769-787 (2002).

Park, J. E., Keller, H.-A. & Ferrara, N. The vascular endothelial growth factor (VEGF) isoforms: differential deposition into the subepithelial extracellular matrix and bioactivity of extracellular matrix-bound VEGF. *Mol. Biol. Cell* **4**, 1317-1326 (1993).

Park, J. E., Chen, H.H., Winer, J., Houck, K.A. & Ferrara, N. Placenta growth factor. Potentiation of vascular endothelial growth factor bioactivity, *in vitro* and *in vivo*, and high affinity binding to Flt-1 but not to Flk-1/KDR. *J. Biol. Chem.* **269**, 25646-25654 (1994).

Partanen, J. and Dumont, D.J. Functions of Tie1 and Tie2 receptor tyrosine kinases in vascular development. *Curr. Top. Microbiol. Immunol.* **237**, 160-172 (1999).

Pellet-Many, C. et al. Neuropilins: structure, function and role in disease. *Biochem J.* **411**, 211-226 (2008).

Persico, M. G. et al. Structure, expression and receptor-binding properties of placenta growth factor (PlGF) *Curr. Top. Microbiol. Immunol.* **237**, 31-40 (1999).

Plouet, J., Schilling, J. & Gospodarowicz, D. Isolation and characterization of a newly identified endothelial cell mitogen produced by AtT20 cells. *EMBO J.* **8**, 3801-3808 (1989).

Powers, C. J. et al. Fibroblast growth factors, their receptors and signaling. *Endocr. Relat. Cancer* **7**, 165-197 (2000).

Presta, L.G. et al. Humanization of an anti-VEGF monoclonal antibody for the therapy of solid tumors and other disorders. *Cancer Res.* **57**, 4593-4599 (1997).

Prewett, M. et al. Antivascular endothelial growth factor receptor (fetal liver kinase 1) monoclonal antibody inhibits tumor angiogenesis. *Cancer Res.* **59**, 5209-5218 (1999).

Provencher, S. W. et al. Estimation of globular protein secondary structure from CD. *Biochemistry* **20**, 33-37 (1981).

Rahimi, N. VEGFR-1 and VEGFR-2: two nonidentical twins with a unique physiognomy. *Front Biosci.* **11**, 819-829 (2006).

Rak, J. and Yu, J.L. Oncogenes and tumor angiogenesis: the question of vascular “supply” and vascular “demand”. *Semin. Canc. Biol.* **14**, 93-104 (2004).

Rastinejad, F. et al. Regulation of the activity of a new inhibitor of angiogenesis by a cancer suppressor gene. *Cell* **56**, 345-355 (1989).

Reuss, B. et al. Fibroblast growth factors and their receptors in the central nervous system. *Cell Tissue Res.* **313**, 139-157 (2003).

Risau, W. Mechanisms of angiogenesis. *Nature* **386**, 671–674 (1997).

Ruch, C. et al. Structure of a VEGF-VEGF receptor complex determined by electron microscopy. *Nat. Struct. Mol. Biol.* **14**, 249-250 (2007).

Ruhrberg, C. Growing and shaping the vascular tree: multiple roles for VEGF. *Bioessays* **25**, 1052-1060 (2003).

Rutherford, C. et al. Endogenously elicited antibodies to platelet-derived growth factor- β and platelet cytosolic protein inhibit aortic lesion development in the cholesterol-fed rabbit. *Int. J. Exp. Pathol.* **78**, 21-32 (1997).

Sato, T. N. et al. Distinct roles of the receptor tyrosine kinases Tie-1 and Tie-2 in blood vessel formation. *Nature* **376**, 70-74 (1995).

Savory, L. J. et al. Viral vascular endothelial growth factor plays a critical role in orf virus infection. *Virology* **74**, 10699-10706 (2000).

Seetharam, L. et al. A unique signal transduction from FLR tyrosine kinase, a receptor for vascular endothelial growth factor (VEGF), *Oncogene* **10**, 135-147 (1995).

Senger, D. R. et al. Tumor cells secrete a vascular permeability factor that promotes accumulation of ascites fluids. *Science* **219**, 983-985 (1983).

Shalaby, F. et al. Failure of blood-island formation and vasculogenesis in Flk-1 deficient mice. *Nature* **376**, 62-66 (1995).

Shi, Q. et al., and Hammond W.P. Evidence for circulating bone marrow-derived endothelial cells. *Blood* **92**, 362-367 (1998).

Shibuya, M. et al. Nucleotide sequence and expression of a novel human receptor-type tyrosine kinase (flt) closely related to the fms family. *Oncogene* **8**, 519-527 (1990).

Shibuya, M. Role of VEGF-FLT receptor system in normal and tumor angiogenesis. *Cancer Res.*, **67**: 281-316 (1995).

Shweiki, D. et al. Patterns of expression of vascular endothelial growth factor (VEGF) and VEGF receptors in mice suggest a role in hormonally regulated angiogenesis. *J. Clin. Invest.* **91**, 2235-2243 (1993).

Soker, S. et al. Neuropilin-1 is expressed by endothelial and tumor cells as an isoform-specific receptor for vascular endothelial growth factor. *Cell* **92**, 735-745 (1998).

Sreerama, N. et al. Estimation of protein secondary structure from CD spectra: comparison of CONTIN, SELCON and CDSSTR methods with an expanded reference set. *Anal. Biochem.* **287**, 252-260 (2000).

Starovasnik, M. A. et al. Solution structure of the VEGF-binding domain of Flt-1 : comparison of its free and bound states. *J. Mol. Biol.* **293**, 531-544 (1999).

Stoepck, A. et al. Results of a phase I dose-escalating study of the antiangiogenic agent, SU5416, in patients with advanced malignancies. *Clin. Cancer Res.* **8**, 2798-2805 (2002).

Sundberg, C. et al. Tumor cell and connective tissue cell interactions in human colorectal adenocarcinoma. Transfer of platelet-derived growth factor- β to stromal cells. *Am. J. Pathol.* **151**, 479-492 (1997).

Suri, C. et al., and Yancopoulos, G.D. Increased vascularization in mice overexpressing angiopoietin-1. *Science* **282**, 468-471 (1998).

Takahashi, T. et al., and Asahara, T. Ischemia- and cytokine-induced mobilization of bone marrow-derived endothelial progenitor cells for neovascularization. *Nat. Med.* **5**, 434-438 (1999a).

Takahashi, T. et al. VEGF activates protein kinase C-dependent, but Ras independent Raf-MEK-MAP kinase pathway for DNA synthesis in primary endothelial cells. *Oncogene* **18**, 2221-2230 (1999b).

Terman, B. I. et al. Identification of a new endothelial cell growth factor receptor tyrosine kinase. *Oncogene* **6**, 1677-1683 (1991).

Thurston, G. et al. Angiopoietin-1 protects the adult vasculature against plasma leakage. *Nat. Med.* **6**, 460-463 (2000).

Ueda, Y. et al. A novel low molecular weight antagonist of vascular endothelial growth factor receptor binding: VGA1155. *Mol. Cancer Ther.* **2**, 1105-1111 (2003).

Venyaminov, S. et al. Determination of protein tertiary structure class from CD spectra. *Anal. Biochem.* **222**, 176-184 (1994).

Waltenberger, J. et al. Different signal transduction properties of KDR and Flt-1, two receptors for vascular endothelial growth factor. *J. Biol. Chem.* **269**, 26988-26995 (1994).

Weis, S.M. et al. Pathophysiological consequences of VEGF-induced vascular permeability. *Nature* **437**, 497-504 (2005).

Wiesmann, C. et al. Crystal structure at 1.7 Angstrom resolution of VEGF in complex with domain 2 of the Flt-1 receptor. *Cell* **91**, 695-704 (1997).

Wiesmann, C. et al. Crystal structure of the complex between VEGF and a receptor –blocking peptide. *Biochemistry* **37**, 17765-17772 (1998).

Wise, L. M. et al. Viral vascular endothelial growth factors vary extensively in amino acid sequence, receptor-binding specificities, and the ability to induce vascular permeability yet are uniformly active mitogens. *J. Biol. Chem.* **278**, 38004-38014 (2003).

Wood, J. M. et al. PTK787/ZK 222584, a novel and potent inhibitor of vascular endothelial growth factor receptor tyrosine kinases, impairs vascular endothelial growth factor-induced responses and tumor growth after oral administration. *Cancer Res.* **60**, 2178-2189 (2000).

Woolard, J. et al. VEGF165b, an inhibitory vascular endothelial growth factor splice variant: mechanism of action, *in vivo* effect on angiogenesis and endogenous protein expression. *Canc. Res.* **64**, 7822-7835 (2004).

Yamazaki, Y. et al. Snake venom Vascular endothelial factors (VEGFs) exhibit potent activity through their specific recognition of KDR (VEGF receptor 2). *J. Biol. Chem.* **278**, 51985-51988 (2003).

Yancopoulos, G. D. et al. Vascular-specific growth factors and blood vessel formation. *Nature* **407**, 242-248 (2000).

Yi, E. S. et al. Platelet-derived growth factor causes pulmonary cell proliferation and collagen deposition *in vivo*. *Am. J. Pathol.* **149**, 539-548 (1996).

Yoshida, A. et al. Differential endothelial migration and proliferation to basic fibroblast growth factor and vascular endothelial growth factor. *Growth Factors*, **13**, 57-64 (1996).

Yu, J. L. et al. Vascular endothelial growth factor isoforms expression as a determinant of blood vessel patterning in human melanoma xenografts. *Canc. Res.* **62**, 1838-1846 (2002).

Zhang, J. D. et al. Three-dimensional structure of human basic fibroblast growth factor, a structural homolog of interleukin 1 beta. *Proc. Natl. Acad. Sci. USA* **88**, 3446-3450 (1991).

Zhu, X. et al. Three-dimensional structures of acidic and basic fibroblast growth factors. *Science* **251**, 90-93 (1991).

Zilberberg, L. et al. Structure and inhibitory effects on angiogenesis and tumor development of a new vascular endothelial growth inhibitor. *J. Biol. Chem.* **278**, 35564-35573 (2003).

Publications

“In Vivo and In Vitro Characterization of CCK8 Bearing a Histidine-Based Chelator Labeled With ^{99m}Tc-Tricarbonyl.”

Luca D. D’Andrea, Irma Testa, MariaRosaria Panico, Rossella Di Stasi, Corradina Caraco`, Laura Tarallo, Claudio Arra, Antonio Barbieri, Alessandra Romanelli, Luigi Aloj.

“A vascular endothelial growth factor mimetic accelerates gastric ulcer healing in an iNOS-dependent manner.”

Genevieve K. Dudar, Luca D. D’Andrea, Rossella Di Stasi, Carlo Pedone, and John L. Wallace.

Comunications

R. Di Stasi, B. Ziaco, D. Capasso, R. Palumbo, M. Serino, E. Benedetti & L. D. D’andrea.

“Design of small protein scaffold to target VEGF receptors”.

10th Naples Workshop on bioactive peptides – Naples June 11-14, 2006.

R. Di Stasi, D. Capasso, C. Pedone & L. D. D’Andrea.

“Extracellular domains of VEGF receptors: expression and characterisation”.

National Congress 2007 of Chemistry Division of Biological Systems – Montagnana, Padova November 8-9, 2007.

R. Di Stasi, D. Capasso, D. Diana, R. Fattorusso, C. Pedone & L. D. D’Andrea.

“Vascular Endothelial Growth Factor (VEGF) and its receptors: key regulators of angiogenesis”.

11th Naples Workshop on bioactive peptides – Naples May 24-27, 2008.

R. Di Stasi, D. Capasso, D. Diana, R. Fattorusso, C. Pedone & L. D. D’Andrea.

“VEGF receptors-peptide interaction: an NMR analysis”.

30th European Peptide Symposium-Helsinki, Finland 31 August-5 September 2008.

R. Di Stasi, D. Capasso, D. Diana, R. Fattorusso, C. Pedone & L. D. D’Andrea.
“Expression of extracellular domains of VEGF receptors and their use in NMR Drug discovery studies”.

53rd National Meeting of the Italian Society of Biochemistry and Molecular Biology and National Meeting of Chemistry of Biological Systems (Italian Chemical Society)-Riccione September 23-26 2008.

In Vivo and In Vitro Characterization of CCK8 Bearing a Histidine-Based Chelator Labeled With ^{99m}Tc -Tricarboxyl

Luca D. D'Andrea,¹ Irma Testa,¹ MariaRosaria Panico,¹ Rossella Di Stasi,¹ Corradina Caracò,² Laura Tarallo,² Claudio Arra,³ Antonio Barbieri,³ Alessandra Romanelli,⁴ Luigi Aloj²

¹Istituto di Biostrutture e Bioimmagini, CNR, 80134 Napoli, Italy

²Area Funzionale di Medicina Nucleare, Istituto Nazionale Tumori, Fondazione "G. Pascale", 80131 Napoli, Italy

³UOS Sperimentazione Animale, Istituto Nazionale Tumori, Fondazione "G. Pascale", 80131 Napoli, Italy

⁴Dipartimento delle Scienze Biologiche, Università di Napoli "Federico II, 80134 Napoli, Italy

Received 2 May 2008; revised 11 June 2008; accepted 16 June 2008

Published online 9 July 2008 in Wiley InterScience (www.interscience.wiley.com). DOI 10.1002/bip.21041

ABSTRACT:

The development of receptor targeting radiolabeled ligands has gained much interest in recent years for diagnostic and therapeutic applications in nuclear medicine. Cholecystinin (CCK) receptors have been shown to be overexpressed in a subset of neuroendocrine and other tumors. We are evaluating binding and biodistribution properties of a CCK8 peptide derivative labeled with ^{99m}Tc (I)-tricarboxyl. The CCK8 peptide was modified at its N-terminus by adding to its N-terminus two lysine-histidine modules (KH), where histidine is coupled to the side chain of the lysine ((KH)₂-CCK8). ^{99m}Tc (I)-tricarboxyl was generated with the IsoLinkTM kit. A431 cells stably transfected with a cDNA encoding for the human CCK2 receptor were utilized to determine binding affinity, internalization, and retention of the labeled peptide, in comparison with wild-type A431 cells. A nude mouse tumor model was obtained by generating A431-CCK2R and A431-control tumors in opposite flanks of the animals. High specific activity labeling with ^{99m}Tc was achieved. In A431-CCK2R cells, specific saturable binding was observed as well as evident

internalization of the radiolabeled peptide after binding. Biodistribution experiments showed rapid, specific localization of (KH)₂-CCK8 on A431-CCK2R xenografts compared with control tumors, although absolute uptake values were not markedly higher compared with background activity. Clearance of unbound radioactivity was both urinary and hepatobiliary. In imaging experiments, while targeting to CCK2R positive tumors could be appreciated, there was poor contrast between target and nontarget areas. (KH)₂-CCK8 shows adequate in vitro and in vivo properties for CCK2R targeting although improvement of biodistribution warrant further development. © 2008 Wiley Periodicals, Inc. *Biopolymers* (Pept Sci) 90: 707–712, 2008.

Keywords: technetium; radiopeptide; imaging; organometallic complexes; carbonyl; cholecystinin receptors

This article was originally published online as an accepted preprint. The "Published Online" date corresponds to the preprint version. You can request a copy of the preprint by emailing the *Biopolymers* editorial office at biopolymers@wiley.com

INTRODUCTION

Radiopharmaceuticals are widely employed in nuclear medicine for the diagnosis and therapy of different diseases. In the last years, many new radiopharmaceuticals have been developed using a target specific approach. In fact, in some diseases, such as cancer,

Correspondence to: Luigi Aloj, Area Funzionale di Medicina Nucleare, Istituto Nazionale Tumori, Fondazione "G. Pascale", Via M. Semmola, 80131, Napoli, Italy; e-mail: luigi.aloj@fondazionepascale.it
© 2008 Wiley Periodicals, Inc.

cells may express on their surface, specific receptors; molecules capable of targeting these receptors can discriminate between normal and cancer cells lowering the toxicity and the side effects of the drug. These radiopharmaceuticals are mainly designed by the following two approaches: integrated and bifunctional. The latter approach is generally accomplished by assembling a targeting molecule, a linker, a chelator, and the radionuclide.¹

Antibodies and peptides are the two classes of compounds widely used as targeting molecules in receptor imaging. In particular, peptides, which recognize the cognate receptor with high binding affinity and specificity, present some advantages over antibodies such as: they are easily synthesized and modified, are relatively inexpensive, have rapid blood clearance, and high tumor to background ratios.¹⁻³ A successful example is represented by the radiolabeled somatostatin analog ¹¹¹In-octreotide widely used in cancer imaging (octreoscan).⁴ After the FDA approval of octreoscan, many other peptides are being investigated.⁵

A well-characterized molecular target for imaging is represented by the cholecystokin (CCK) receptors.⁶ CCK receptors, CCK1R and CCK2R, are membrane bound receptors belonging to the superfamily of G-protein-coupled receptors (GPCRs) and are predominantly located in the gastrointestinal tract and the central nervous system.⁷ They differ in the affinity for gastrin; CCK1R has low affinity, whereas CCK2R binds both gastrin and cholecystokin (CCK) with high affinity. CCK2R is overexpressed in a variety of tumors such as medullary thyroid carcinoma, small cell lung cancer, astrocytomas, stromal ovarian tumors, and some gastroenteropatic tumors.⁸ Several CCK and gastrin derivatives have been characterized over the past years for the purpose of in vivo receptor targeting, and the feasibility of using CCK8-based peptides to target CCK2R in vivo has been shown.^{6,9,10} The C-terminal sequence of cholecystokin, CCK8, is capable of binding both CCK receptors, but shows higher affinity and selectivity for CCK2R⁹ and has been extensively used for imaging with different chelators.⁹⁻¹⁷

Several radionuclides are being used in nuclear medicine, and ^{99m}Tc(I) is rapidly gaining in popularity since the introduction by Alberto and coworkers^{18,19} of a one-pot procedure to synthesize stable organometallic Tc(I)-complexes [^{99m}Tc(OH)₂(CO)₃]⁺ (TcCO). ^{99m}Tc(I) presents very favorable physical properties for application as radiopharmaceuticals. Its half-life ($t_{1/2} = 6$ h) is long enough to carry out chemical synthesis and get useful images after administration to the patient. At the same time, it is short enough to permit administration of relatively high amounts of ^{99m}Tc radioactivity without exposing the patient to excessive radiation doses. The 140 keV photons are ideal for nuclear imaging

applications, and ^{99m}Tc isotope is readily available from commercial ⁹⁹Mo-^{99m}Tc generators.^{1,20}

In the TcCO complex, the water molecules can be replaced by ligands to obtain very stable d⁶ low-spin complexes. Preferred ligands are molecules possessing, as coordinating atoms, sp² nitrogens such as present in the side chain of the amino acid histidine.¹⁹ Ligands replacing all the three water molecules can form very stable complexes, avoiding trans-chelation reactions, which may occur in vivo, and the generation of free Tc. Recently, Alberto et al. reviewed the ligands (mono-, bi-, and tridentate) available for peptide labeling with TcCO.²¹ Histidine is a convenient ligand to functionalize peptides because of its small dimension, and it can be easily introduced during chain assembly on the resin. When His is inserted in a peptide chain, it can act as monodentate ligand for TcCO, but when positioned at the N-terminus, it acts as bidentate ligand. The α-NH₂ group and the δ-N aromatic amine are efficient chelators for the fac-[^{99m}Tc(CO)₃]⁺ core under formation of a six-member ring. Several articles have been reported the utility of histidine and histidine-based ligand labeled with TcCO for imaging applications.²²⁻²⁸

Aim of this work was to characterize the in vitro and in vivo properties of CCK8 tagged with a chelator composed of two N-terminal His-like residues and labeled with ^{99m}Tc(I)-tricarbonyl. The presence of multiple His units could favor the metal complexation and allow to achieve higher specific activities. This in turn would allow targeting of higher amounts of radioactivity per unit of peptide molecule, a feature that may prove advantageous for therapeutic applications using ^{186/188}Re(I)-tricarbonyl.

EXPERIMENTAL SECTION

All amino acids and coupling reagents (HOBT and HBTU) were purchased from Novabiochem (Läufelfingen, Switzerland), *N,N*-dimethylformamide (DMF) from Lab-Scan (Dublin, Ireland), DIPEA and trifluoroacetic acid (TFA) from Romil (Cambridge, UK), acetic anhydride from Applied Biosystem Dichloromethane, Piperidine, 1,2-ethanedithiol (EDT) from Fluka (Steinheim, Germany), and triisopropylsilane from Aldrich (Steinheim, Germany). Acetonitrile HPLC grade was from Riedel-de Haën (Schnelldorf, Germany).

Peptide Synthesis

Peptide amide was synthesized using ABI 433 peptide synthesizer (Applied Biosystem) on solid phase using Rink Amide MBHA resin (Novabiochem) and standard Fmoc (*N*-(9-fluorenyl)methoxycarbonyl) chemistry. All the amino acids presented standard protection group on the side chain except for the lysines, which were protected with methyltrityl group (Mtt) to allow selective deprotection. Lysines were selectively deprotected with a solution of 1% TFA, 5%

TIS in DCM, and after neutralization (20% DIPEA in DMF) FmocHis(Trt)-OH was coupled to the resin. After Fmoc deprotection with piperidine the peptide was cleaved from the resin, and removal of side-chain protecting groups was achieved by treatment with a mixture of TFA, water, EDT, TIS (94:2.5:2.5:1) at room temperature for 3 h. Then the peptide ((KH)₂-CCK8) was precipitated with ethyl ether and lyophilized. Crude peptide was purified by HPLC on a C18 Column (Juppiter, Phenomenex) using a linear gradient of acetonitrile/water (0.1% TFA) from 5 to 40% in 25 min. Purity and identity of the synthesized peptide was assessed by HPLC (Agilent 1100 series) and MALDI-ToF mass spectrometry (Voyager DE-Perceptive Biosystem).

Radiolabeling

Carboxyl aquaion [$^{99m}\text{Tc}(\text{OH})_2(\text{CO})_3$]⁺ was prepared from a commercial kit (ISOLINK, Mallinckrodt, Petten) according to the manufacturer's instructions (1 ml volume; 200–1000 MBq ^{99m}Tc). Small aliquots of the ^{99m}Tc -CO complex (100–150 μL) were incubated with the peptide (10–50 nmol) at room temperature. Complex formation was verified by RP-HPLC. Final specific activities of the radiolabeled peptide used in the experiments were 1850–3700 GBq/mmol.

In Vitro Cellular Assays

All in vitro cellular assays were performed on A431 cells overexpressing CCK2R receptor (A431-CCK2R).¹⁰ Cells were plated at a density of 1–200,000 cells/well in 12-well multiwell plates, 2 or 3 days prior to the experiments. These conditions allowed for the cells to be almost confluent at the time of the assay.

To assess binding affinity of the compound, duplicate wells were incubated with serial dilutions of [TcCO](KH)₂-CCK8 in culture medium at 4°C for 1 h, with concentrations ranging from 0.05 to 120 nM. To assess nonspecific binding, 100- to 1000-fold excess unlabeled peptide was added to some of the wells. At the end of incubation period free radioactivity was recovered, wells washed with two rapid rinses in PBS and bound activity recovered by solubilization cells in 0.1N NaOH. Radioactivity was measured with a Wallac Wizard gamma counter (Wallac Oy, Turku, Finland). The amount of bound compound was normalized for protein content that was determined by utilizing a commercially available kit (Bio-Rad Laboratories, USA).

Binding curves were analyzed using a Macintosh computer and Kaleidagraph software (Abelbeck Software, Version 3.0.5, distributed by Synergy Software, Reading, PA). Dissociation constants (K_d) and apparent number of binding sites per cell (B_{max}) were derived by fitting the data to the following equation:

$$\text{Bound} = \frac{B_{\text{max}} * [[\text{TcCO}](\text{KH})_2\text{-CCK8}]}{K_d + [[\text{TcCO}](\text{KH})_2\text{-CCK8}]}$$

Cellular internalization was determined by comparing differences in accumulation of the compound incubated with A431-CCK2R cells at 4°C, temperature at which most metabolic processes are blocked, and at 37°C, where all metabolic processes including receptor internalization are active. Cells were incubated with 20 nM [TcCO](KH)₂-CCK8 at the two temperatures, for 60 and 120 min. After 120 min of incubation some wells were rinsed with PBS to

remove unbound radioactivity and were subsequently incubated for an additional hour at 4°C with 30 μM unlabeled peptide, in order to displace any surface bound radioactivity. Radioactivity associated to cells was determined after washing away unbound radioactivity and subsequently normalized for protein content, as described earlier.

In Vivo Studies

Mice bearing xenografts of A431-CCK2R and A431-control cells were generated by injecting 100 μL of the respective cell suspensions at a density of $2 \times 10^7 \text{ ml}^{-1}$ in PBS in opposite flanks of 6-week-old CD-1 nude mice (weight 17–23 g). Tumors were allowed to grow for 10–14 days. Final tumor weight was between 0.5 and 1 g at the time of the biodistribution and imaging experiments.

Biodistribution Studies. The time course of tissue and tumor distribution of [TcCO](KH)₂-CCK8 was determined following injection of $\sim 3.7 \text{ MBq/mouse}$ (0.2–0.5 nmol peptide) of labeled peptide in the lateral tail vein. At least five animals per time point were used. The animals were killed 30 and 120 min after injection. Blood, lungs, liver, spleen, kidneys, stomach, intestines, muscle, and xenograft samples were weighed and radioactivity determined in the gamma counter. Dilutions of the injected compound were simultaneously counted for accurate determination of the injected dose. The relative amount of radioactivity in the organs was calculated and expressed as percentage of the injected dose/gram tissue (%ID/g) normalized to a 20 g mouse. In some animals, gamma camera imaging was performed after sacrificing the mouse to assess visualization of CCK2R positive tissues.

Metabolite Analysis. To test stability of [TcCO](KH)₂-CCK8, the compound was injected into a nude mouse and a blood sample was recovered 120 min postinjection. The blood samples were centrifuged to recover serum and then CH_3CN was added to precipitate high molecular weight proteins. The resulting soluble fraction was subjected to RP-HPLC and radioactivity assessed by collecting 1 min fractions that were subsequently measured in a gamma counter. Similarly, experiments aimed at determining tissue metabolism of the compound were carried out on homogenates obtained from mouse tissue samples and xenografts that were freshly prepared as previously described.¹⁰ Aliquots of [TcCO](KH)₂-CCK8 were incubated with the homogenates for times ranging from 0 to 60 min, extracted with CH_3CN and analyzed with RP-HPLC as above.

RESULTS AND DISCUSSION

Peptide Design and Synthesis

The synthesis of the CCK8 peptide, (KH)₂-CCK8, tagged with the multiple bifunctional ligand based on histidine as chelator agent, was entirely carried out on solid phase. The bifunctional ligand is composed of two lysines, spaced by a β -alanine, each bearing a His residue on its side chain. In this way the two His assume a N-terminal-like position. The β -alanine acts as spacer, in order to reduce electrostatic and steric repulsions between the chelator groups. β -alanine was chosen as spacer because of its conformational preference: the dihedral angle μ (N-C β -C α -C') can adopt only the trans

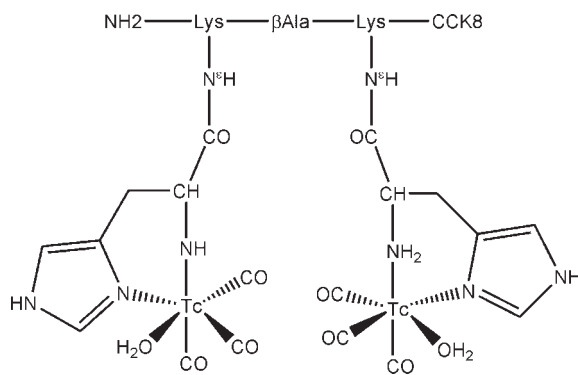


FIGURE 1 Schematic representation of the labeled peptide $(\text{KH})_2\text{-CCK8}$. The amino acid sequence of CCK8 is: Asp-Tyr-Met-Gly-Trp-Met-Asp-Phe-amide.

(180°) and/or gauche ($+60^\circ$) conformations²⁹ keeping the two His residues far away from each other. The peptide sequence is reported in Figure 1.

The peptide and the ligand are entirely synthesized in solid phase, this is an advantage over peptide-chelate conjugates that need to be prepared coupling in solution the chelating units. The product is obtained with high yields and can be purified by HPLC yielding a high homogeneous product. Moreover, the modular composition of the chelating unit allows the design of a class of ligands in which the physicochemical properties of the whole molecule, such as hydrophilicity, could be easily modulated.

Radiolabeling and Quality Control

The purified peptide was efficiently labeled using the isolink kit at high specific activity starting from the carbonyl aquation $[\text{}^{99\text{m}}\text{Tc}(\text{OH}_2)_3(\text{CO})_3]$. The reaction was followed by reverse phase HPLC and a mixture, most presumably, of mono and double labeled species, were obtained. There were no purification steps for the radiolabeled material prior to experimental use.

Receptor Binding and Internalization

Initially, we tested whether $[\text{TcCO}](\text{KH})_2\text{-CCK8}$ was capable of binding A431 cells overexpressing the CCK2R in vitro. Figure 2 shows data from a saturation binding experiment with increasing concentration of peptide $[\text{TcCO}](\text{KH})_2\text{-CCK8}$. The experiment shows rapid initial binding of the compound to the CCK2R expressing cells and a slight increase in cell associated activity over time suggesting that part of the radioactivity is internalized. Nonspecific binding, as assessed by incubation of the compound with nonreceptor expressing cells or in receptor expressing cells in the presence of 100-fold excess unlabeled peptide, was very low. These experiments were performed at 4°C , in order to block receptor internaliza-

tion and thus measure only ligand-receptor interaction. The peptide binds to the CCK2 receptor with a dissociation constants (K_d) of ~ 30 nM and with an apparent receptor number (B_{max}) of 5.8 pmol/mg protein. The binding was saturable. All parameters were in agreement with previously characterized CCK8-based molecules¹⁰ and are in the range useful for receptor-binding of radiopharmaceuticals.³⁰ This data show that the introduction of the bis-His chelating unit does not affect the binding of the targeting molecule to the receptor.

The CCK receptors, such as GPCRs, internalize after the ligand binding event. A radiopharmaceutical targeting the CCK2R can take advantage of this biological mechanism because the receptor turn over always recycle free receptor on the cell surface, and the segregation of the peptide in the cytosol shift the ligand-binding equilibrium toward the receptor-ligand complex formation. To evaluate if the peptide was being internalized by the cells, we performed parallel experiments in which A431-CCK2R cells were incubated with 20 nM $[\text{TcCO}](\text{KH})_2\text{-CCK8}$ at 4°C (internalization blocked) or 37°C (internalization active). The results are reported in Figure 3. The radioactivity is progressively accumulated in cells incubated at 37°C with labeled peptide alone (60 min vs. 120 min), whereas the levels of cell-associated radioactivity are constant in cells incubated at 4°C at 60 and 120 min, suggesting that internalization is occurring to some extent at 37°C . Again, the presence of the multifunctional ligand does not appear to alter the biological activity of the CCK8 peptide portion.

In Vivo Characterization

The in vivo characterization was carried out in nude mice bearing xenografts of A431-CCK2R and A431-control cells.

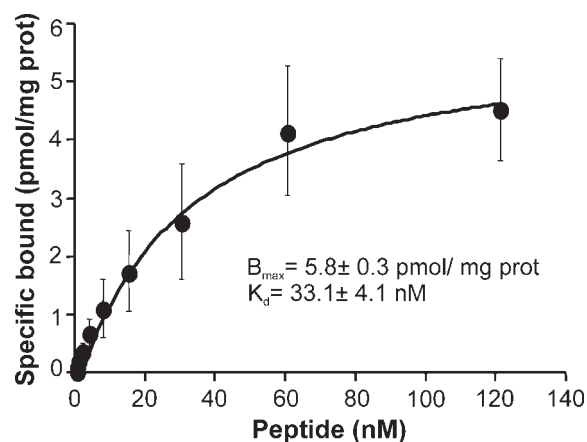


FIGURE 2 Receptor binding. A431 cells overexpressing CCK2R were incubated with increasing concentration of TcCo labeled peptide. The radioactivity of bound compound was normalized for protein content.

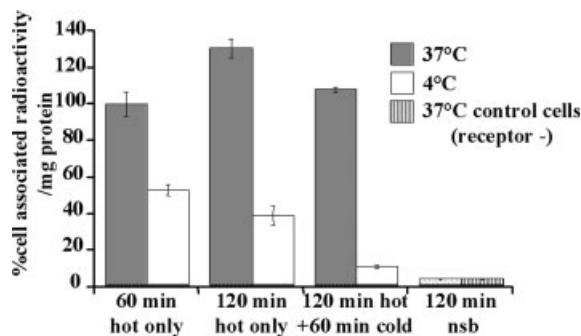


FIGURE 3 Peptide internalization. A431-CCK2R cells were incubated with 20 nM $[\text{TcCO}](\text{KH})_2\text{-CCK8}$ at 4°C and 37°C for 60 and 120 min. An additional incubation of one hour at 4°C with 30 μM unlabeled peptide was performed in order to displace any surface bound radioactivity. Radioactivity associated to cells was normalized for protein content. NSB. Nonspecific binding was assessed by incubating control A431 cells at 37°C for 120 min with tracer amounts of labeled peptide or by incubating A431-CCKBR cells at 4°C with the radiolabeled peptide in the presence of excess (30 μM) cold peptide.

With this approach, two xenografts displaying identical properties regarding to blood flow, vascular permeability, etc. are used, and the two tumors differ only in the ability to express CCK2 receptors. As we have previously shown,¹⁰ this model allows an accurate assessment of specific and nonspecific interactions of the ligand and the evaluation of its imaging properties. We have evaluated the biodistribution (Figure 4), metabolite analysis (Figure 5), and the imaging properties (Figure 6) of the peptide $[\text{TcCO}](\text{KH})_2\text{-CCK8}$.

The uptake of $[\text{TcCO}](\text{KH})_2\text{-CCK8}$ in the A431-CCK2R xenografts was higher than in A431-control tumors with a target to nontarget ratio (receptor positive vs. receptor negative tumor) of 2.3:1 at 120 min postinjection indicating a good uptake, retention and that the binding specificity is

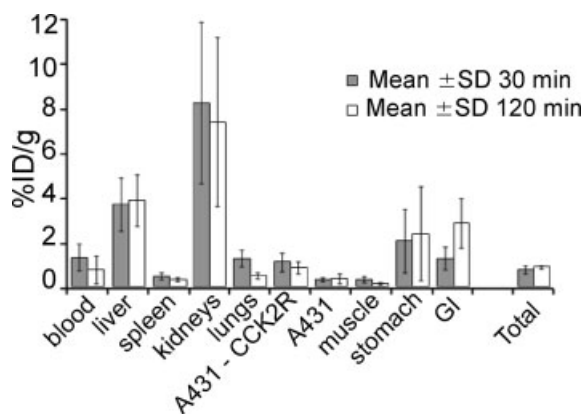


FIGURE 4 Peptide biodistribution. Analysis of peptide organ distribution 30 or 120 min after injection. ID/g, injected dose/gram tissue.

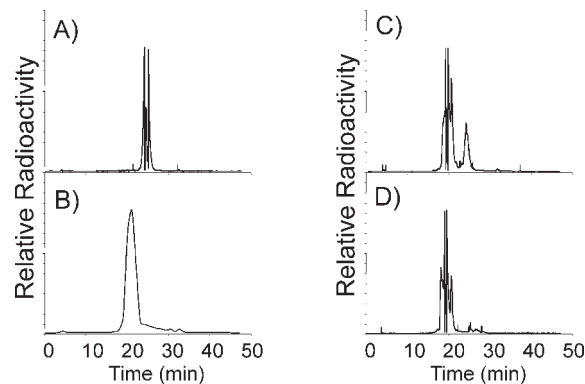


FIGURE 5 Metabolite analysis. RP-HPLC traces of (A) $[\text{TcCO}](\text{KH})_2\text{-CCK8}$ peptide control, (B) serum at 120 min post injection, (C) liver homogenates after 1 h incubation at 37°C, and (D) kidney homogenates after 1 h incubation at 37°C.

maintained in vivo. The route of clearance of radioactivity was mostly through the kidneys, although a significant portion of radioactivity showed hepatobiliary clearance. In general, the clearance was rapid and evident by the 30 min time point. Retention in all organs (see Figure 4) was lower than 4% ID/g after 2 h except for the kidney (7.35% ID/g); blood

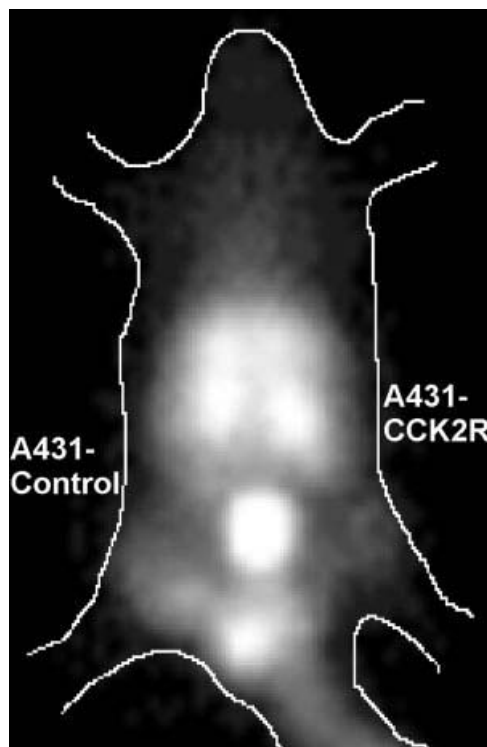


FIGURE 6 γ -camera images. Animals were sacrificed 2 h after injection of $[\text{TcCO}](\text{KH})_2\text{-CCK8}$ peptide. Accumulation of the peptide was seen in a CCK2R-positive xenograft (right thigh) but not in the control tumor (left thigh). Hot spots in the abdomen are consistent with liver and kidney accumulation.

levels of 0.75% ID/g at 2 h indicate fairly rapid plasma clearance. We also evaluated the stability of the peptide conjugate under different conditions (see Figure 5). The compound was injected into a nude mouse, and a blood sample was recovered 120 min postinjection. HPLC analysis showed degradation of the starting compound to hydrophilic byproducts and the starting material was no longer detectable (Figures 5A and 5B). As previous experience with CCK8-based ligands¹⁰ indicate that metabolism in the organs rather than in serum plays a major role, the compound was incubated with tissue homogenates obtained from liver and kidney (Figures 5C and 5D). In both cases, rapid degradation of the compound to very hydrophilic byproducts was observed; however, in kidney extracts the degradation was more complete, whereas in the liver we could still observe a significant amount of the starting material.

Imaging properties of [TcCO](KH)₂-CCK8 were assessed by performing gamma camera images 2 h after injection (see Figure 6). Concentration of the compound in the CCK2R positive tumor can be appreciated; however, the image also shows high-level background activity in kidney, liver, and gastrointestinal tract as expected from the biodistribution data.

CONCLUSIONS

We have reported the chemical synthesis, *in vitro* and *in vivo* biological properties of a new molecule, [TcCO](KH)₂-CCK8, based on CCK8 peptide as targeting agent bearing an amino acid-based chelator and labeled with the technetium(I) carbonyl. The compound shows specific binding to CCK2R receptors with high affinity, low nonspecific binding, and cellular internalization. The specificity of compound-receptor interaction is maintained *in vivo*. However, imaging applications of this compound could benefit from reduction of the relatively high-background radioactivity levels, likely linked to significant hepatobiliary clearance. The ease of synthesis and the modular design of this class of ligands allow their modification and further development with the aim of favoring renal clearance through increased hydrophilicity.

REFERENCES

- Liu, S.; Edwards, D. S. *Chem Rev* 1999, 99, 2235–2268.
- Aloj, L.; Morelli, G. *Curr Pharm Des* 2004, 10, 3009–3031.
- Benedetti, E.; Morelli, G.; Accardo, A.; Mansi, R.; Tesauro, D.; Aloj, L. *BioDrugs* 2004, 18, 279–295.
- Kwekkeboom, D.; Krenning, E. P.; de Jong, M. *J Nucl Med* 2000, 41, 1704–1713.
- Heppeler, A.; Froidevaux, S.; Eberle, A. N.; Maecke, H. R. *Curr Med Chem* 2000, 7, 971–994.
- Aloj, L.; Panico, M. R.; Caraco, C.; Zannetti, A.; Del Vecchio, S.; Di Nuzzo, C.; Arra, C.; Morelli, G.; Tesauro, D.; De Luca, S.; Pedone, C.; Salvatore, M. *Biopolymers* 2002, 66, 370–380.
- Wank, S. A. *Am J Physiol* 1998, 274, G607–G613.
- Reubi, J. C.; Schaer, J. C.; Waser, B. *Cancer Res* 1997, 57, 1377–1386.
- Aloj, L.; Panico, M.; Caraco, C.; Del Vecchio, S.; Arra, C.; Affuso, A.; Accardo, A.; Mansi, R.; Tesauro, D.; De Luca, S.; Pedone, C.; Visentin, R.; Mazzi, U.; Morelli, G.; Salvatore, M. *Cancer Biother Radiopharm* 2004, 19, 93–98.
- Aloj, L.; Caraco, C.; Panico, M.; Zannetti, A.; Del Vecchio, S.; Tesauro, D.; De Luca, S.; Arra, C.; Pedone, C.; Morelli, G.; Salvatore, M. *J Nucl Med* 2004, 45, 485–494.
- Ertay, T.; Unak, P.; Bekis, R.; Yurt, F.; Biber, F. Z.; Durak, H. *Nucl Med Biol* 2001, 28, 667–678.
- Morelli, G.; De Luca, S.; Tesauro, D.; Saviano, M.; Pedone, C.; Dolmella, A.; Visentin, R.; Mazzi, U. *J Pept Sci* 2002, 8, 373–381.
- Reubi, J. C.; Waser, B.; Schaer, J. C.; Laederach, U.; Erion, J.; Srinivasan, A.; Schmidt, M. A.; Bugaj, J. E. *Eur J Nucl Med* 1998, 25, 481–490.
- Laverman, P.; Roosenburg, S.; Gotthardt, M.; Park, J.; Oyen, W. J.; de Jong, M.; Hellmich, M. R.; Rutjes, F. P.; van Delft, F. L.; Boerman, O. C. *Eur J Nucl Med Mol Imaging* 2008, 35, 386–392.
- Melis, M.; Krenning, E. P.; Bernard, B. F.; de Visser, M.; Rolleman, E.; de Jong, M. *Nucl Med Biol* 2007, 34, 633–641.
- Agostini, S.; Bolzati, C.; Didone, E.; Cavazza-Ceccato, M.; Refosco, F.; Aloj, L.; Arra, C.; Aurilio, M.; Tornesello, A. L.; Tesauro, D.; Morelli, G. *J Pept Sci* 2007, 13, 211–219.
- Laverman, P.; Behe, M.; Oyen, W. J.; Willems, P. H.; Corstens, F. H.; Behr, T. M.; Boerman, O. C. *Bioconjug Chem* 2004, 15, 561–568.
- Alberto, R.; Schibli, R.; Egli, A.; Schubiger, P. A.; Abram, U.; Kaden, T. A. *J Am Chem Soc* 1998, 120, 7987–7988.
- Waibel, R.; Alberto, R.; Willuda, J.; Finnern, R.; Schibli, R.; Stichelberger, A.; Egli, A.; Abram, U.; Mach, J. P.; Pluckthun, A.; Schubiger, P. A. *Nat Biotechnol* 1999, 17, 897–901.
- Metzler-Nolte, N. *Angew Chem Int Ed Engl* 2001, 40, 1040–1043.
- Alberto, R.; Pak, J. K.; van Staveren, D.; Mundwiler, S.; Benny, P. *Biopolymers* 2004, 76, 324–333.
- von Guggenberg, E.; Behe, M.; Behr, T. M.; Saurer, M.; Seppi, T.; Decristoforo, C. *Bioconjug Chem* 2004, 15, 864–871.
- Zhang, K.; An, R.; Gao, Z.; Zhang, Y.; Aruva, M. R. *Nucl Med Biol* 2006, 33, 505–512.
- Maes, V.; Garcia-Garayoa, E.; Blauenstein, P.; Tourwe, D. *J Med Chem* 2006, 49, 1833–1836.
- Egli, A.; Alberto, R.; Tannahill, L.; Schibli, R.; Abram, U.; Schaffland, A.; Waibel, R.; Tourwe, D.; Jeannin, L.; Iterbeke, K.; Schubiger, P. A. *J Nucl Med* 1999, 40, 1913–1917.
- La Bella, R.; Garcia-Garayoa, E.; Langer, M.; Blauenstein, P.; Beck-Sickinger, A. G.; Schubiger, P. A. *Nucl Med Biol* 2002, 29, 553–560.
- La Bella, R.; Garcia-Garayoa, E.; Bahler, M.; Blauenstein, P.; Schibli, R.; Conrath, P.; Tourwe, D.; Schubiger, P. A. *Bioconjug Chem* 2002, 13, 599–604.
- Bullok, K. E.; Dyszlewski, M.; Prior, J. L.; Pica, C. M.; Sharma, V.; Piwnica-Worms, D. *Bioconjug Chem* 2002, 13, 1226–1237.
- Di Blasio, B.; Pavone, V.; Lombardi, A.; Pedone, C.; Benedetti, E. *Biopolymers* 1993, 33, 1037–1049.
- Eckelman, W. C. *Nucl Med Biol* 1994, 21, 759–769.

A vascular endothelial growth factor mimetic accelerates gastric ulcer healing in an iNOS-dependent manner

Genevieve K. Dudar,¹ Luca D. D'Andrea,² Rossella Di Stasi,² Carlo Pedone,² and John L. Wallace¹

¹Inflammation Research Network, University of Calgary, Calgary, Alberta, Canada; and ²Istituto di Biostrutture e Bioimmagini, Consiglio Nazionale delle Ricerche, Napoli, Italy

Submitted 5 May 2008; accepted in final form 20 June 2008

Dudar GK, D'Andrea LD, Di Stasi R, Pedone C, Wallace JL. A vascular endothelial growth factor mimetic accelerates gastric ulcer healing in an iNOS-dependent manner. *Am J Physiol Gastrointest Liver Physiol* 295: 374–381, 2008. First published June 26, 2008; doi:10.1152/ajpgi.90325.2008.—Angiogenesis is crucial to all types of wound healing, including gastric ulcer healing. The most potent promoter of angiogenesis is vascular endothelial growth factor (VEGF). We hypothesized that a 15-amino acid peptide designed to mimic the angiogenic action of VEGF would accelerate gastric ulcer healing. Gastric ulcers were induced in mice by serosal application of acetic acid. Treatment with the VEGF mimetic accelerated gastric ulcer healing when administered orally or intraperitoneally, at a dose of 50 ng/kg or greater. Such healing was not observed when the reverse sequence pentadecapeptide or the full-length VEGF protein was administered. Contrary to our hypothesis, the VEGF mimetic did not significantly increase angiogenesis in the ulcerated stomach. The enhancement of ulcer healing by the VEGF mimetic occurred independently of cyclooxygenase-2 (COX-2) activity but was blocked by inhibitors of inducible nitric oxide synthase (iNOS). These results demonstrate that a VEGF mimetic is a potent stimulus for gastric ulcer healing, even when given orally. The effects of the mimetic were independent of stimulatory effects on angiogenesis and COX-2 activity but were dependent on iNOS-derived NO production.

stomach; nitric oxide; cyclooxygenase; angiogenesis; prostaglandin; gastric mucosa

CHRONIC GASTRIC ULCER HEALING involves epithelial cell migration and proliferation, matrix remodeling, and angiogenesis. These processes can be modulated by a plethora of transcription factors, growth factors, and cytokines (36). Growth factors that influence angiogenesis have been of particular interest to many investigators (13, 23, 31). Vascular endothelial growth factor (VEGF), a 46-kDa homodimeric glycoprotein, is the most potent stimulator of angiogenesis (31). It is produced by a variety of cell types including macrophages, smooth muscle cells, fibroblasts, megakaryocytes, and neoplastic cells (2, 17).

Several studies have provided evidence for a role of VEGF in gastric ulcer healing. For example, expression of VEGF was detected in the margins of human gastric ulcers (32). The same group observed that rat gastric fibroblasts could express VEGF, and this expression was enhanced when the fibroblasts were exposed to growth factors that stimulated ulcer healing (e.g., epidermal growth factor and hepatocyte growth factor) (33). Expression of VEGF was observed to be elevated following induction of gastric ulcers in rats, in parallel with increases in angiogenesis (29).

There is also a link among prostaglandin synthesis by the gastric mucosa, VEGF expression, and angiogenesis. Although indomethacin suppressed ulcer healing and angiogenesis in rats, it did not affect gastric VEGF expression (29). It has been known for several years that cyclooxygenase-2 (COX-2) makes an important contribution to the healing of ulcers throughout the gastrointestinal tract (15, 20, 25, 28). Again, this may be linked to the role of VEGF in ulcer healing. COX-2 and VEGF have been colocalized in fibroblasts in the ulcer bed (19). A selective COX-2 inhibitor suppressed VEGF release from human gastric fibroblasts, and this could be reversed by addition of prostaglandin E₂ (PGE₂) to the culture medium (19).

The possibility that VEGF can be exploited therapeutically to improve gastric ulcer healing has been investigated. Jones et al. (10) observed enhanced ulcer healing in rats following a single injection of naked DNA encoding VEGF. This effect was significantly reduced by cotreatment with an antibody directed against VEGF. We exploited the platelet as a rich source of VEGF to examine its effects on gastric ulcer healing. Ulcer healing could be substantially accelerated by oral treatment with a suspension of human platelets, and this effect was reversed by immunoneutralization of VEGF (40).

In the present study, we have examined the effects of a 15-amino acid peptide that adopts a helical conformation in aqueous solution that resembles the α -helical region (17–25) of the VEGF protein (4). This peptide has been shown to bind to both the VEGF-1 and VEGF-2 receptors and to induce endothelial cell proliferation, activate the same signaling cascades as VEGF, and stimulate capillary formation in vitro (4). We have examined the ability of this VEGF mimetic to influence experimental ulcer healing and characterized the dependence of such effects on angiogenesis and on COX-2 and nitric oxide synthase (NOS) activity.

MATERIALS AND METHODS

Animals. All experiments were approved by the University of Calgary Animal Care Committee. Male Wistar rats weighing 150–175 g and male C57BL/6 mice weighing 20–25 g were obtained from Charles River Laboratories (Montreal, Quebec, Canada). The animals had free access to a standard laboratory chow and were housed in a room with a 12-h:12-h light-dark cycle.

Peptides. The VEGF mimetic used in these studies is a 15-amino acid peptide (KLTWQELYQLKYKGI), synthesized as described by D'Andrea et al. (4). The NH₂ terminus of the peptide is acetylated, whereas the COOH terminus is capped with an amide group. The effects of a peptide with the reverse sequence of the VEGF mimetic (IGKYKLQYLEQWTLK) were also assessed. As with the VEGF

Address for reprint requests and other correspondence: J. Wallace, Dept. of Pharmacology & Therapeutics, Univ. of Calgary, 3330 Hospital Dr. NW, Calgary, Alberta, T2N 4N1, Canada (e-mail: wallacej@ucalgary.ca).

The costs of publication of this article were defrayed in part by the payment of page charges. The article must therefore be hereby marked "advertisement" in accordance with 18 U.S.C. Section 1734 solely to indicate this fact.

mimetic, the NH₂ terminus of the reverse peptide is capped with an acetyl group and the COOH terminus ends in an amide group.

Gastric ulcer induction. Gastric ulcers were induced in mice according to the method outlined by Wang et al. (45), with slight modifications (41). In brief, a laparotomy was performed under halothane anesthesia, and the stomach was externalized. A 1-ml syringe, with its barrel cut and filed smooth, was placed firmly against the serosal side of the stomach. Acetic acid [200 μ l of 20% (vol/vol)] was added to the syringe such that it was in contact with the serosal surface for 1 min. The acetic acid was removed from the syringe by aspiration and replaced with several rinses of sterile saline. The stomach was then placed back to its original anatomical position, and the midline incision was closed with sutures.

The procedure used to induce gastric ulcers in rats was similar to that employed for mice, with a few differences. The rats were fasted overnight before the surgery. Acetic acid (80% vol/vol) was applied to the serosal wall of the stomach for 1 min with the barrel of a 3-ml syringe.

Measurement of gastric ulcer area. In each experiment, a group of mice or rats was euthanized on *day 3* after ulcer induction. This provided data on the size of ulcers before treatment. Groups of animals were similarly euthanized at various times after beginning treated with test drugs. In all cases, the stomach was excised and pinned out (mucosal surface up) onto a wax block. A 25-mm² paper grid was placed adjacent to the ulcer, and a photograph was taken. The photograph was then enlarged and used for planimetric measurement of the ulcer area (performed by an observer unaware of the treatments the animals had received). The area of ulceration was then converted into units of mm² using the paper grid as a reference. In some experiments, samples of gastric tissue were processed for further evaluation (e.g., immunohistochemistry).

Effects of the VEGF mimetic on ulcer healing. The ability of the VEGF mimetic to accelerate ulcer healing was first examined in the mouse. Beginning 3 days after ulcer induction, mice were treated twice-daily intraperitoneally with the VEGF mimetic (100 ng/kg) or vehicle (sterile 0.9% saline). Groups of 5–7 mice were euthanized on *days 5, 7, and 10* after ulcer induction, and gastric ulcer areas were measured.

Next, the ability of different doses of the VEGF mimetic to enhance gastric ulcer healing was assessed. Beginning on *day 3* after ulcer induction, mice were treated intraperitoneally with vehicle ($n = 16$) or the VEGF mimetic at 25 ng/kg ($n = 4$), 50 ng/kg ($n = 13$), or 100 ng/kg ($n = 4$). The mice were euthanized on *day 7* after ulcer induction for measurement of ulcer area.

Whether or not the VEGF mimetic would be effective when administered orally was then examined. Groups of mice were treated twice daily with vehicle or the VEGF mimetic (50 ng/kg), each being given either intraperitoneally or orally ($n = 5$ –9 per group). The mice were euthanized on *day 7* for measurement of gastric ulcer area.

A series of experiments was performed to determine whether the beneficial effects of the VEGF mimetic on ulcer healing could be observed with the full-length VEGF protein. Groups of 6–9 rats were treated twice daily with VEGF (1 μ g/kg) or vehicle, given either orally or intraperitoneally, beginning on *day 3* after ulcer induction and continuing until *day 7*. The mice were then euthanized, and ulcer areas were measured. The dose of VEGF used in this experiment represents an equimolar dose to 50 ng/kg of the VEGF mimetic.

The effects of the VEGF mimetic on gastric ulcer healing were then compared with the effects of a peptide with the same length as the mimetic but with the reverse sequence. Twice daily intraperitoneal treatment with vehicle ($n = 6$), the VEGF mimetic (50 ng/kg, $n = 6$), or the reverse sequence peptide (50 ng/kg ip, $n = 7$) was conducted over a 3-day period beginning on the third day after ulcer induction. The mice were then euthanized, and ulcer areas were determined.

The experiments described above all involved the use of mice. The following experiment was performed to determine whether the VEGF mimetic could influence ulcer healing in rats. Beginning on *day 3* after

ulcer induction, groups of 5 rats each were treated twice daily intraperitoneally with the VEGF mimetic (50 ng/kg) or vehicle. The rats were euthanized on *day 7* after ulcer induction for measurement of gastric ulcer area.

Gastric acid secretion. Since agents that suppress gastric acid secretion can accelerate ulcer healing in this model (9), we examined the possibility that the VEGF mimetic might suppress gastric acid secretion in the mouse. Mice were fasted overnight and anesthetized with halothane. The pyloric sphincter was ligated, and the mice were allowed to recover consciousness. The mice were then treated intraperitoneally with vehicle ($n = 4$) or the VEGF mimetic (100 ng/kg, $n = 5$). Three hours later, the mice were anesthetized with halothane, the lower gastro-esophageal junction was clamped, and the stomach was carefully excised. The contents of the stomach were collected into a tube and the volume of the fluid determined gravimetrically. The pH and the titratable acidity of the gastric juice were determined, as described previously (1).

Angiogenesis. Gastric tissues harvested at the end of some of the above-described experiments were assessed for the extent of angiogenesis occurring in the ulcer bed and at the ulcer margin. Microvessels were visualized via immunohistochemical staining of CD31, an endothelial cell-specific marker (18). Tissue samples were immersed in formalin-free zinc fixative and embedded into paraffin blocks. Sections (7 μ m) of the tissues were then cut and placed onto positively charged glass slides, heated overnight at 60°C, and stored until further processing.

The sections were deparaffinized and rehydrated using an ethanol gradient and then boiled in citrate buffer for 10 min to achieve epitope retrieval. The tissue was blocked with normal rabbit serum blocking solution for 1 h before overnight incubation at 4°C with rat anti-mouse CD31 antibody (PharMingen, San Diego, CA). Afterward, an endogenous peroxidase-blocking step was performed with the use of 3% hydrogen peroxide in 0.01 M PBS (pH 7.4) solution for 10 min at room temperature. The primary antibody that bound to the tissue sections was detected using the horseradish peroxidase-Streptavidin method (Vector Laboratories, Burlington, ON, Canada). The microvessels were detectable once the tissue underwent a reaction with diaminobenzidine. The stained microvessels in the granulation tissue were counted in a blind manner under a microscope at a magnification of 400 \times . The results were reported as the number of microvessels per mm² of tissue.

Role of COX-2. COX-2 plays an important role in the healing of ulcers in mice and rats (15, 19) and has also been shown to regulate release of VEGF from gastric fibroblasts (19). We therefore investigated the possibility that COX-2 activity may be necessary for the enhancement of ulcer healing by the VEGF mimetic. Groups of mice with gastric ulcers were treated twice daily, from *day 3* to *day 7*, with a selective COX-2 inhibitor (lumiracoxib, 10 mg/kg po, $n = 8$), with the VEGF mimetic (50 ng/kg ip, $n = 14$), or with both the VEGF mimetic and lumiracoxib ($n = 9$). An additional group of mice was treated with the vehicles for lumiracoxib and the VEGF mimetic (1% carboxymethylcellulose and 0.9% saline, respectively). On *day 7*, the mice were euthanized and ulcer areas were measured. Lumiracoxib is a selective inhibitor of COX-2 (8). We confirmed that the 10-mg/kg dose of lumiracoxib produced a selective inhibition of COX-2 in mice. As described in detail elsewhere (38, 46), injection of carrageenan or zymosan into an air pouch on the rat or mouse results in a marked stimulation of PGE₂ synthesis, with this synthesis occurring almost exclusively via COX-2. Oral pretreatment with lumiracoxib (10 mg/kg) reduced zymosan-induced PGE₂ synthesis by 90% ($P < 0.01$) while not significantly affecting whole blood thromboxane synthesis [the latter occurring exclusively via COX-1 (37)].

Role of NOS. NO contributes significantly to gastric mucosal defense (42, 44) and has been shown to contribute significantly to experimental ulcer healing (12, 14). Expression of inducible NOS (iNOS) has been noted in inflammatory cells at the base of gastric ulcers in rodents (14). NO has also been reported to be a crucial

mediator of VEGF-dependent angiogenesis (22, 47). Indeed, there is evidence of reciprocal regulation between NO and VEGF in the context of angiogenesis (11).

We performed studies to determine whether NOS activity was required for the enhancement of ulcer healing by VEGF and further examined whether selective inhibition of the inducible isoform of NOS (iNOS) contributed to VEGF mimetic-induced ulcer healing. Beginning 3 days after the ulcer induction, groups of mice were treated twice daily intraperitoneally with saline ($n = 7$), the VEGF mimetic (50 ng/kg, $n = 7$), nitro-L-arginine methyl ester (L-NAME) (15 mg/kg, $n = 4$), both the VEGF mimetic and L-NAME (15 mg/kg, $n = 5$), N^{ϵ} -(iminoethyl)-L-lysine (L-NIL) (3 mg/kg, $n = 5$), or both the VEGF mimetic and L-NIL ($n = 5$). On *day 7*, the treated mice were euthanized, and ulcer areas were determined. L-NAME is a nonselective inhibitor of NOS (24); that is, it inhibits all three of the identified isoforms of this enzyme. L-NIL is a selective inhibitor for the inducible isoform of NOS (21).

Materials. Indomethacin was purchased from Sigma Chemicals (St. Louis, MO) and was dissolved in 5% sodium bicarbonate. Lumiracoxib was purchased from SynphaBase AG (Muttens, Switzerland) and was suspended in 1% carboxymethylcellulose sodium. L-NAME (Sigma) and L-NIL (Sigma) were dissolved in 0.9% saline. VEGF was purchased from Chemicon International (Temecula, CA) and was dissolved in sterile distilled water.

Statistical analysis. All data are expressed as the means \pm SE. Comparisons of data among multiple groups were performed with one-way ANOVA followed by Dunnett's multiple comparison test. Comparisons between two groups were conducted using the unpaired Student's *t*-test. An associated probability of less than 5% was considered significant.

RESULTS

Enhancement of gastric ulcer healing by a VEGF mimetic. Gastric ulcers were clearly visible and of relatively consistent size 3 days after application of acetic acid to the serosal surface of the mouse stomach. The ulcers penetrated into the submucosal layer. In mice treated twice daily with vehicle, the size of the ulcers decreased over time (Fig. 1). A significantly more pronounced reduction of ulcer area was observed in mice treated twice daily with the VEGF mimetic.

The VEGF mimetic accelerated ulcer healing in a dose-dependent manner (Fig. 2). Intraperitoneal treatment at a dose of 25 ng/kg did not significantly affect gastric ulcer healing compared with that in mice treated with vehicle. However, at doses of 50 and 100 ng/kg, the VEGF mimetic significantly enhanced ulcer healing.

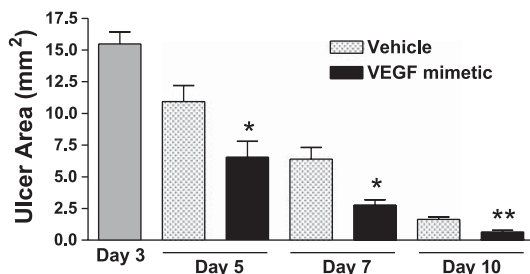


Fig. 1. Time course of gastric ulcer healing in mice treated intraperitoneally with vehicle or the vascular endothelial growth factor (VEGF) mimetic. Treatment with vehicle or the VEGF mimetic (100 ng/kg) was initiated on *day 3* (note that the *day 3* bar is indicative of the size of ulcers before initiation of treatment). Data represent means \pm SE of at least 5 mice per group. * $P < 0.05$, ** $P < 0.01$ vs. the corresponding vehicle-treated group.

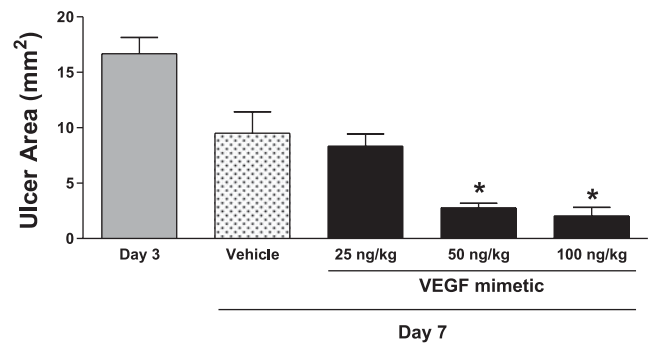


Fig. 2. Dose-dependent improvement of ulcer healing by a VEGF mimetic in mice. The VEGF mimetic and vehicle were administered intraperitoneally twice daily beginning on *day 3*. Data represent means \pm SE for at least 5 mice per group. * $P < 0.05$ vs. the vehicle-treated group.

The VEGF mimetic also significantly enhanced ulcer healing when given orally (Fig. 3). Thus oral treatment with the VEGF mimetic from *days 3* through *7* after induction of ulcers resulted in significantly smaller ulcers compared with treatment orally with vehicle that were not significantly different than what was observed in mice treated intraperitoneally with the VEGF mimetic.

In contrast to the improved healing observed in mice treated with the VEGF mimetic, treatment with the full-length VEGF protein did not significantly affect ulcer healing when given either intraperitoneally or orally (Fig. 3). Also, intraperitoneal treatment with a peptide with the reverse sequence of the VEGF mimetic did not significantly affect ulcer healing compared with vehicle treatment (8.6 ± 0.8 vs. 10.8 ± 1.4 mm², respectively; $n = 6-7$).

As in mice, the ulcers in rats were well established 3 days after application of acetic acid to the serosal surface of the stomach. The mean ulcer area at *day 3* was 118 ± 6 mm². By *day 7*, the mean ulcer area in rats treated with vehicle had declined to 91 ± 10 mm², but a significantly greater reduction of ulcer area was observed in the rats treated intraperitoneally with 100 ng/kg of the VEGF mimetic (35 ± 15 mm²; $P < 0.05$ vs. the vehicle-treated group; $n = 4$ per group).

Lack of effect of the VEGF mimetic on acid secretion. Intraperitoneal administration of the VEGF mimetic at a dose (100 ng/kg) that had a significant effect on ulcer healing did not have any detectable effect on gastric acid secretion. The

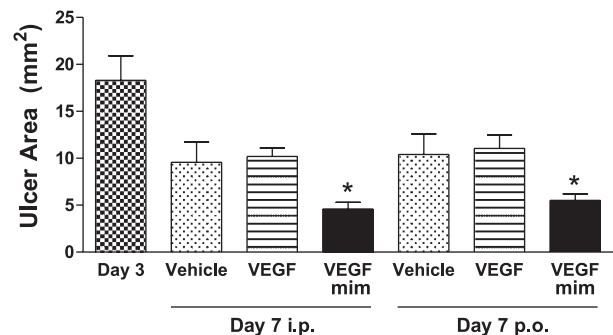


Fig. 3. Effects of oral (po) vs. intraperitoneal (ip) administration of the VEGF mimetic (mim) (50 ng/kg) or the full-length VEGF peptide (1 μ g/kg; equimolar to the dose of the VEGF mimetic) on gastric ulcer healing. Twice daily treatment was started on *day 3* after ulcer induction and continued until *day 7*. * $P < 0.05$ vs. the corresponding vehicle-treated group ($n = 6-9$ per group).

volume of gastric juice recovered from the pylorus-ligated stomach 3 h after administration of the VEGF mimetic did not differ significantly from that collected from vehicle-treated rats (0.62 ± 0.09 vs. 0.66 ± 0.06 ml, respectively). The titratable acidity in the gastric juice was also similar in the VEGF mimetic-treated vs. vehicle-treated mice (10.4 ± 2.7 vs. 10.1 ± 1.3 meq, respectively).

Effects of the VEGF mimetic on ulcer healing are COX-2 independent. As in the experiments described above, mice treated with the VEGF mimetic (50 mg/kg) from day 3 to day 7 had an average ulcer area that was significantly smaller than that in the vehicle-treated mice (Fig. 4). Treatment with lumiracoxib, a selective inhibitor of COX-2, did not affect ulcer healing compared with vehicle-treated mice. Moreover, mice treated with the combination of lumiracoxib and the VEGF mimetic still exhibited a significant improvement in the extent of healing compared with vehicle-treated mice.

Effects of the VEGF mimetic on ulcer healing are NO dependent. Treatment with L-NAME did not significantly affect ulcer healing (Fig. 5). However, when L-NAME was coadministered with the VEGF mimetic, ulcer healing occurred to a similar extent as was observed with vehicle treatment; that is, a significant effect of the VEGF mimetic on ulcer healing was no longer apparent.

To determine whether selective inhibition of iNOS would produce the same inhibitory effect on VEGF-induced enhancement of ulcer healing, the effects of treatment with L-NIL were examined. As was the case with L-NAME, treatment with L-NIL did not influence ulcer healing compared with vehicle (Fig. 5). However, mice cotreated with L-NIL and the VEGF mimetic did not exhibit the extent of ulcer healing that was observed in mice treated with the VEGF mimetic alone.

Effects of the VEGF mimetic on angiogenesis. The effects of the VEGF mimetic on angiogenesis were examined by quantifying the number of microvessels in the ulcer bed (granulation tissue) and in the ulcer margin. Angiogenic microvessels were clearly identifiable in the ulcer bed and ulcer margin after staining for CD31 (Fig. 6). Little if any staining for CD31 was detected in gastric tissue from healthy mice (i.e., no ulcers). The number of microvessels in the ulcer margin did not change significantly between days 3 and 5 after ulcer induction, but there was a significant increase in angiogenesis in the granu-

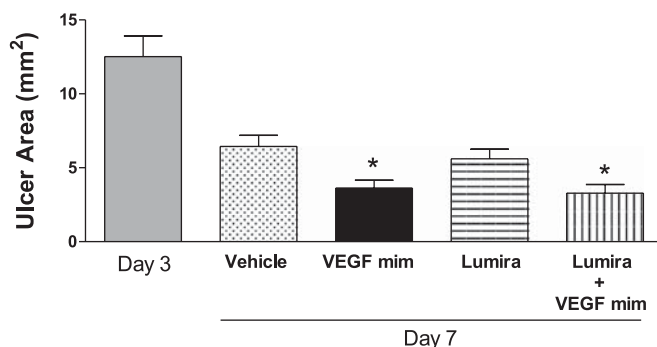


Fig. 4. Effects of treatment with a selective cyclooxygenase-2 (COX-2) inhibitor (lumiracoxib, 10 mg/kg) on the ability of a VEGF mimetic (50 ng/kg) to improve ulcer healing in mice. Vehicle and the VEGF mimetic were administered intraperitoneally, whereas lumiracoxib was administered orally. Data represent means \pm SE, with $n = 8-14$ mice per group. * $P < 0.05$ vs. the vehicle-treated group.

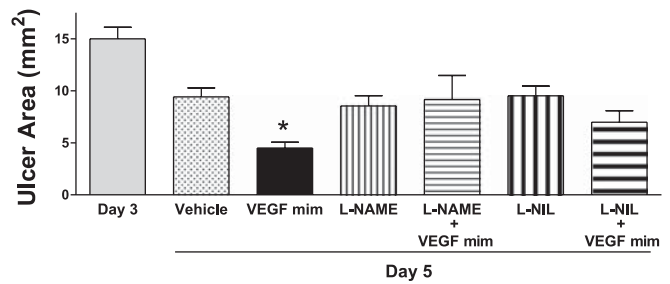


Fig. 5. Gastric ulcer area in mice treated with vehicle or the VEGF mimetic (50 ng/kg ip), alone or in conjunction with a nitric oxide synthase (NOS) inhibitor [either nitro-L-arginine methyl ester (L-NAME), 15 mg/kg ip, or *N*⁶-(iminoethyl)-L-lysine (L-NIL), 3 mg/kg ip]. Data represent means \pm SE; $n = 4-7$ mice per group. * $P < 0.05$ vs. the corresponding vehicle-treated group.

lation tissue (Figs. 6 and 7). In mice treated with the VEGF mimetic, the extent of angiogenesis was similar to that in the vehicle-treated group.

Treatment with L-NIL did not significantly affect the extent of angiogenesis compared with vehicle-treated mice, either in the ulcer bed or the ulcer margin (Fig. 7). However, in both tissues, cotreatment of mice with L-NIL and the VEGF mimetic resulted in a significant reduction of the extent of angiogenesis ($P < 0.05$ compared with the vehicle-treated group and compared with the group treated with the VEGF mimetic alone).

DISCUSSION

VEGF is the most potent known stimulator of angiogenesis (31), a process integral to all types of wound healing. In the present study, we examined the effects on gastric ulcer healing of a VEGF mimetic modeled on a portion of the VEGF region responsible for binding to and activating the VEGF receptors. This pentadecapeptide significantly accelerated gastric ulcer healing in mice and rats. Significant effects were observed with a dose as low as 50 ng/kg and when given orally or intraperitoneally. The effect of the mimetic was specific, in that the reverse-sequence pentadecapeptide did not significantly affect ulcer healing. Moreover, an equimolar dose of VEGF did not affect ulcer healing, whether given orally or intraperitoneally. Contrary to our hypothesis, the beneficial effects of the VEGF mimetic on ulcer healing did not appear to be due to enhancement of angiogenesis.

Reconstruction of the destroyed vascular network within the ulcerated site is integral to healing because granulation tissue formation and tissue deposition are dependent upon nutrient availability and nutrients are delivered to the injured site via capillaries. As observed previously (15, 16), there was a marked increase in microvessel density in response to the induction of an ulcer in the stomach. However, treatment with the VEGF mimetic did not increase the extent of angiogenesis above that observed in vehicle-treated rats. Our hypothesis that the VEGF mimetic would enhance angiogenesis was based on the fact that the mimetic was designed to replicate the region of the VEGF protein responsible for interacting with the VEGF receptors that are known to trigger angiogenesis in vitro (4). Indeed, previous studies of the VEGF mimetic demonstrated that this peptide can bind to the VEGF receptors, initiate VEGF-induced signaling cascades, and stimulate angiogenesis in vitro (4).

In considering other potential mechanisms of action of the VEGF mimetic, we first considered the possibility that the

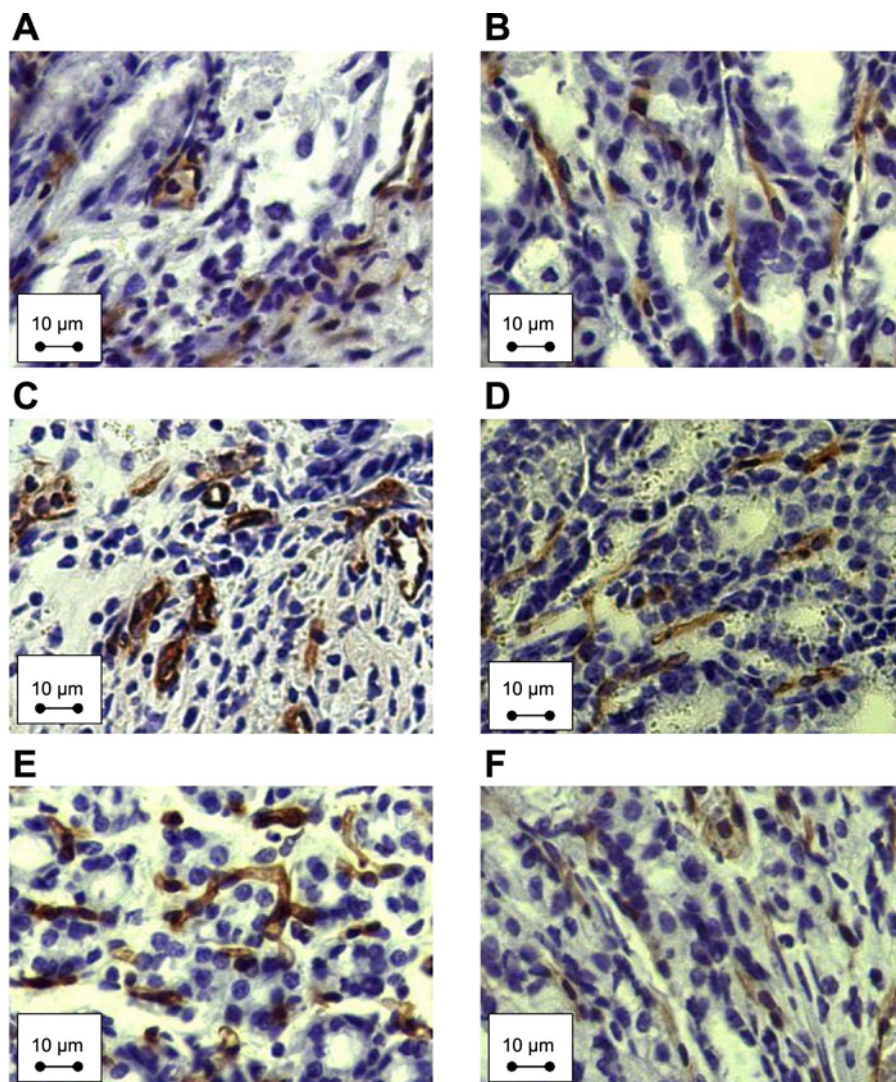


Fig. 6. Immunohistochemical staining of the endothelial cell marker CD31 in granulation tissue (A–C) and the ulcer margin (D–F). A and D show *day 3* mice, B and E show *day 5* vehicle-treated mice (ip), and C and F show *day 5* VEGF mimetic-treated mice (50 ng/kg ip).

mimetic might reduce gastric acid secretion since inhibitors of acid secretion are the mainstay of treatment of gastric ulcers and have been shown to be effective in this model (9). However, the mimetic, when administered at a dose that was effective in enhancing ulcer healing, had no effect on the volume of gastric juice or its acidity.

We then examined the possibility that the beneficial effects of the VEGF mimetic were mediated via COX-2. COX-2 plays an important role in gastric mucosal defense (43) and can be rapidly upregulated in response to mucosal irritants, including aspirin (6). Prostaglandins produced in the ulcerated mouse stomach are largely derived from COX-2 (19), and inhibition of COX-2 activity has been shown to significantly delay ulcer healing (15, 20, 28). Moreover, treatment with conventional nonsteroidal anti-inflammatory drugs (NSAIDs) and selective COX-2 inhibitors at doses that delay ulcer healing in rats was also found to alter the ratios of pro- and antiangiogenic factors (VEGF and endostatin, respectively) in serum. COX-2-derived prostaglandins can stimulate the release of VEGF (19), whereas NSAIDs can interfere with downstream proangiogenic signaling of VEGF (30). In the present study, we found that treatment with a selective COX-2 inhibitor (lumiracoxib) did not inter-

fer with the beneficial effects of the VEGF mimetic on ulcer healing in mice. Importantly, we confirmed that the dose of lumiracoxib used in these experiments produced a significant (>90%) inhibition of COX-2 activity in the mouse.

Like prostaglandins, NO contributes significantly to gastric mucosal defense and healing (42, 44). Inhibitors of NO synthesis have been shown to delay ulcer healing in rodent models (12, 14), while NO donors can significantly accelerate healing in these models (7, 12, 15). Expression of iNOS is apparent in inflammatory cells in the ulcer bed in rats (14). The delay in gastric ulcer healing that occurs following administration of inhibitors of NO synthesis has been associated with diminished angiogenesis and impaired blood flow at the ulcer margin (3, 12, 35). In the present study, the potential role of NO synthesis in the actions of the VEGF mimetic was examined through the use of a nonselective NOS inhibitor (L-NAME) and a selective iNOS inhibitor (L-NIL). Neither of these inhibitors, alone, significantly affected ulcer healing when administered over a period of 4 days. However, both inhibitors interfered with the ability of the VEGF mimetic to enhance ulcer healing. Moreover, inhibition of iNOS activity resulted in a significant reduction of angiogenesis in the ulcer bed and ulcer margin of

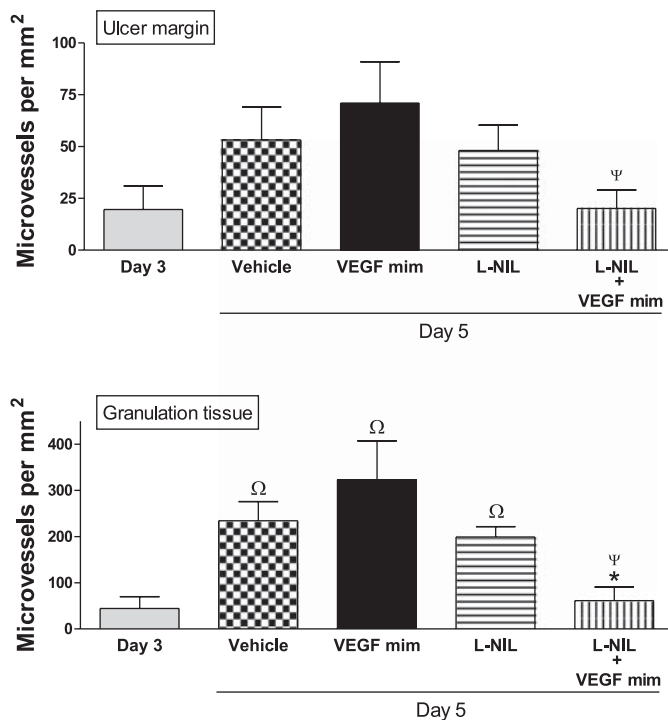


Fig. 7. Angiogenesis in the ulcer margin and granulation tissue (ulcer bed) of mice treated intraperitoneally with vehicle, the VEGF mimetic (50 ng/kg), or a selective inhibitor of inducible NOS (L-NIL, 3 mg/kg ip). Treatment was initiated on *day 3* after ulcer induction, and tissues were harvested for determination of extent of angiogenesis (CD31-positive staining microvessels) on *day 5* after ulcer induction. Data represent means \pm SE, with $n = 12$ – 14 mice per group. $\Omega P < 0.05$ vs. the *day 3* group; $\Psi P < 0.05$ vs. the vehicle-treated group; $\Psi P < 0.05$ vs. the group treated only with the VEGF mimetic. There were no statistical differences between the vehicle and the VEGF mimetic-treated groups.

mice treated with the VEGF mimetic to levels even lower than those observed in vehicle-treated rats. This is consistent with the findings of previous studies that NO is also crucial for VEGF-dependent angiogenesis (22, 47), but, to our knowledge, this is the first demonstration of a beneficial effect on healing being mediated by iNOS.

Gastrointestinal ulceration and bleeding remain significant clinical concerns, particularly in patients taking NSAIDs on a chronic basis (39). Cotherapy with proton pump inhibitors is the most common approach to preventing ulceration and promoting the healing of existing ulcers in these patients. However, there is still a need for agents that will promote more rapid and effective healing. In terms of therapeutic utility, it is noteworthy that the VEGF mimetic was as effective in promoting ulcer healing when given orally as when given systemically. This is in contrast to the experiments in the present study and in a previous study (40), showing that oral (or systemic) administration of the full-length VEGF protein did not affect ulcer healing. Of course, it is possible that higher doses of the full-length VEGF protein would accelerate ulcer healing, but in the present study we tested a dose equimolar to an effective dose of the mimetic. We previously observed that administration of a suspension of human platelets to rats with gastric ulcers resulted in a marked acceleration of ulcer healing in a VEGF-dependent manner (40). We speculated that the effectiveness of VEGF delivered in this way, vs. administration

of the VEGF itself, may indicate the need for “presentation” of the VEGF by the platelet. For example, the release of VEGF from platelets that have bound to damaged tissue may result in a high local concentrations and possibly protection from proteolytic actions or denaturation by luminal acid. In the case of the VEGF mimetic, certain modifications were made to enhance its biological half-life; thus, the NH_2 - and COOH -terminal modifications of the peptide make it more resistant to proteolytic degradation by exopeptidases (4). Also, the fact that the mimetic, when given orally, accelerated gastric ulcer healing to the same extent as when given systemically suggests that the mimetic is stable in gastric acid, at least for a period of time sufficient to affect the healing process. The importance of VEGF in ulcer healing and/or maintenance of mucosal integrity in humans is supported by the recent reports of gastrointestinal ulceration occurring in patients with colorectal cancer treated with an anti-VEGF antibody (bevacizumab) (27).

We utilized a mouse model of gastric ulceration that involves serosal application of acetic acid for a brief period of time. This is a clinically irrelevant means of inducing an ulcer; nevertheless, this model has several advantages for use in a study such as the present one. The size of the ulcers is reproducible from animal to animal (thus facilitating studies of rates of healing), and the ulcers are histologically similar to human gastric ulcers (45). Importantly, a previous study using the same model demonstrated that ulcer healing could be accelerated by local injection of naked DNA encoding VEGF (10), and our own studies demonstrated that ulcer healing in this model could be enhanced in a VEGF-dependent manner by administration of rat or human platelets (16, 40). Gastric ulcers in humans are mainly associated with the use of NSAIDs or with colonization of the stomach by *Helicobacter pylori* (*H. pylori*). Unfortunately, repeated oral administration of NSAIDs to rodents does not reproducibly result in gastric ulceration (indeed, severe intestinal ulceration is more common, often leading to perforation and death) (5, 26). Although there are several animal models of *H. pylori* infection, gastric ulceration is not a consistent feature of any such models.

In summary, the studies described herein demonstrate that a 15-amino acid mimetic of VEGF is a very potent stimulus for gastric ulcer healing in rodents and is active when given orally or systemically. The acceleration of healing by this mimetic is dependent upon iNOS activity but not on COX-2 activity. From the present studies, it would appear that the acceleration of ulcer healing induced by the VEGF mimetic is not related to an enhancement of angiogenesis in the ulcerated tissue. Given its oral bioavailability and potency, this mimetic may have therapeutic utility for the treatment of ulceration in the gastrointestinal tract.

ACKNOWLEDGMENTS

The authors are grateful to Webb McKnight, Gary Martin, and Mike Dickey for their assistance in performing these studies.

GRANTS

This work was supported by a grant from the Canadian Institutes of Health Research. Dr. Wallace holds a Canada Research Chair in Inflammation and is an Alberta Heritage Foundation for Medical Research Scientist.

REFERENCES

- Barnett K, Bell CJ, McKnight W, Dickey M, Sharkey KA, Wallace JL. Role of cyclooxygenase-2 in modulating gastric acid secretion in the normal and inflamed rat stomach. *Am J Physiol Gastrointest Liver Physiol* 279: G1292–G1297, 2000.
- Berse B, Brown LF, Van de Water L, Dvorak HF, Senger DR. Vascular permeability factor (vascular endothelial growth factor) gene is expressed differentially in normal tissues, macrophages, and tumors. *Mol Biol Cell* 3: 211–220, 1992.
- Brzozowski T, Konturek PC, Sliwowski Z, Drozdowicz D, Hahn EG, Konturek SJ. Importance of nitric oxide and capsaicin-sensitive afferent nerves in healing of stress lesions induced by epidermal growth factor. *J Clin Gastroenterol* 25: S28–S38, 1997.
- D'Andrea LD, Iaccarino G, Fattorusso R, Sorriento D, Carannante C, Capasso D, Trimarco B, Pedone C. Targeting angiogenesis: structural characterization and biological properties of a de novo engineered VEGF mimicking peptide. *Proc Natl Acad Sci USA* 102: 14215–14220, 2005.
- Davies NM, Røseth AG, Appleyard CB, McKnight W, Del Soldato P, Calignano A, Cirino G, Wallace JL. NO-naproxen vs. naproxen: ulcerogenic, analgesic and anti-inflammatory effects. *Aliment Pharmacol Ther* 11: 69–79, 1997.
- Davies NM, Sharkey KA, Asfaha S, MacNaughton WK, Wallace JL. Aspirin causes rapid up-regulation of cyclo-oxygenase-2 expression in the stomach of rats. *Aliment Pharmacol Ther* 11: 1101–1108, 1997.
- Elliott SN, McKnight W, Cirino G, Wallace JL. A nitric oxide releasing nonsteroidal anti-inflammatory drug accelerates gastric ulcer healing in rats. *Gastroenterology* 109: 524–530, 1995.
- Esser R, Berry C, Du Z, Dawson J, Fox A, Fujimoto RA, Haston W, Kimble EF, Koehler J, Peppard J, Quadros E, Quintavalla J, Toscano K, Urban L, van Duzer J, Zhang X, Zhou S, Marshall PJ. Preclinical pharmacology of lumiracoxib: a novel selective inhibitor of cyclooxygenase-2. *Br J Pharmacol* 144: 538–550, 2005.
- Ito M, Segami T, Tsukahara T, Kojima R, Suzuki Y. Effect of cimetidine and omeprazole on gastric ulcer healing of rats with limited food intake time. *Eur J Pharmacol* 263: 245–251, 1994.
- Jones MK, Kawanaka H, Baatar D, Szabo IL, Tsugawa Pai R, Koh GY, Kim I, Sarfeh J, Tarnawski AS. Gene therapy for gastric ulcers with single local injection of naked DNA encoding VEGF and angiopoietin-1. *Gastroenterology* 121: 1040–1047, 2001.
- Kimura H, Esumi H. Reciprocal regulation between nitric oxide and vascular endothelial growth factor in angiogenesis. *Acta Biochim Pol* 50: 49–59, 2003.
- Konturek SJ, Brzozowski T, Majka J, Pytko-Polonczyk J, Stachura J. Inhibition of nitric oxide synthase delays healing of chronic gastric ulcers. *Eur J Pharmacol* 239: 215–217, 1993.
- Konturek SJ. Role of growth factors in gastroduodenal protection and healing of peptic ulcers. *Gastroenterol Clin North Am* 19: 41–65, 1990.
- Ma L, Wallace JL. Endothelial nitric oxide synthase modulates gastric ulcer healing in rats. *Am J Physiol Gastrointest Liver Physiol* 279: G341–G346, 2000.
- Ma L, del Soldato P, Wallace JL. Divergent effects of new cyclooxygenase inhibitors on gastric ulcer healing: Shifting the angiogenic balance. *Proc Natl Acad Sci USA* 99: 13243–13247, 2002.
- Ma L, Elliott SN, Cirino G, Buret A, Ignarro LJ, Wallace JL. Platelets modulate gastric ulcer healing: role of endostatin and vascular endothelial growth factor release. *Proc Natl Acad Sci USA* 98: 6470–6475, 2001.
- Maloney JP, Silliman CC, Ambruso DR, Wan J, Tudor RM, Voelkel NF. In vitro release of vascular endothelial growth factor during platelet aggregation. *Am J Physiol Heart Circ Physiol* 275: H1054–H1061, 1998.
- Mesri M, Morales-Ruiz M, Ackermann EJ, Bennett CF, Pober JS, Sessa WC, Altieri DC. Suppression of vascular endothelial growth factor-mediated endothelial cell protection by surviving targeting. *Am J Pathol* 158: 1757–1765, 2001.
- Miura S, Tatsuguchi A, Wada K, Takeyama H, Shinji Y, Hiratsuka T, Futagami S, Miyake K, Gudis K, Mizokami Y, Matsuoka T, Sakamoto C. Cyclooxygenase-2-regulated vascular endothelial growth factor release in gastric fibroblasts. *Am J Physiol Gastrointest Liver Physiol* 287: G444–G451, 2004.
- Mizuno H, Sakamoto C, Matsuda K, Wada K, Uchida T, Noguchi H, Akamatsu T, Kasuga M. Induction of cyclooxygenase 2 in gastric mucosal lesions and its inhibition by the specific antagonist delays healing in mice. *Gastroenterology* 112: 387–397, 1997.
- Moore WM, Webber RK, Jerome GM, Tjoeng FS, Misko TP, Currie MG. L-N6-(1-iminoethyl)lysine: a selective inhibitor of inducible nitric oxide synthase. *J Med Chem* 37: 3886–3888, 1994.
- Morbideilli L, Chang CH, Douglas JG, Granger HJ, Ledda F, Ziche M. Nitric oxide mediates mitogenic effect of VEGF on coronary venular endothelium. *Am J Physiol Heart Circ Physiol* 270: H411–H415, 1996.
- Podolsky DK. Review article: healing after inflammatory injury—coordination of a regulatory peptide network. *Aliment Pharmacol Ther*, 14 Suppl 1: 87–93, 2000.
- Rees DD, Palmer RM, Schulz R, Hodson HF, Moncada S. Characterization of three inhibitors of endothelial nitric oxide synthase in vitro and in vivo. *Br J Pharmacol* 101: 746–752, 1990.
- Reuter BK, Asfaha S, Buret A, Sharkey KA, Wallace JL. Exacerbation of inflammation-associated colonic injury in rat through inhibition of cyclooxygenase-2. *J Clin Invest* 98: 2076–2085, 1996.
- Reuter BK, Davies NM, Wallace JL. Nonsteroidal anti-inflammatory drug enteropathy in rats: role of permeability, bacteria, and enterohepatic circulation. *Gastroenterology* 112: 109–117, 1997.
- Saif MW, Elfiky A, Salem RR. Gastrointestinal perforation due to bevacizumab in colorectal cancer. *Ann Surg Oncol* 14: 1860–1869, 2007.
- Schmassmann A, Peskar BM, Stettler C, Netzer P, Stroff T, Flogerzi B, Halter F. Effects of inhibition of prostaglandin endoperoxide synthase-2 in chronic gastro-intestinal ulcer models in rats. *Br J Pharmacol* 123: 795–804, 1998.
- Suzuki N, Takahashi S, Okabe S. Relationship between vascular endothelial growth factor and angiogenesis in spontaneous and indomethacin-delayed healing of acetic acid-induced gastric ulcers in rats. *J Physiol Pharmacol* 49: 515–527, 1998.
- Szabo IL, Pai R, Soreghan B, Jones MK, Baatar D, Kawanaka H, Tarnawski A. NSAIDs inhibit the activation of egr-1 gene in microvascular endothelial cells. A key to inhibition of angiogenesis? *J Physiol Paris* 95: 379–383, 2001.
- Szabo S, Vincze A. Growth factors in ulcer healing: lessons from recent studies. *J Physiol Paris* 94: 77–81, 2000.
- Takahashi M, Kawabe T, Ogura K, Maeda S, Mikami Y, Kaneko N, Terano A, Omata M. Expression of vascular endothelial growth factor at the human gastric ulcer margin and in cultured gastric fibroblasts: a new angiogenic factor for gastric ulcer healing. *Biochem Biophys Res Commun* 234: 493–498, 1997.
- Takahashi M, Maeda S, Ogura K, Terano A, Omata M. The possible role of vascular endothelial growth factor (VEGF) in gastric ulcer healing: effect of sofalcone on VEGF release in vitro. *J Clin Gastroenterol* 27: S178–S182, 1998.
- Takahashi M, Ogura K, Maeda S, Mori K, Mafune K, Mikami Y, Terano A, Omata M. Promoters of epithelialization induce expression of vascular endothelial growth factor in human gastric epithelial cells in primary culture. *FEBS Lett* 418: 115–118, 1997.
- Takeuchi K, Kato S, Takehara K, Asada Y, Yasuiro T. Role of nitric oxide in mucosal blood flow response and the healing of HCl-induced lesions in the rat stomach. *Digestion* 58: 19–27, 1997.
- Tarnawski AS. Cellular and molecular mechanisms of gastrointestinal ulcer healing. *Dig Dis Sci* 50: S24–S33, 2005.
- Wallace JL, Bak A, McKnight W, Asfaha S, Sharkey KA, MacNaughton WK. Cyclooxygenase 1 contributes to inflammatory responses in rats and mice: implications for gastrointestinal toxicity. *Gastroenterology* 115: 101–109, 1998.
- Wallace JL, Chapman K, McKnight W. Limited anti-inflammatory efficacy of cyclo-oxygenase-2 inhibition in carrageenan-airpouch inflammation. *Br J Pharmacol* 126: 1200–1204, 1999.
- Wallace JL, del Soldato P. The therapeutic potential of NO-NSAIDs. *Fundam Clin Pharmacol* 17: 11–20, 2003.
- Wallace JL, Dickey M, McKnight W, Dudar GK. Platelets accelerate gastric ulcer healing through presentation of vascular endothelial growth factor. *Br J Pharmacol* 148: 274–278, 2006.
- Wallace JL, Dickey M, McKnight W, Martin GR. Hydrogen sulfide enhances ulcer healing in rats. *FASEB J* 21: 4070–4076, 2007.
- Wallace JL, Miller MJ. Nitric oxide in mucosal defense: a little goes a long way. *Gastroenterology* 119: 512–520, 2000.

43. **Wallace JL, McKnight W, Reuter BK, Vergnolle N.** NSAID-induced gastric damage in rats: requirement for inhibition of both cyclooxygenase 1 and 2. *Gastroenterology* 119: 706–714, 2000.
44. **Wallace JL, Tigley AW.** Review article: new insights into prostaglandins and mucosal defence. *Aliment Pharmacol Ther* 9: 227–235, 1995.
45. **Wang JY, Yamasaki S, Takeuchi K, Okabe S.** Delayed healing of acetic acid-induced gastric ulcers in rats by indomethacin. *Gastroenterology* 96: 393–402, 1989.
46. **Zanardo RC, Brancaleone V, Distrutti E, Fiorucci S, Cirino G, Wallace JL.** Hydrogen sulfide is an endogenous modulator of leukocyte-mediated inflammation. *FASEB J* 20: 2118–2120, 2006.
47. **Ziche M, Morbidelli L, Choudhuri R, Zhang HT, Donnini S, Granger HJ, Bicknell R.** Nitric oxide synthase lies downstream from vascular endothelial growth factor-induced but not basic fibroblast growth factor-induced angiogenesis. *J Clin Invest* 99: 2625–2634, 1997.

